TU Delft Delft University of Technology

SPACE CHARGE ANALYSIS OF EPOXY BASED NANOCOMPOSITES

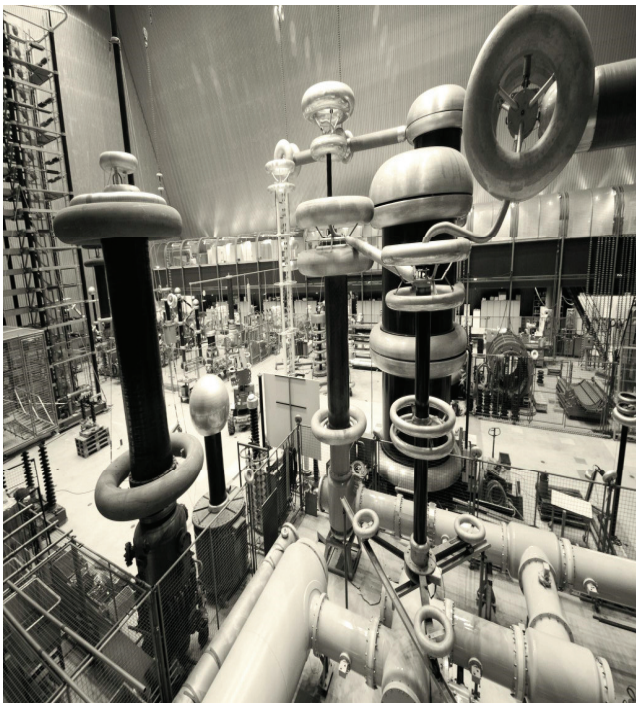

8/21/2015

Debarshi Saha

The High Voltage Laboratory, TU Delft, The Netherlands.

Space Charge analysis of epoxy based nanocomposites

A DISSERTATION PRESENTED
BY
DEBARSHI SAHA
TO
THE ELECTRICAL ENGINEERING, MATHEMATICS & COMPUTER SCIENCE FACULTY

IN PARTIAL FULFILLMENT OF THE REQUIREMENTS
FOR THE DEGREE OF
MASTER OF SCIENCE
IN THE SUBJECT OF
ELECTRICAL ENGINEERING

DELFT UNIVERSITY OF TECHNOLOGY
DELFT, ZUID-HOLLAND, THE NETHERLANDS

AUGUST 2015

Space Charge analysis of epoxy based nanocomposites

Abstract

HVDC is an established technology that has been in commercial use for 60 years. During the last three decades, space charge phenomena in HVDC insulation have been investigated worldwide. Many techniques have been developed for the experimental observation of space charge. Further research into these techniques, and development of novel dielectric materials is also progressing at a quick pace worldwide.

Epoxy resins are widely used as electrical insulation in electrical engineering applications such as transformers, bus bars, electrical machines etc. Excellent adhesive properties, resistance to heat and chemicals, good mechanical properties and very good electrical insulating properties make epoxy a favoured insulating material. Accumulation of space charge within a polymeric dielectric material, may be associated with gradual degradation.The accumulation of space charge inside polymeric material modifies conduction through the material- and leads to local field enhancement within the material and might contribute to its aging.

Some research groups worldwide have now been able to document some significant improvements that can be made in the electrical, and other, properties of polymer composites through the incorporation of nanoparticulates. In this research work, the space charge analysis of epoxy-based nano-composites has been performed. The nano-filler of choice is hexagonal boron nitride cast into the epoxy matrix by volume%, ranging from 0% (neat, unfilled epoxy resin), to a maximum of 5%. Thin plaque samples, ranging from a thickness of 0.46 mm till 0.59 mm have been used to characterize our measurements. Because of excellent thermal and chemical stability, boron nitride materials are traditionally used as parts of high-temperature equipment. Boron nitride has potential use in nanotechnology. The fact that BN structurally is similar to graphite, which also exhibits the property that nano-particles can reduce the development of space charge, coupled with the fact of it possessing high thermal conductivity, is reason enough to investigate the effect of fillers in neat epoxy, and whether the properties of the material have been enhanced or diminished.

The main goal of this thesis is to characterize the experimental samples with regard to their threshold for charge accumulation and space charge dynamics, and to investigate the effect of fill-grade loading & the contribution of nano-fillers to the space charge behaviour of epoxy. The effect of particle distribution on space charge behaviour is also researched to provide a holistic understanding of the nano-dielectric performance.

Contents

1 Introduction **2**
- 1.1 General words . . . 2
- 1.2 HVDC electrical power transmission technology . . . 2
- 1.3 Dielectric (Insulation) materials for HVDC technology . . . 4
- 1.4 Space charge phenomena in insulation materials . . . 4
- 1.5 Nano composite dielectric materials development . . . 5
- 1.6 Objective of the present study . . . 6
- 1.7 Outline of the thesis . . . 6

2 Background scientific theory upon space charge measurements **8**
- 2.1 Space charge accumulation . . . 8
- 2.2 Salient features & criterion . . . 8
- 2.3 The macroscopic viewpoint . . . 8
- 2.4 The microscopic viewpoint . . . 10
- 2.5 Trapped space charge accumulation threshold . . . 15
- 2.6 Dielectric polarization . . . 16
- 2.7 Dielectric properties of epoxy resin . . . 19
- 2.8 Polymer Nanocomposites . . . 19
- 2.9 Space charge analysis parameters . . . 24

3 Experimental procedures **25**
- 3.1 Experimental techniques adopted . . . 25
- 3.2 An introduction to test specimens . . . 25
- 3.3 Space charge measurements . . . 26

4 Experimental results & analysis **42**
- 4.1 The effect of fill grade upon nano-filler incorporation in host material . . . 42
- 4.2 Analysis of effect of filler content on nanocomposites . . . 70
- 4.3 The effect of nano-particle distribution upon space charge behaviour . . . 72
- 4.4 Threshold Field measurements upon samples . . . 80
- 4.5 The Ultrasonic measurement of sound velocity in Epoxy-hBN nanocomposites . . . 87

5 Conclusion & Recommendations for future work **91**
- 5.1 Conclusions . . . 91
- 5.2 Future scope of research work . . . 93

References **95**

Listing of figures

1.2.1 The HVDC transmission system,© 2015, ABB. 3

2.4.1 The energy-band model 10
2.4.2 Charge trapping, injection for metal-insulator surfaces[101]. 12
2.4.3 Log-log plot of current density J vs. voltage V[101]. 15
2.6.1 The phenomenon of dielectric polarization, in a parallel-plate capacitor 17
2.8.1 The interface ab between two phases A and B, and change of chosen material property[1,55]. 21
2.8.2 Electrical situation at a metal electrode-dielectric interface, the 2 electrical layers[1]. 22
2.8.3 Multi core model for nano-particle and polymer interfaces(Tanaka) 23

3.2.1 All test specimens, arranged by increasing fill grade. 26
3.3.1 A simplified diagram of a generic pulsed electro-acoustic system sample cell and detector, ©J.M. Alison, 1998[93] 28
3.3.2 Principle behind the PEA method[19]. 29
3.3.3 The PEA measurement setup schematic 30
3.3.4 General schematic of the PEA test bench 32
3.3.5 Setup photograph-3 (Plaque sample loaded on PEA base) 33
3.3.6 Setup photograph-4 (HV electrode, with circular carbon-black semicon) 34
3.3.7 The preliminary observations from raw data. 36
3.3.8 Signal filtered by Butterworth & Gaussian filtering, polarity corrected. 37
3.3.9 Deconvoluted signal 38
3.3.10 Obtained space charge profile 39
3.3.11 Obtained Contour Plot, space charge dynamics investigated. 39
3.3.12 Obtained Average charge density plot. 41

4.1.1 Neat epoxy processed signal contour plot, 8 $\frac{kV}{mm}$, 25 degrees 43
4.1.2 Neat epoxy processed signal contour plot, 30 $\frac{kV}{mm}$, 25 degrees 43
4.1.3 Neat epoxy processed signal contour plot, 30 $\frac{kV}{mm}$, 45 degrees 44
4.1.4 Neat epoxy processed signal contour plot, 8 $\frac{kV}{mm}$, 45 degrees 45
4.1.5 Neat epoxy processed average charge density plot, 30 $\frac{kV}{mm}$, 25 & 45 degrees 45
4.1.6 Neat epoxy processed average charge density plot, 30 $\frac{kV}{mm}$, 25 & 45 degrees 46
4.1.7 E-hBN-0.2-A processed signal contour plot, 30 $\frac{kV}{mm}$, 25 degrees 47
4.1.8 E-hBN-0.2-A processed signal contour plot, 30 $\frac{kV}{mm}$, 45 degrees 47
4.1.9 E-hBN-0.2-B processed signal contour plot, 30 $\frac{kV}{mm}$, 25 degrees 48
4.1.10 E-hBN-0.2-B processed signal contour plot, 30 $\frac{kV}{mm}$, 45 degrees 48
4.1.11 E-hBN-0.2-C processed signal contour plot, 30 $\frac{kV}{mm}$, 25 degrees 49
4.1.12 E-hBN-0.2-C processed signal contour plot, 30 $\frac{kV}{mm}$, 45 degrees 49
4.1.13 E-hBN-0.2-A average charge density vs time plot[poling], 30 $\frac{kV}{mm}$, 45 degrees 50

4.1.14E-hBN-0.2-A average charge density vs time plot[depoling], 30 $\frac{kV}{mm}$, 45 degrees . . . 50
4.1.15E-hBN-0.2-B average charge density vs time plot[poling], 30 $\frac{kV}{mm}$, 45 degrees . . . 51
4.1.16E-hBN-0.2-B average charge density vs time plot[depoling], 30 $\frac{kV}{mm}$, 45 degrees . . . 51
4.1.17E-hBN-0.2-C average charge density vs time plot[poling], 30 $\frac{kV}{mm}$, 45 degrees . . . 52
4.1.18E-hBN-0.2-C average charge density vs time plot[depoling], 30 $\frac{kV}{mm}$, 45 degrees . . . 52
4.1.19E-hBN-0.5 processed signal contour plot, 30 $\frac{kV}{mm}$, 25 degrees . . . 53
4.1.20E-hBN-0.5 processed signal contour plot, 30 $\frac{kV}{mm}$, 45 degrees . . . 54
4.1.21E-hBN-0.5 average charge density vs time plot[poling], 30 $\frac{kV}{mm}$, 45 degrees . . . 54
4.1.22E-hBN-0.5 average charge density vs time plot[depoling], 30 $\frac{kV}{mm}$, 45 degrees . . . 55
4.1.23E-hBN-0.6 processed signal contour plot, 30 $\frac{kV}{mm}$, 25 degrees . . . 56
4.1.24E-hBN-0.6 processed signal contour plot, 30 $\frac{kV}{mm}$, 45 degrees . . . 56
4.1.25E-hBN-0.6 average charge density vs time plot[poling], 30 $\frac{kV}{mm}$, 45 degrees . . . 57
4.1.26E-hBN-0.6 average charge density vs time plot[depoling], 30 $\frac{kV}{mm}$, 45 degrees . . . 57
4.1.27E-hBN-1-A processed signal contour plot, 30 $\frac{kV}{mm}$, 25 degrees . . . 58
4.1.28E-hBN-1-A processed signal contour plot, 30 $\frac{kV}{mm}$, 45 degrees . . . 59
4.1.29E-hBN-1-B processed signal contour plot, 30 $\frac{kV}{mm}$, 25 degrees . . . 59
4.1.30E-hBN-1-B processed signal contour plot, 30 $\frac{kV}{mm}$, 45 degrees . . . 60
4.1.31E-hBN-1-C processed signal contour plot, 30 $\frac{kV}{mm}$, 25 degrees . . . 61
4.1.32E-hBN-1-C processed signal contour plot, 30 $\frac{kV}{mm}$, 45 degrees . . . 62
4.1.33E-hBN-1-A average charge density vs time plot[poling], 30 $\frac{kV}{mm}$, 45 degrees . . . 62
4.1.34E-hBN-1-A average charge density vs time plot[depoling], 30 $\frac{kV}{mm}$, 45 degrees . . . 63
4.1.35E-hBN-1-B average charge density vs time plot[poling], 30 $\frac{kV}{mm}$, 45 degrees . . . 63
4.1.36E-hBN-1-B average charge density vs time plot[depoling], 30 $\frac{kV}{mm}$, 45 degrees . . . 64
4.1.37E-hBN-1-C average charge density vs time plot[poling], 30 $\frac{kV}{mm}$, 45 degrees . . . 64
4.1.38E-hBN-1-C average charge density vs time plot[depoling], 30 $\frac{kV}{mm}$, 45 degrees . . . 65
4.1.39E-hBN-5-A processed signal contour plot, 30 $\frac{kV}{mm}$, 25 degrees . . . 66
4.1.40E-hBN-5-A processed signal contour plot, 30 $\frac{kV}{mm}$, 45 degrees . . . 66
4.1.41E-hBN-5-B processed signal contour plot, 30 $\frac{kV}{mm}$, 25 degrees . . . 67
4.1.42E-hBN-5-B processed signal contour plot, 30 $\frac{kV}{mm}$, 45 degrees . . . 67
4.1.43E-hBN-5-A average charge density vs time plot[poling], 30 $\frac{kV}{mm}$, 45 degrees . . . 68
4.1.44E-hBN-5-A average charge density vs time plot[depoling], 30 $\frac{kV}{mm}$, 45 degrees . . . 68
4.1.45E-hBN-5-B average charge density vs time plot[poling], 30 $\frac{kV}{mm}$, 45 degrees . . . 69
4.1.46E-hBN-5-B average charge density vs time plot[depoling], 30 $\frac{kV}{mm}$, 45 degrees . . . 69
4.3.1 Samples E-hBN-0.2-C & E-hBN-0.5 . . . 73
4.3.2 Samples E-hBN-1-C & E-hBN-5-B . . . 74
4.3.3 Samples E-hBN-0.2-A & E-hBN-1-B . . . 75
4.3.4 Sample E-hBN-5-A . . . 75
4.3.5 Samples E-hBN-0.2-B & E-hBN-0.6 . . . 76
4.3.6 Samples E-hBN-1-A . . . 76
4.3.7 Comparison between average charge density plot, 30 $\frac{kV}{mm}$, 45 degrees . . . 77
4.3.8 Comparison between average charge density plot, 30 $\frac{kV}{mm}$, 45 degrees . . . 77
4.3.9 Comparison between average charge density plot, 30 $\frac{kV}{mm}$, 45 degrees . . . 78
4.3.10Comparison between average charge density plot, 30 $\frac{kV}{mm}$, 45 degrees . . . 79
4.3.11Comparison between average charge density plot, 30 $\frac{kV}{mm}$, 45 degrees . . . 79
4.3.12Comparison between average charge density plot, 30 $\frac{kV}{mm}$, 45 degrees . . . 80
4.4.1 Neat epoxy threshold field plot, 45 degrees . . . 81
4.4.2 E-hBN-0.2-C threshold field plot, 45 degrees . . . 82

4.4.3 E-hBN-0.5 threshold field plot, 45 degrees . . . 83
4.4.4 E-hBN-0.6 threshold field plot, 45 degrees . . . 84
4.4.5 E-hBN-1-C threshold field plot, 45 degrees . . . 85
4.4.6 E-hBN-5-B threshold field plot, 45 degrees . . . 86
4.5.1 The Phased Array Ultrasonic Flaw detector Omniscan MX2, ©Olympus NDT Canada, Inc. . . . 88
4.5.2 The sample, wedge connected to setup for measurement. . . . 88
4.5.3 Fill grade vs. Acoustic velocity . . . 89
4.5.4 Fill grade vs. Acoustic velocity(95% C.I.) . . . 90

5.2.1 Schematic representation: Deconvolution technique . . . 102
5.2.2 Switch box for PEA setup . . . 106
5.2.3 HVDC pulse generator for PEA setup . . . 106
5.2.4 HVDC supply for PEA setup . . . 107
5.2.5 Oscilloscope used for data acquisition from PEA setup . . . 107
5.2.6 PEA setup, sample loaded onto base . . . 108
5.2.7 PEA setup, HV electrode in position . . . 109
5.2.8 PEA setup, HV electrode with semicon strip . . . 109
5.2.9 The Omniscan MX2 Flaw detector . . . 110
5.2.10 The Omniscan MX2 Flaw detector, sample underneath optical wedge, gel for application on surface . . . 110
5.2.11 The selection of traces, for E-hBN-0.5, 30 kV/mm, 45 degrees . . . 112
5.2.12 The selection of traces, for E-hBN-0.5, 30 kV/mm, 45 degrees[magnified] . . . 112
5.2.13 Neat epoxy contour plots-1 . . . 113
5.2.14 Neat epoxy contour plots-2 . . . 113
5.2.15 E-hBN-0.2-C contour plots-1 . . . 114
5.2.16 E-hBN-0.2-C contour plots-2 . . . 114
5.2.17 E-hBN-0.5 contour plots-1 . . . 115
5.2.18 E-hBN-0.5 contour plots-2 . . . 115
5.2.19 E-hBN-0.6 contour plots-1 . . . 116
5.2.20 E-hBN-0.6 contour plots-2 . . . 116
5.2.21 E-hBN-1-C contour plots-1 . . . 117
5.2.22 E-hBN-1-C contour plots-2 . . . 117
5.2.23 E-hBN-5-B contour plots-1 . . . 118
5.2.24 E-hBN-5-B contour plots-2 . . . 118

To my parents, who showed me the light of day- and the Lord Krishna.

"The embodied soul is eternal in existence, indestructible, and infinite, only the material body is factually perishable- therefore fight, o Arjuna!"

— The Bhagavad Gita (Chapter 2, Verse 3)

Acknowledgments

Any project of importance undertaken owes its success entirely to the wonderful persons involved with it, just as this one. Apart from my own efforts, many people contributed to the success of this thesis research, in a direct/indirect manner. I would like to express my heartfelt gratitude to all of them.

Firstly, I would like to express my appreciation to Dr. Ir. Peter H.F. Morshuis for giving me the opportunity to participate in such an interesting project. His lectures were what made me embark on this journey, and it has been my privilege to have been a recipient of his knowledge.

It is with great joy that I provide a shout-out to my two enthusiastic, knowledgeable and fantastic supervisors, Ir. I.A. Tsekmes & Dr. Roman Kochetov. Both of them taught me in their own ways to pay attention to the finer details in work, a fact which crossed over in life as well. One usually had monosyllabic answers and an air of nonchalance, whilst the other could be really worked up in the frenzy of exposition. They were polar opposites in some ways, but my perfect friends- a fact which I realized only when I learnt how to really think about science, and not just imagine about it, grasping at straws wading in the enormous deluge of data. One was an avid globe trotter, whilst the other was a really voracious reader. But, they were (and still are) the links of completion between an artist and an engineer.

One special person I would like to earnestly thank is Dr. Riccardo Bodega (and of course his wonderful family- Yvonne & Matteo!), whose august company I have heartily enjoyed at all times. I have met many individuals on my journey of life, and few (like him) have left a lasting effect on me. He is one fine mentor, and I hope we remain the best of friends!

It is with a deep sense of satisfaction & gratitude that I thank Dr. Andrei Anisimov, post-doctoral researcher at the Aerospace NDT laboratory (TU Delft) for helping me out with the measurement of sound velocity using ultrasonic techniques. I highly appreciate his meticulousness and valuable time spared for me, and I look forward to a fruitful & exciting collaboration between the respective research groups in the future!

The High Voltage Laboratory is indeed a beautiful place, and the wonderful people at the helm are to be acknowledged herein as well! My gratitude goes out to Ing. Paul Van Nes & Mr. Wim Termorshuizen, for their assistance, guidance & help at all times.

Finally, I would like to thank my family who inspired, encouraged and fully supported me in every aspect of my life. They have been truly the leading light for me. I would like to thank my friends as well, especially Mr. Ramin K Barak & Mr. Subhronil Chaudhuri, my 'geek friend with a heart of gold'! May our friendship age like fine wine!

An ode to Space Charge!

These little electrons make me wonder,
and I wonder where they wander!
They ain't giving off any discharge,
and yet they show up as space charge!
It's a damned job, hunting them down-
Hundreds of graphs get plotted & rejected, with me looking like a clown!
They like lurking in 'bumps' and 'humps',
they show up in my graphs as mis-shapen lumps!
Gaussian filters convoluted my dreams, the amplifier response keeps me up at night-
I wonder whether I'll ever get the interfaces right?
Ideas flow past thick and fast, time slips by-
The setup has a mind of its own, and the oscilloscope leaves me high & dry!
It's no fun being an electron, if you are being perturbed by a pulse-
So, dear electron, kindly stop being annoyed and respond to my impulse!
You like wandering down the alleyways of Life, and this leads to 'scatter'-
So, please stick together, be nice neighbours- and let me work on things that matter!!

— Debarshi Saha (December 12, 2014)

I want to build a billion tiny factories, models of each other, which are manufacturing simultaneously. The principles of physics, as far as I can see, do not speak against the possibility of maneuvering things atom by atom. It is not an attempt to violate any laws; it is something, in principle, that can be done; but in practice, it has not been done because we are too big.

Richard P. Feynman

1 Introduction

1.1 General words

Nanotechnology is the *big* science of very *small* things! The topic of *Nano-dielectrics* was introduced primarily by *Lewis* in a 1994 paper [1], but it was not until the experimental work of *Henk et al.* [2] and an US/European team [3] that it became clear that there may, indeed, be advantages to be gained in the field of electrical insulation, by the inclusion of nano-particulates. Nanotechnology, sometimes shortened as 'nanotech', deals with the manipulation and manufacturing of structures of which at least one of the dimensions is less than 100 nanometers. Epoxy resin, by virtue of its eminent dielectric, physical and chemical properties, is widely used in such direct current (DC) equipment as bushings for converter transformers, smoothing reactors and composite post insulators[19]. However, when epoxy resin is subjected to DC voltage, the accumulation of space charge may lead to serious local electric field distortion, from a Laplacian to a Poissonian distribution inside the material and thus threaten to reduce its insulation life span. As many improvements in material properties are harnessed from using nano-composites, a lot of electrical properties are also seen to have been enhanced making use of nano-composites. A significant number of literature results show enhancement of electrical properties using nano-composites[4,5,8]. Some of the significant advantages of using nanoscale fillers instead of micrometer-scale fillers are reported as an increase in the electrical breakdown strength, improvement in mechanical strength & stiffness of composites, increased electrical conductivity, improved viscosity control, increase in strength of material & enhanced resistance to wear and tear[20]. *Ajayan* [4] mentions that, the permittivity of polymers can be increased with the addition of many metal oxide fillers, on both the micro- and nanoscale. Once hailed as the 'panacea' for such conditions(nanodielectrics), this work sheds light on the effect of nano-particle inclusion into host epoxy matrix.

1.2 HVDC electrical power transmission technology

HVDC transmission is an efficient technology designed to deliver large amounts of electricity over long distances with low losses. It can also interconnect incompatible AC networks and stabilize the surrounding electrical grid. HVDC transmission is widely recognized as being advantageous for long-distance, bulk power delivery, asynchronous interconnections and long submarine cable crossings.

Each transmission link has its own set of requirements justifying the choice of HVDC, but the most common points of advantage in favor include:

- Asynchronous interconnections
- Long distance water crossing
- Lower losses
- Controllability
- Environmental concerns
- Limit short-circuit currents
- Lower investment cost

An HVDC transmission link consists of *three* main components: a station to convert the alternating current of the grid to direct current, the transmission equipment itself in the form of cables and overhead lines, and another station that converts DC back into AC so that it can be used by consumers.

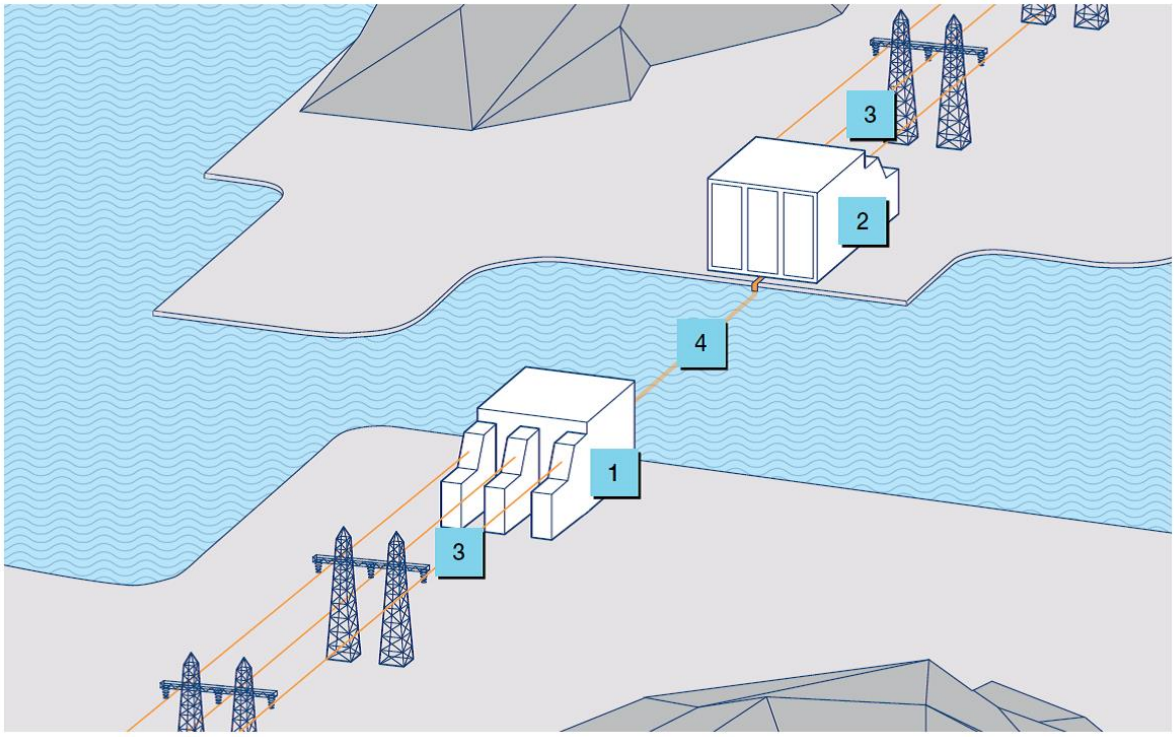

Figure 1.2.1: The HVDC transmission system,© 2015, ABB.

Key legends 1 denote the HVDC converter station rectifier, 2-the HVDC converter station inverter, 3 and 4 the locations of AC & DC transmission.

However, the electric field distribution at DC voltage differs greatly from that at AC voltage. The field distribution at DC is determined by the conductivity σ of the insulation which is not constant and depends strongly on the temperature and the electric field. Surface charges and space charges play an important role too. As a result, the intermediate fields are space,

temperature and time dependent. This makes the determination of the electric field at DC voltage a far more complex matter than the equivalent case at AC voltage.

HVDC has a higher initial cost – the converter stations – but because the means of transmission (the overhead lines and the cables) are less expensive per kilometer with DC, there is a break-even distance. Hence, to reduce electrical losses and costs – and sometimes because it is the only possible solution, HVDC is rapidly gaining great importance. For example, the rapidly growing Indian power system is being constructed as several regional power systems interconnected with HVDC transmission lines and back-to-back converters with centralized control of these HVDC elements (*Koshcheev 2001*).

Likewise, in China, 800-kV HVDC will be the main mode used to transmit large capacity over very long distances from large hydropower and thermal power bases. Other applications involve long-distance transmission projects with few tie-ins of power supplies along the line (*Yinbiao 2005*).

1.3 Dielectric (Insulation) materials for HVDC technology

Polymeric HVDC insulation materials were developed in the 1990's in parallel with the development of voltage source converter technology. Successful field testing of both cable and converter was carried out in 1994. The unidirectional electric field imposed by a DC line has a strong effect on the integrity of dielectric materials traditionally made for AC applications. In the early years of the first DC lines, it became clear that specific dielectrics were needed.

High resistivity is required for DC applications. According to IEC 61325 standard, the specifications for dielectric materials can be summarized through two main requirements, both of them are of prime importance to prevent harmful consequences on the dielectric:

- Ionic migration
- Thermal runaway

In fact, both are linked together through the resistivity of the dielectric. A continuous transverse current crossing the body of the dielectric (different from the surface leakage current) can generate a temperature increase and subsequently a local decrease of resistivity. The persistence of this phenomenon can bring the dielectric to puncture or shatter through an avalanche phenomenon, which is the visible aspect of a thermal runaway[21]. The unidirectional current going through the body of the dielectric can also generate some depletion of the atomic structure of the material, reducing the material's electrical and/or thermo mechanical (as per IEC or ANSI) and electromechanical properties[49]. Therefore, major suppliers for the DC insulators market have significantly increased the electric resistivity of their dielectric materials to provide a correct solution to these particular stress conditions[21]. However, it must be taken into account that **higher resistivity does not always mean better performance under DC conditions**. Operating conditions & desired electrical/thermal/mechanical objectives often determine manufacturing decisions regarding the production of dielectric materials.
Compliance with ionic migration performance test requires firstly an appropriate resistivity value but also excellent purity and homogeneity of the dielectric materials.

1.4 Space charge phenomena in insulation materials

One of the intrinsic properties of the DC polymeric materials is the accumulation of charges. Insulating materials allow a weak electrical conduction. This weak flow of charge within the insulation may not be uniform, because of a local inhomogeneity of the material. When an inequality occurs between the flow of charges into a region and the flow of charges out of that region, charge accumulates in that region. In an AC situation, the flow of charges inverts its direction too quickly to allow a significant growth of space charge at the insulation inhomogeneities, at least for conventional insulating materials. This means that the space charge field can be neglected. However, under a DC stressing condition, the flow of charge maintains the same direction. This allows a build-up of charge, which, in general, significantly affects the electric field distribution inside the insulation.

The existence of space charge causes 2 main problems:

- Space charge distorts any electrical field present according to Poisson's equation.

$$\vec{\nabla}.\vec{E} = \frac{\rho}{\varepsilon_o \varepsilon_r} \tag{1.1}$$

- Energy is required to separate charged particles of different polarity. This energy is stored in the system and may be used to damage or deform the material locally.

$$W_e = \frac{\varepsilon_o \varepsilon_r E^2}{2} \tag{1.2}$$

Space charge may accumulate in a solid dielectric when a DC voltage is applied across it. The electric field distribution is distorted and if the space charge density is sufficiently high, the local field strength may exceed the breakdown strength of the dielectric, leading to a failure[47,48]. Polymer structure and degree of crystallinity can influence the dielectric strength and space charge formation.

1.5 Nano composite dielectric materials development

Dielectrics possess many distinctive features. They contain few charge species and polymer chains mostly interact with other polymer chains in the vicinity. Dielectrics are also substances for which the intrinsic spatial electronic distribution strongly tends, under the influence of an external EMF, to resist any change; in other words, a polarizable compound. For electrotechnical applications, one would seek dielectrics with low electrical conductivity, or low dielectric constant for integrated circuitry, and one that can sustain a high electric field gradient[22].

In this context, a *nanodielectric* would consist of a multi-component dielectric possessing nanostructures, the presence of which leads to changes in one or several of its dielectric properties[91].

Nanodielectrics can be named as *'molecularly tailored materials'*- hence the structure of a nanodielectric would include the nano-structuring of solid bulk materials with appropriate nano-sized filler content. Dispersing nanoparticles into polymers sometimes lead to enhancement of thermal and mechanical properties of the composite with respect to the conventional (conventional: unfilled, without the presence of nanoparticles) material and it is hoped that similar effects could be observed on electrical performances. Improvement of electrical behaviour has indeed been reported on different types of PNC(polymer nano-composites)[4,8,55,66]. Such modifications are attributed, besides to the presence of the filler, to the much higher surface area to volume ratio, as compared to the same ratio between polymer molecules themselves[72]. This aspect of increase is associated with the presence of nanoparticles.

One of the starting points for nano-dielectric materials development was the realization that nanodielectrics behaved in a completely different way to the micro-filled composites[22]. It was speculated that the "interaction zone" around the particles was having a dominant effect in the case of nano-particles. Because of their extended surface area, nanoparticles may change the very nature of the polymer, alter the depth and density of trap sites, thus reducing charge carrier mobility and energy. It is also possible that the structure between the polymer and the nanoparticle is the key to the trapping mechanism[91]; this is where the "assumed" charge layer may develop. Finally, the most fundamental effect may be that nanoparticles embedded in a dielectric matrix create an enormous number of nanoscopic electrochemical interfaces and these regions thus created may determine some of the features of nanodielectrics. In order to gain an understanding about the dielectric behaviour of nanocomposites, space charge measurements are being conducted worldwide- since the characterization of space charge dynamics in nanocomposites possibly help in determination of electrical behaviour for the structured materials.

The first successful nanocomposites incorporated nanoscale clay into a polymer host material. Initial results regarding the permittivity of polymer-based nanocomposites were astounding since they defied conventional wisdom. Introducing a small fraction of nanoscale filler material into a polymer host reduces the relative permittivity. Traditional theories would suggest that a composite of two materials would have a relative permittivity with a value between the values of the constituent elements, instead of sometimes being lower than either of them[88,89]. The reason for this unique behaviour turned out to

be an immobilization of polymer chains surrounding the nanoparticles[89]. The main parameters affecting the properties of a nanocomposite can be identified as follows:

- Filler size, material and aspect ratio
- Surface functionalization
- Fillgrade
- Host material
- Type of synthesis (in-situ, ex-situ, mixing process, polymerization, etc.)
- Sample homogeneity as regards the incorporation of nano-particles into the host material

1.6 Objective of the present study

This project investigates the effect of addition of h-BN (hexagonal boron nitride) nanoparticles, of average size about 70 nm, to epoxy resin, cast in the form of thin circular plaques, varying in thickness from 0.46 mm minimally till 0.56 mm maximally. Different filler concentrations by volume% have been chosen, with the lowest as 0.2 volume% till the highest of 5 volume%, and incorporated into the epoxy host material. The space charge characterization of the samples is performed by the Pulsed Electro-acoustic technique, and the resultant nano-filler incorporated materials are characterized in terms of space charge accumulation in the samples, depletion rate, accumulation rate, charge accumulation characteristics. 3 distinct techniques of sample production have been adopted, to incorporate the h-BN nanoparticles into the epoxy base, in case of the same fill-grade, and the study of these techniques is briefly performed as well. The investigation mainly concerns the effect of fill grade upon space charge dynamics, and the influence of sample homogeneity upon space charge behaviour. Boron nitride was chosen for the investigation due to its excellent thermal conductivity properties, and also because it has certain structural similarity to graphite nano-particles[55].

1.6.1 Scientific contribution of the work

The main scientific contribution of this research work lies in the space charge behaviour characterization upon the addition of boron nitride nano-fillers, by pre-determined fill-grades, using different synthesis techniques (between similar filler concentrations) to examine the effect of particle distribution upon global space charge behaviour. Fixed conditions of temperature and relative humidity levels make this work unique in the light of other research literature upon polymer nanocomposites.

1.7 Outline of the thesis

In Chapter 1, the general ground for the discussion of the research work conducted is set. The world of HVDC technology is introduced, and the motivation behind the research of nano-dielectrics is briefly discussed.

In Chapter 2, the basic background theory related to space charge phenomena is presented, along with a discussion of various theoretical models. In the following chapter, Chapter 3, the experimental methods used for the space charge measurements are described in detail.

In Chapter 4, the experimental results with regard to the space charge measurements are presented and discussed. Primarily, the method of data acquisition & subsequent extensive mathematical processing are discussed. The effect of fill grade upon nano-filler incorporation in host material, is characterized by the space charge behaviour of the specimens. The effect of nano-particle distribution upon space charge behaviour is studied in detail, with a comparative analysis between

nanocomposite production techniques as follow up. The results of threshold field measurements upon selected specimens are presented,with the analysis of the effect of fill-grade upon space charge accumulation thresholds. A discussion of electrical behaviour of polymeric specimens upon nano-filler incorporation is embarked upon, threshold field results obtained are correlated with electrical behaviour. Finally, a holistic comparison of this scientific work is made with previous research literature, rounding off the chapter with our current state of knowledge, and a brief summary of results.

The final chapter, Chapter 5, contains the conclusions drawn from the measurements and some recommendations for future research on polymer nanocomposites.

There are two possible outcomes: If the result confirms the hypothesis, then you've made a measurement. If the result is contrary to the hypothesis, then you've made a discovery.

Enrico Fermi

2

Background scientific theory upon space charge measurements

2.1 Space charge accumulation

In this section, the underlying physical phenomena of the processes behind the investigated parameters in this research work are discussed. Space charge phenomena is usually examined in literature from 2 main viewpoints, namely, the macroscopic and microscopic point of view.

2.2 Salient features & criterion

Space charge accumulates within dielectrics when it is retained in traps even after applied voltage is removed[76]. The accumulation of space charge within a dielectric alters the field distribution within the dielectric. Charges trapped in deep or shallow traps store electromechanical energy, cause local field intensification and give rise to radiative recombination and excitation. These processes can in turn produce early damage through increased rate of hot electron generation, bond dissociation, micro-cavity enlargement and internal strains[77].

2.3 The macroscopic viewpoint

From a macroscopic point of view, space charge accumulates when the current density $\boldsymbol{J}$ is divergent. Therefore, when the flow of charged particles into a region of space differs from the flow out of that region, a net charge builds up in time in this region[76]. The main statement in the macroscopic view is the fact that space charge accumulation occurs only when the total current density $\boldsymbol{J}$ through a region of space is divergent, due to factors like: at an electrode-dielectric interface, at a dielectric-dielectric interface, in the case of a temperature gradient and in the case of inhomogeneities. They are specifically listed below for clarity:

- Electrode-dielectric interface
- Dielectric-dielectric interface
- In the presence of a temperature gradient

- In case of gross inhomogeneities
- In case of morphological inhomogeneities

Each of these factors are separately discussed below:

1) **The electrode-dielectric interface**: The flow of charged particles through the interface is determined by the charge injection/extraction mechanisms and their field and temperature dependence. On the other hand, the flow of charged particles through the dielectric is governed by the charge transport mechanism of the dielectric and its field and temperature dependence. Therefore, the build-up of space charge depends on the difference:

$$J_{injection}(E, Tconstant) - J_{transmission}(E, Tconstant) = \Delta J_{interface} \tag{2.1}$$

Here, $J_{injection}$ is the injection current density and $J_{transmission}$ is the current density through the dielectric. Three cases can be distinguished which are described below.

- $J_{injection}$=$J_{transmission}$: In this case the interface is called ohmic and no space charge is accumulated as the amount of charges injected/extracted from the electrodes is just enough to replace the charges that are removed from/ towards the interface by transport.
- $J_{injection}$ <$J_{transmission}$: In this case the electrode interface cannot convey the charges as fast as the dielectric can conduct them. Therefore, positive hetero-charge will build up in front of the cathode and negative hetero-charge in front of the anode. The hetero-charge increases the electric field in front of the electrode and hence the injection current while reducing the bulk field and the transport current. Eventually, a steady state situation is achieved when the two currents coincide.
- $J_{injection}$ >$J_{transmission}$: In this case the electrodes yield more charges than the dielectric can conduct. Therefore, negative homo-charge builds up in front of the cathode and positive homo-charge in front of the anode. The homo-charge decreases the electric field in front of the electrode and hence the injection current while increasing the bulk field and the transport current. Eventually, a steady state situation is achieved when the two currents coincide.

2) **The dielectric-dielectric interface**: Space charge accumulation at the interface of two different dielectrics is described by the Maxwell –Wagner theory. A hypothetical capacitive configuration is used to describe the phenomena at the interface between two different dielectrics which is called Maxwell capacitor. When crossing an interface between two different dielectrics both the permittivity ε and the conductivity σ jump to another value. The difference in conductivity between the two dielectrics results in a change in current density. Because of the different current densities, charge accumulates at the interface (total current density is divergent). Furthermore, the difference in permittivity results in a difference in field strength E across the boundary according to equation:

$$E_{n2} = \frac{\varepsilon_1}{\varepsilon_2} E_{n1} \tag{2.2}$$

The difference in field strength then results in again a difference in current density and thus charge accumulates at the boundary. In general space charge accumulates at every boundary where the quotient $\frac{\varepsilon}{\sigma}$ changes.

3) **In presence of a temperature gradient**: The transport current density in the bulk material is temperature dependent. A temperature gradient in the material therefore causes a difference in transport current density leading to space charge accumulation. Therefore, space charge ρ is generated in the dielectric according to the equation:

$$\rho = J.\nabla(\frac{\varepsilon}{\sigma}) \tag{2.3}$$

This effect can also be explained by the fact that the conductivity is temperature dependent. The conductivity thus changes along the temperature gradient, and the quotient $\frac{\varepsilon}{\sigma}$ changes.

4) **Gross & morphological inhomogeneity**: Material inhomogeneity is found in most types of insulation materials. Many insulation materials contain fillers which have a different conductivity and permittivity than the host material resulting in a large amount of boundaries in the material. Space charge will accumulate at those boundaries. The conductivity of the amorphous parts is higher than the crystalline parts. Space charge will therefore accumulate at the boundaries between the crystalline and amorphous parts in polymers.

2.4 The microscopic viewpoint

In the microscopic view of space charge physics three different mechanisms are important: *trapping, injection and conduction of space charge*. **Trapping** is the fastening of charges at a fixed location in the insulation material, **injection** is the emission or extraction of charges at the electrodes and **conduction** is the transportation of charges through the bulk material.

An overview of this section necessitates knowledge about the atomic model proposed by Niels Bohr. At this point it is essential to mention the difference between insulators, semi-conductors and conductors. Their different behaviour can be explained by using the atom model of Niels Bohr. According to that, a number of electrons move in separate orbits around the nucleus of an atom. Not every orbit is possible; a limited number of orbits which are situated at discrete distances from the nucleus are available. An electron may leap from one orbit to another; it cannot move in between, every orbit represents a distinct energy level. Therefore, the conductivity of a material depends on the size of the band gap[79]. If this gap is large it is extremely improbable that an electron can pass the gap and add to the conductivity. The width of this gap is expressed in electron volts eV. A graphical representation is provided below for clearer comprehension of the above.The band gap for an insulator is larger than 2 eV, for a semi-conductor is between 0.2 and 1 eV and finally for a conductor is less than 0.2 eV.

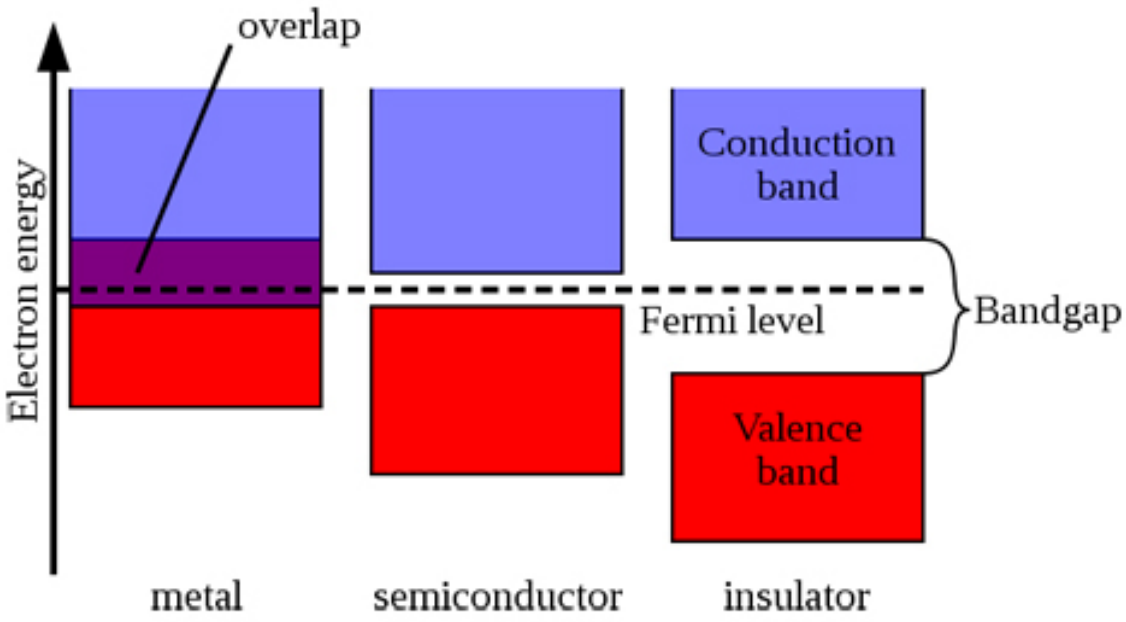

Figure 2.4.1: The energy-band model

2.4.1 Trapping of charge carriers

Impurity and defect states in insulators profoundly influence their electrical and optical properties[47,48]. This makes it possible to use these properties to obtain information about the nature of the states. The reason why space-charge forces play

a prominent role in the electrical properties of insulators as compared to, say, semiconductors at room temperature, is that these solids normally have a relatively low density of free carriers and consequently charge unbalance is easily produced by electrical fields[46,47]. Alteration of electric field distribution, increased stress at certain locations- may occur through the use of ohmic contacts which facilitate the direct injection of excess charge into the insulator. The character and magnitude of these effects is due largely to the presence of localized states which can trap and store charge in an equilibrium with the free, mobile charge[49]. The study of space charge-limited currents can therefore yield such information as the density, location-in-energy and capture cross sections of the trapping states.

Incompletely bound atoms at crystal defects give rise to dangling bonds which can be satisfied by either the removal or donation of an electron (or both) and thus behave as states within the band gap[23]. However, these energy states are not extended throughout the crystal, they only exist in the vicinity of chemical or structural defects (often in amorphous regions). Electrons and holes entering these localized states are therefore not available for conduction and may have to acquire considerable energy before they can leave[47]. These states are called traps. A trap for electrons is called acceptor and a trap for holes, donor. Donors have energy levels immediately above the top of the valence band and acceptors have energy levels immediately below the bottom of the conduction band. Furthermore, traps may take the form of sites where the field from an electron or hole can re-orient the local structure thereby creating a potential well from which escape may be difficult. The depth of a trap is defined as the energy that a charge carrier needs in order to be liberated. These are called self-traps.

Self-trapped charge is a form of space charge in which a region of an insulation contains localized charge of one polarity which is not compensated by an equal concentration of opposite polarity charge. This causes local field enhancement according to Poisson's equation.

$$\nabla E = \frac{\rho_c}{\varepsilon} \tag{2.4}$$

Where ρ_c is the charge density $(\frac{C}{m^3})$ and ε is the permittivity. Self-traps can be deep and keep charges for a considerable time, up to many hours or even days. Electrons can escape from localized states given sufficient energy and drift to other localized states under the influence of the local electric field.

The occurrence of chemical traps is related to the additives in polymers, which tend to concentrate in the amorphous regions. These additives consist of anti-oxidants which are added to the material to counteract thermal aging, residues of the chemical processes during production such as cross-linking by-products and finally, impurities which cannot be prevented in any material. Small differences in additives can have large effects in the number of traps, so that the ability to store space charge is greatly affected by the type and concentration of additives.

2.4.2 Injection & extraction of charge carriers

It is a direct consequence of the energy-band picture for an insulator that an ohmic contact furnishes a reservoir of free electrons which are injected into the insulator (upon gain of sufficient energy) in the region of the contact. A theoretical thermodynamic model, pertaining to the injection of electrons/holes from a metal to an insulator, across a metal-insulator interface is first briefly discussed. Care should be taken to note that charge injection behaviour across a metal-semicon-insulator interface (as in our work) may differ from the generalized model presented. A previous investigation[33] has revealed that semi-conductive materials seem to have a large influence on charge injection and removal at the electrodes. Therefore, this particular interface plays a major role in space charge injection/accumulation in the insulation bulk.

General model for charge injection across metal-insulator surfaces

This model is illustrated in Fig-2.4.2(A) which shows a simplified energy-band diagram for an insulator, with a discrete trap level, in ohmic contact with a metal in thermal and electrical equilibrium. When voltage is applied across the insulator, as shown in Fig-2.4.2(B), this reservoir will inject electrons into the bulk of the insulator. The metal, in turn, is tightly coupled

to the reservoir and readily replenishes it so long as the current is well below its saturation value for the particular contact at the given temperature[101]. The exact theory for charge injection from metal to an insulator, across an interface, is based on three equations—a current flow equation, Poisson's equation, and an equation of state relating the free-electron density to the trapped-electron density at the same position[101]. The sign conventions are provided as follows:

$$\mathbf{J} = -J\mathbf{x}, \mathbf{E} = E\mathbf{x}, E = \frac{dV}{dx} \tag{2.5}$$

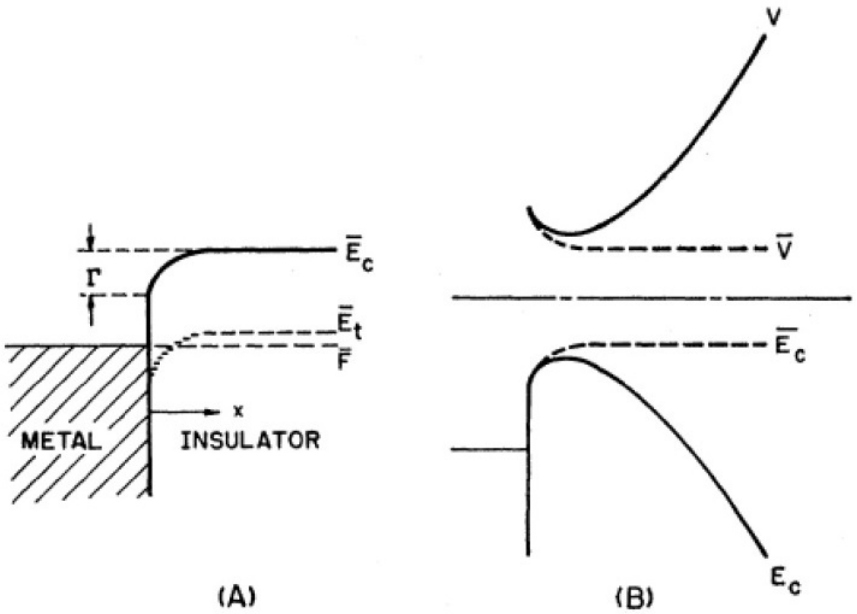

Figure 2.4.2: Charge trapping, injection for metal-insulator surfaces[101].

The equations are thus provided, keeping the sign conventions presented earlier in mind:

$$J = e\mu E - eD(\frac{dn}{dx}) = constant \tag{2.6}$$

$$\frac{\varepsilon}{e}\frac{dE}{dx} = (n - n_o) + (n_t - n_x) \tag{2.7}$$

Wherein, n_o and n_x are in thermal equilibrium.

Also, $\mathbf{J}$ is the current density, J=$|\mathbf{J}|$, $\mathbf{E}$ is the electric field intensity; E=$|\mathbf{E}|$, e is the magnitude of the electronic charge; μ is the electronic mobility; D is the diffusion constant for electrons; ε is the static dielectric constant of the insulator; n and n_t are the densities of free and trapped electrons, respectively; they are functions of position x; n_o and n_x are the values of n and n_t, respectively, in the bulk neutral crystal in thermal and electrical equilibrium (no applied voltage). Fig-2.4.2(A) depicts the contact in thermal and electrical equilibrium. Fig-2.4.2(B) depicts the contact in steady state under an applied voltage. V is the electric potential, E_c the total free-carrier energy. The corresponding thermodynamic equilibrium quantities, V_o and E_{co} are indicated.

The conduction and the emission of charges in epoxy are mainly performed by electrons. Injection of electrons at the cathode and extraction of electrons at the anode are the main mechanisms for the emission of charges in epoxy. In order for a charge to leave the metal and enter the insulation, a potential barrier has to be passed. The height of this barrier depends on the interface properties. The required energy for electrons to cross this 'potential barrier' is given by the equation:

$$W = \Phi - X \tag{2.8}$$

Where Φ is the work function of the metal and X is the electron affinity of the insulator. Two main processes of charge injection are considered. The first one is the Schottky injection and the other one is the Fowler-Nordheim injection.[76] The Schottky process is valid for "low" fields up to 100 $\frac{kV}{mm}$. Due to the applied electric field the potential barrier is reduced and an electron can travel across the barrier. The Schottky injection current density depends on temperature T and electric field E, according to the equation provided below:

$$J = AT^2 exp[-\frac{\Phi - e\sqrt{\frac{eE}{4\pi\varepsilon_o\varepsilon_r}}}{kT}] \tag{2.9}$$

Where, A is a constant, T is the temperature and Φ is the total barrier height.
On the other hand, the Fowler – Nordheim injection is valid for "high" fields above 100 $\frac{kV}{mm}$. In this case the barrier becomes very thin, less than 1 nm at 1000 $\frac{kV}{mm}$. Therefore, electrons can pass through narrow potential barriers despite having insufficient energy to surmount them, this is known as tunnelling. The injection current density, according to the equation provided below, depends strongly on electric field E and there is no or small temperature dependence.

$$J = BE^2 exp[\frac{-C\Phi^{\frac{3}{2}}}{E}] \tag{2.10}$$

Where, B and C are constants and $\varphi = \Phi - E_f$.

2.4.3 Conduction of charge carriers

Conduction occurs when charge carriers move in response to an electric field. However, in many dielectrics charge carriers spend most of their time in traps and they cannot move even if an electric field is applied. Between traps, the travel velocity of electrons is approximately 10^5 $\frac{m}{s}$[47]. For "*shallow*" traps, the trapping time is short. A "*shallow*" trap has a lower potential well value, and hence the electron can escape this sort of trap quite easily. In traps of 1 eV depth, electrons can spend more than an hour. The mobility of these electrons is effectively reduced by the traps. This is called trap-limited mobility or trap-limited conduction. However, conduction in the band gap by this method is very slow since carriers spend most of their time in traps and very little travelling between them (trap-limited conduction). If an insulator already contains charge, then it is likely to be deeply trapped. This is known as space charge and can result in the increase of the mobility of other charges.

The Poole-Frenkel mechanism

In solid-state physics, the Poole–Frenkel effect (also known as Frenkel-Poole emission) is a means by which an electrical insulator can conduct electricity. It is named after Yakov Frenkel, who published on it in 1938 and also after H. H. Poole (Horace Hewitt Poole, 1886-1962), Ireland. Electrons can move (slowly) through an insulator by the following method. The electrons are generally trapped in localized states (loosely speaking, they are *"stuck"* to a single atom, and not free to move around the crystal). Occasionally, random thermal fluctuations will give that electron enough energy to get out of its localized state, and move to the conduction band. Once there, the electron can move through the crystal, for a brief amount of time, before relaxing into another localized state (in other words, *"sticking"* to a different atom). The Poole–Frenkel effect describes how, in a large electric field, the electron doesn't need as much thermal energy to get into the conduction band (because part of this energy comes from being pulled by the electric field), so it does not need as large a thermal fluctuation and will be able to move more frequently. In this case, barriers which are localizing carriers within the dielectric are lowered

by the applied electric field in contrast to the Schottky effect where the electrode-insulator barrier is lowered. As a result there is an increase in the conduction. The conduction current density is given by the equation provided below:

$$J = \sigma_o E * exp[-\frac{e\Phi - \beta\sqrt{E}}{2kT}] \tag{2.11}$$

The resonance tunnelling mechanism

A quantum well, in the general use of this term, is a potential structure which spatially confines the electron[68]. According to quantum mechanics, an electron subjected to potential confinement has its energy quantized and a discrete energy spectrum would be expected for the electron system[79]. However, the electron remains free to move in the perpendicular direction. This results in the creation of a two-dimensional electron gas of quasi-bound states. Resonant tunnelling refers to tunnelling in which the electron transmission coefficient through a structure is sharply peaked about certain energies. The emergence of these peaks can be qualitatively explained by introducing infinite walls as boundary conditions. It is usually possible to do this far from the quantum well itself. Then the calculation of the quantized energy levels in a quantum well of arbitrary shape is the solution of an eigenvalue problem. For electrons with an energy corresponding approximately to the virtual resonant energy level of the quantum well, the transmission coefficient is close to unity. That is, an electron with this resonant energy can cross the double barrier without being reflected. This resonance phenomenon is similar to that taking place in the optical Fabry-Perot resonator or in a microwave capacitive-coupled transmission-line resonator. Conduction mainly takes place in the amorphous regions of polymeric materials where defects occur in the crystal structure. In order for the conduction of the amorphous parts of the molecular chains to be explained, the theory of hopping is devised. There are many dislocations in the chain, where an electron can be trapped. The potential barrier between two traps is so high that an electron cannot pass this barrier. However, from the point of view of quantum mechanics, the position of an electron can also be regarded as the probability that an electron is located on the other side of the barrier. This probability depends on the distance between traps. As this distance is small, the probability differs from zero, so that an electron can sometimes appear on the other side of the barrier. A pure tunnelling process is only valid at zero Kelvin temperature, because at higher temperatures the exponential reduction of the electron wave function with distance limits the range over which it can be effective and also the principle of energy conservation restricts the participating sites to similar energy levels. Hence, thermally assisted tunnelling occurs from site to site. According to that, thermal promotion at one site raises the electron to a level which is similarly energetic with that of an empty neighbouring site. Tunnelling between the two sites is allowed at this energy level and there will be a finite probability that the electron resides at the previously empty site.

2.4.4 Space charge limited conduction

A power law dependence of the current density J on the electric field E has been found for electrical conduction in insulating polymers. This statement is described in mathematical terms as provided below:

$$J = aE^n \tag{2.12}$$

Different values of n characterize various conduction mechanisms. n=1 signifies the case of Ohmic conduction and carrier concentration & mobility are field independent. Space charge limited conduction SCLC occurs when the conduction is the result of the injection of excess carriers from an Ohmic contact into a material of very low mobility. In case that traps are present in the dielectric, some of the carriers become trapped and do not contribute to the conduction. A graphical representation of the logarithmic plot of limiting current density **J** versus voltage **V** characteristics for space charge limited currents in an insulator with traps is presented below.

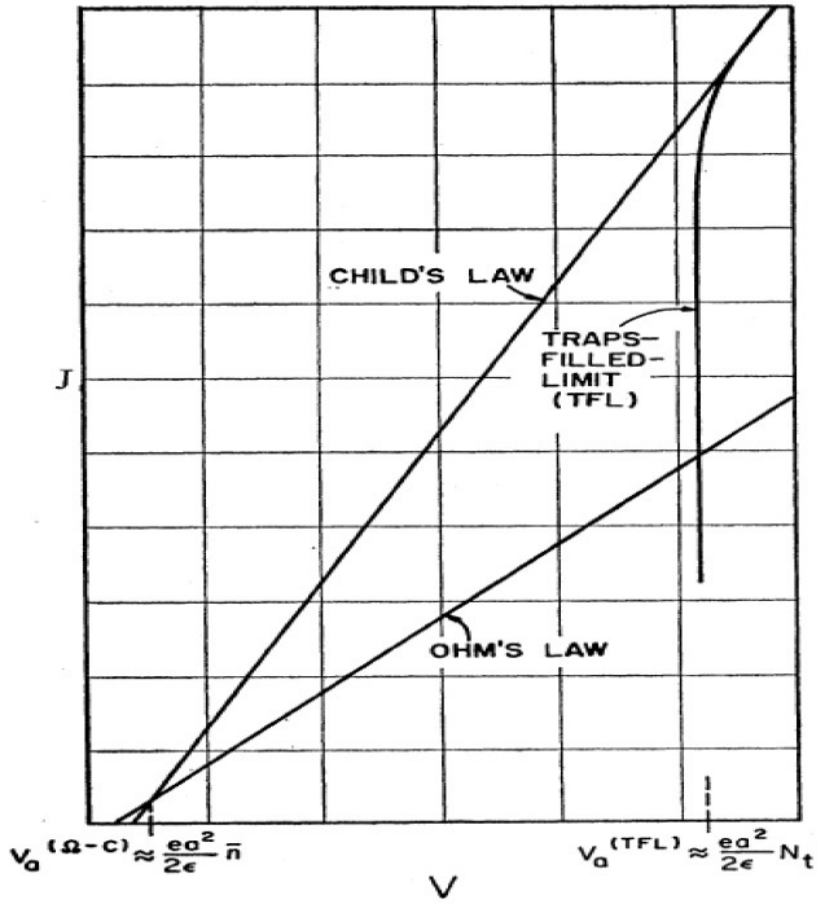

Figure 2.4.3: Log-log plot of current density J vs. voltage V[101].

At a sufficiently high voltage the charge carrier number density being injected is approximately equal to the number density of traps[101]. In this case the traps are considered as deep. When all the traps are filled the so-called trap-filled limit is reached and the number of electrons available for conduction increases which results in the rapid raise of the current density. The SCLC current density is given by the equation provided below:

$$J = \frac{9}{8} * \frac{\varepsilon \mu V^2}{L^3} \tag{2.13}$$

Where ε is the relative permittivity, μ is the carrier mobility, V the applied voltage and L is the sample thickness.

2.5 Trapped space charge accumulation threshold

The starting point of our measurements is the fact that that it is often possible to define a critical field separating an ohmic type of conduction from a non-linear regime in the current-voltage characteristic of solid dielectrics. In the SCLC theory

[34,44] this critical field corresponds to the start of space charge accumulation. There are techniques to detect this threshold field via conduction current measurements, space charge measurements and electroluminescence measurements. The presence of space charge modifies the internal field distribution in a dielectric. In a parallel plate configuration the electric field is uniform when the total space charge is zero. A linear relationship exists between the current and the applied voltage (Ohmic behaviour). In this case, the charge contributed by the mobile carriers is compensated by an equal amount of counter charge, and the net charge density is zero. An increase in the voltage causes the accumulation of some amount of space charge (both mobile and trapped), so that a non-linear relationship is established between current and voltage. In order to evaluate the charge injection capabilities of different electrodes, an electrical threshold for the inception of space charge accumulation in a given situation is determined by plotting the logarithm of average space charge density, an equivalent to the integration of the space charge density within the specimen divided by its thickness, against the logarithm of the applied field. A life model which describes the mechanism of insulation degradation due to the presence of space charges, is based on the assumption that even if the applied electric field is not large enough to inject hot electrons which are able to break inter or intra-molecular bonds, the trapped charges are responsible for local storage of electromechanical and electrostatic energy which may favour degradation reactions via a process of lowering an activation energy barrier. This occurs above a level of electric field, which changes with material used, and it is called **threshold for trapped space charge accumulation**. It has been proposed in literature [34] that the threshold for electrical aging under DC field may be close to the threshold above which space charge becomes trapped in the insulation. This lends great importance to the investigation of the threshold as a '*safe operating limit*' for the material under consideration. Therefore, the meaning and investigation of such a threshold can acquire fundamental importance in electrical insulation characterization, since working at electric stresses below the threshold means some degree of safety with regard to electrical aging(via this phenomenon) and thus high reliability in service, provided that there are no other significant stresses acting on the insulation.
In this research work, the PEA method has been used extensively to determine the space charge concentration along the insulation thickness. The determination of the electrical threshold requires an electric field E- average space charge density ρ characteristic, in order to single out the electric field above which space charges become steadily and noticeably resident in insulation and increase with field. Therefore, measurements at different voltage levels are required.

2.6 Dielectric polarization

Materials can be broadly divided into three categories: conductors, semi-conductors and insulators. Free charges in a conductor will respond to exactly cancel out an applied field. The charges in an insulator will respond to an applied field in such a way as to partially cancel an applied electric field. The situation in an insulator is more complicated, however, since a molecule in the insulator will also experience a field due to the response of the insulator. There is a reaction field due to the response of the medium to charges on the molecule and there is a local field due to polarization of the material in the applied field. These issues are important for relating the molecular polarizability to the bulk polarization. Dielectric polarization occurs when a dipole moment is formed in an insulating material because of an externally applied electric field. When a current interacts with a dielectric (insulating) material, the dielectric material will respond with a shift in charge distribution with the positive charges aligning with the electric field and the negative charges aligning against it. A diagrammatic representation is shown below.

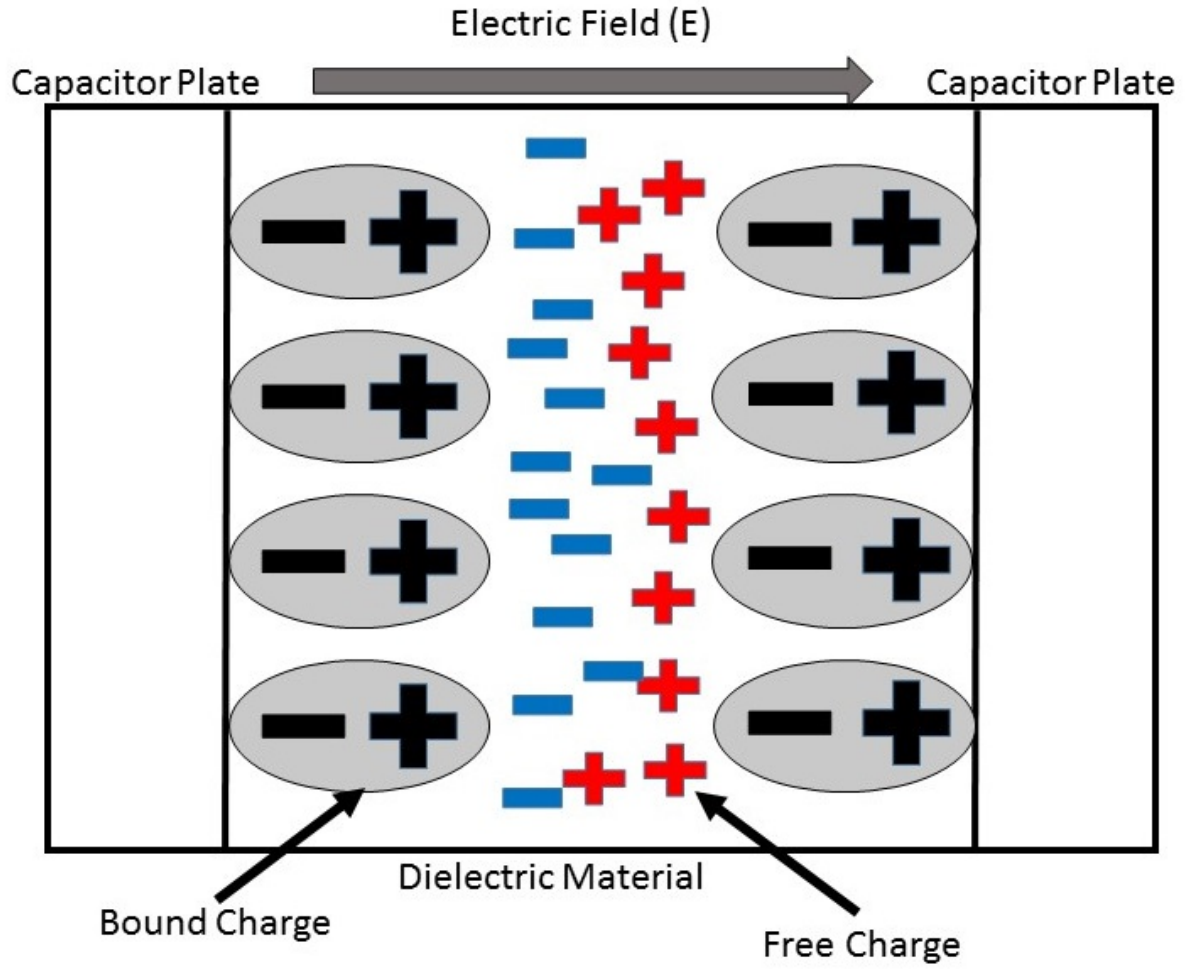

Figure 2.6.1: The phenomenon of dielectric polarization, in a parallel-plate capacitor

As soon as a dielectric is exposed to an electric field (generated by a voltage across electrodes embedded in the insulation), the positive and negative charges become oriented and form different kind of dipoles even on atomic scales. A local charge imbalance is thus induced within the neutral species as the centres of gravity for the equal amounts of positive and negative charges q become separated by a finite distance d, thus creating a dipole with a dipole moment, given by $\overrightarrow{p} = q\,\overrightarrow{d}$. Due to chemical interactions between dissimilar atoms forming molecules, many molecules will have a stable distance d between the charge centres, thus forming permanent dipoles, which are usually randomly oriented and distributed within the material, as long as no external field is applied. To explain how the dielectric constant relates to the electronic polarizability of a material, the polarization or P of a material should be determined. The polarization of a material is defined as the total dipole moment per unit volume, and its equation is, as given below:

$$P = Na_eE = X_e\varepsilon_oE \tag{2.14}$$

The X term is known as the electric susceptibility of the material given by the equation $X = \varepsilon_r - 1$. Then, from substituting $\varepsilon_r - 1$ for X, an equation relating the relative permittivity and the electronic polarizability is determined, by the equation as provided below:

$$\varepsilon_r = 1 + \frac{N\varepsilon_e}{\varepsilon_o} \tag{2.15}$$

Where N is the number of molecules per unit volume. While this equation does relate the dielectric constant with the electronic polarizability, it only represents the material as a whole, and does not take into effect the local field, or the field experienced by a molecule in a dielectric. This field is known as the Lorentz field, and the equation to define this is provided

below:

$$E_{loc} = E + \frac{P}{3\varepsilon_0} \tag{2.16}$$

By substituting this value back for the field used in the previous method, the following equation is determined, as provided by the equation below:

$$\frac{\varepsilon_r - 1}{\varepsilon_r + 2} = \frac{Na_e}{3\varepsilon_0} \tag{2.17}$$

This equation is known as the Clausius-Mossotti equation and is the way to interchange between the microscopic property of electronic permittivity and the dielectric constant. In addition to knowing the electronic polarizability of a material, there are also other sub-factors, such as chemical composition and bond type that determine the total dielectric behaviour of a material. However, electronic polarization is always inherent in a dielectric material. Polarization arises from a finite displacement of charges in a steady electric field and this is to be contrasted with the complementary physical phenomenon of electrical conduction which arises from a finite average velocity of motion of charges in a steady electric field.
Dipoles are polarizing species which are incapable of leading to a continuing conduction current in a static electric field, since the charges in question cannot be completely separated or dissociated under normal conditions. A dipole could only become dissociated in a field that would be sufficiently large to break the strong bonding forces of the neutral dipolar molecule and this is not normally possible in solids and liquids where various forms of electrical breakdown take place at much lower fields. The main mechanisms that produce macroscopic polarization are listed below:

- **Electronic polarization**: A slight relative shift of positive and negative electric charge in opposite directions within an insulator, or dielectric, induced by an external electric field. Polarization occurs when an electric field distorts the negative cloud of electrons around positive atomic nuclei in a direction opposite the field. This slight separation of charge makes one side of the atom somewhat positive and the opposite side somewhat negative. In some materials whose molecules are permanently polarized by chemical forces, such as water molecules, some of the polarization is caused by molecules rotating into the same alignment under the influence of the electric field. One of the measures of polarization is electric dipole moment, which equals the distance between the slightly shifted centres of positive and negative charge multiplied by the amount of one of the charges. This effect is extremely fast and thus, effective up to optical frequencies.

- **Ionic polarization**: Ionic polarization is a mechanism that contributes to the relative permittivity of a material. This type of polarization typically occurs in ionic crystal elements such as NaCl, KCl, and LiBr. There is no net polarization inside these materials in the absence of an external electric field because the dipole moments of the negative ions are cancelled out with the positive ions. However, when an external field is applied, the ions become displaced, which leads to an induced polarization. The positive charges will flow with the field and the negative charges will flow against the field, causing a net average dipole moment per ion to form. A process which is effective up to infrared frequencies.

- **Orientational Polarization**: Orientational polarization arises when there is a permanent dipole moment in the material. Materials such as HCl and H_2O will have a net permanent dipole moment because the charge distributions of these molecules are skewed. For example, in a molecule of HCl, the chlorine atom will be negatively charged and the hydrogen atoms will be positively charged causing the molecule to be dipolar. The dipolar nature of the molecule should cause a dipole moment in the material, however, in the absence of an electric field, the dipole moment is cancelled out by thermal agitation resulting in a net zero dipole moment per molecule. When an electric field is applied however, the molecule will begin to rotate in order to align the molecule with the field, causing a net average dipole moment per molecule. Under the influence of an electric field the dipoles will be oriented only partially, so again, a linear dependence of polarization and electric field exists. An effect which is effective up to infrared frequencies. Unlike electronic polarizability and ionic polarizability, orientational polarizability is temperature dependent. This is an important factor to consider when choosing a dielectric material for electronic and optical applications.

- **Interfacial polarization**: Interfacial or space charge polarization occurs when there is an accumulation of charge at an interface between two materials or between two regions within a material because of an external field. This

can occur when there is a compound dielectric, or when there are two electrodes connected to a dielectric material. This type of electric polarization is different from orientational and ionic polarization because instead of affecting bound positive and negative charges i.e. ionic and covalent bonded structures, interfacial polarization also affects free charges as well. As a result interfacial polarization is usually observed in amorphous or polycrystalline solids. The electric field will cause a charge imbalance because of the dielectric material's insulating properties. However, the mobile charges in the dielectric will migrate over maintain charge neutrality. This then causes interfacial polarization. This phenomenon is often very 'slow' and generally active in the power frequency range and below.

- **Space charge accumulation**: Presence of trapped charge polarizes the surrounding medium. A very slow process, which takes place below the power frequency.

2.7 Dielectric properties of epoxy resin

Dielectric, by definition, means any insulating medium which intervenes between two conductors. In simple terms, it suggests the absence of conduction and describes materials which are not electrical conductors. Dielectric materials can be used for making capacitors, providing an insulating barrier between two conductors (as in cross over and multi-layered circuits) and for encapsulating circuits. Dielectric properties, specifically for epoxy adhesives, refer to the electrical properties of a material.
There are four dielectric properties typically associated with epoxy products: VR (Volume Resistivity), Dk (Dielectric Constant), Df (Dissipation factor) and dielectric strength. For epoxies, some general guidelines are presented herein:

- Volume Resistivity (VR) is defined as the measured electrical resistance through a material when a voltage is applied for a specific amount of time. For an insulative product, it is generally greater than or equal to 0.1 teraohm-meter at 25 degrees Celsius and greater than or equal to 1.0 megaohm-meter at 125 degrees Celsius, according to ASTM D257, for an insulative product.
- Dielectric Constant (Dk) is defined as a material's ability to store a charge when used as a capacitor dielectric. It is usually less than or equal to 6.0 at both 1 kHz and 1 MHz, according to ASTM D150, and is a unit less value because it is measured in ratios.
- Dissipation Factor (Df) (also called loss factor or dielectric loss) is defined as the power dissipated by a dielectric, generally less than or equal to 0.03 at 1 kHz and less than or equal to 0.05 at 1 MHz, according to ASTM D150.
- Dielectric Strength (sometimes referred to as breakdown voltage) is the maximum electric field a material can withstand before breaking down. It is an important property for many applications that will be running a high current or amperage. ***As a general rule-of-thumb, the dielectric strength of an epoxy is roughly 500 volts per*** $2.54 * 10^{-5}$ ***metre at 23 degrees Celsius for an insulating product.***

2.8 Polymer Nanocomposites

Polymer nanoscience is the study and application of nanoscience to polymer-nanoparticle matrices, where nanoparticles are those with at least one dimension of less than 100 nm[20]. PNC consist of a polymer or copolymer having nanoparticles or nanofillers dispersed in the polymer matrix. The dispersion of inorganic nanometric size additives in polymers can improve their electrical, mechanical & thermal properties[72,73]. When particles of nanometric size are introduced in a polymer matrix, an interfacial region is assumed to be formed around each particle. These interfacial regions, which seem to interact, play a dominant role in the improved dielectric properties that the polymer nanocomposites might exhibit[7,19,20,22]. The size of the particle is of prime importance as well, since the surface area-to-volume ratio increases as the particles get smaller. This leads to an increasing dominance of the behaviour of atoms on the surface area of particle over that of those interior of the particle. This affects the properties of the particles when they are reacting with other particles. Because of

the larger surface area possessed by the nanoparticles, the interaction with the other particles within the mixture is more and this affects barrier properties, flammability resistance, electrical/electronic properties, membrane properties, polymer blend compatibilization.

2.8.1 The vitality of physical interfaces

The *'interface'* is often defined as:

- A surface forming a common boundary of two bodies, spaces, or phases (an oil-water interface).
- The place at which independent and often unrelated systems meet and act on or communicate with each other (the man-machine interface)[102].

The properties of the interface are not well defined. The heterogeneity at the contact may lead to local charge concentrations and non-uniform electric fields. The altered properties of nanocomposites are due to the behavior of the interfacial interaction zone which surrounds the nanoparticles. The characteristics of the interfacial interaction zone are the following: 1) mobility, which depends on the physico-chemical bonds created on the common surface, and 2) formation at the interface of a layer/layers, which may affect the local conductivity. The effect of these two mechanisms is due to the considerable increase of the interfacial surface area[6]. Moreover, the Maxwell-Wagner polarization is not so evident in the case of the nanocomposites, as it is with conventional polymers. This is because of the size of the nanoparticles, which as they become too small, they do not present the Maxwell-Wagner polarization. Maxwell-Wagner polarization changes significantly as the dimensions of inserted particles approach the length of polymer chain [25]. With the addition of nanoparticles in a base polymer, the aforementioned mobility and the structure of the surrounding polymer change considerably. The nanoparticles have a large surface area and this is the reason as to why the interaction zones in a nanocomposite are much larger than in a conventional polymer or in a polymer containing microparticles. In [1], it is proposed that around the nanoparticles a Stern layer and a diffuse double layer (layer Gouy-Chapman) are formed, which have a high conductivity in opposition to the low conductivity of the surrounding material. Charge movement through these layers is relatively easy [3]. In this way, a current flow is possible between the nanoparticles. In another paper [26], it was noted that the significant interfacial polarization in conventional polymers is mitigated in nanocomposites, where a short-range highly immobilized layer develops near the surface of the nanoparticle. This layer affects a much larger region surrounding the nanoparticle in which conformational behavior and chain kinetics are greatly altered.
Thus, in summary we can state that physical interfaces indeed play a very significant role. Interfacial characteristics are not only determined by the size-induced properties, but also the surface chemistry of the particles. Two main features proving the *vitality* of interfaces can thus be enumerated:

- **The mobility ascribed to the physical and chemical bonding occurring at the interface.**
- **The electrical activity in the interfacial region which can influence local conductivity.**

The impact of both of these mechanisms relies on the substantial increase in the interface area which is characteristic of nanocomposites[6,9]. There is still a lot to be definitively stated for the role of physical interfaces- and much to discover.

2.8.2 Charge behaviour of nanocomposites & popular theoretical models

Various models and theoretical constructs for describing nanocomposites have been introduced in recent years. Most of them emphasize upon the interface formed between nanoparticle and host material. The nanometric interfaces and their dielectric and conductive properties were firstly pointed out by Lewis in 1994[1]. When particles are embedded in a polymer matrix, a layer, consisting of immobilized polymer, is formed around each particle. The local chain conformation and the chain kinetics of these layers are changed[26]. In the context of incorporation of nano-sized fillers in polymer matrices, it is thought that fundamental to controlling the dielectric strength of insulating polymers is the cohesive energy [23] density and the associated free volume [23] of a polymer structure.

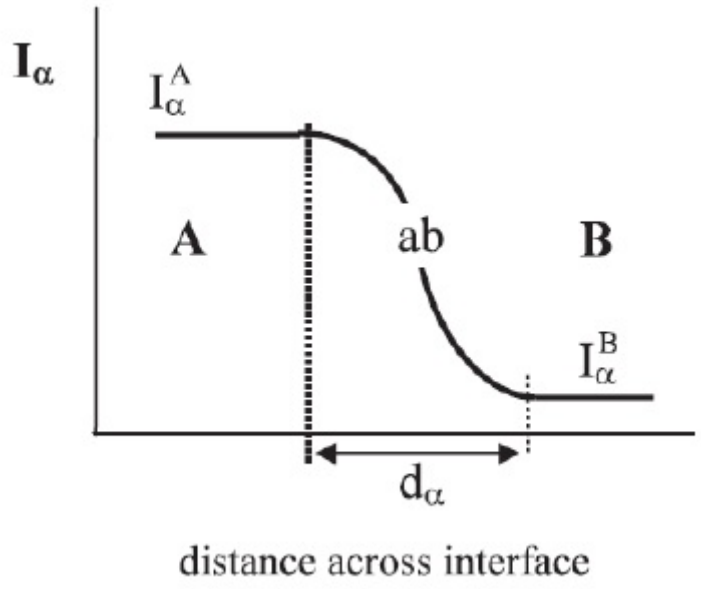

Figure 2.8.1: The interface ab between two phases A and B, and change of chosen material property[1,55].

Why do nanoparticles inserted into conventional polymers alter the various properties of nanocomposites? The improvement may be due to the interfaces present because of the numerous nanoparticles, or the reorganization of polymer chain morphology, or modifications in polymer chain kinetics, even the possible alteration of trap and energy band structure. It is most certain that what is valid in conventional physics, is not necessarily valid for nanocomposites. Some of the most interesting models that have been developed with respect to the interpretation of the interaction between a polymer and nanofiller in nanocomposites are the following:

- **Lewis' model**: In 1994, Lewis highlighted the importance of interfaces with nanometric thickness, considering interfaces as areas with altered electrochemical and electromechanical behavior[1]. Lewis' suggestion is based on the basic idea that the intensity I_a of a material property a does not change abruptly, but gradually changes over some nanometers, across the interface.(Figure-2.8.1 refers to this phenomenon) The intensity a can be any physical or chemical property. (Examples include the free electron concentration at a hot metal surface in vacuum, the normal electric field at a metal-n-type semiconductor contact.) A nanoparticle can become charged, when embedded in a matrix with different dielectric properties. The surrounding matrix responds by developing a counter charge in order to compensate the charge of the nanoparticle. This can be achieved either by the reorganization process of electrochemistry (i.e., the polarization of the material that surrounds the nanoparticle), or by the establishment of layers around the nanoparticle, if the surrounding matrix contains mobile ions[73]. Lewis suggested that 2 layers with different electrical properties are formed around each nanoparticle, namely a Stern layer & a diffuse Gouy-Chapman layer. The first layer of ions is the Stern or Helmholtz double layer, which is formed on the nanoparticle surface. A second layer, the diffuse electrical double layer, is created around the first one, by a distribution of positive and negative ions. This layer determines the dielectric properties of the nanocomposite, since it changes the internal charge activity.

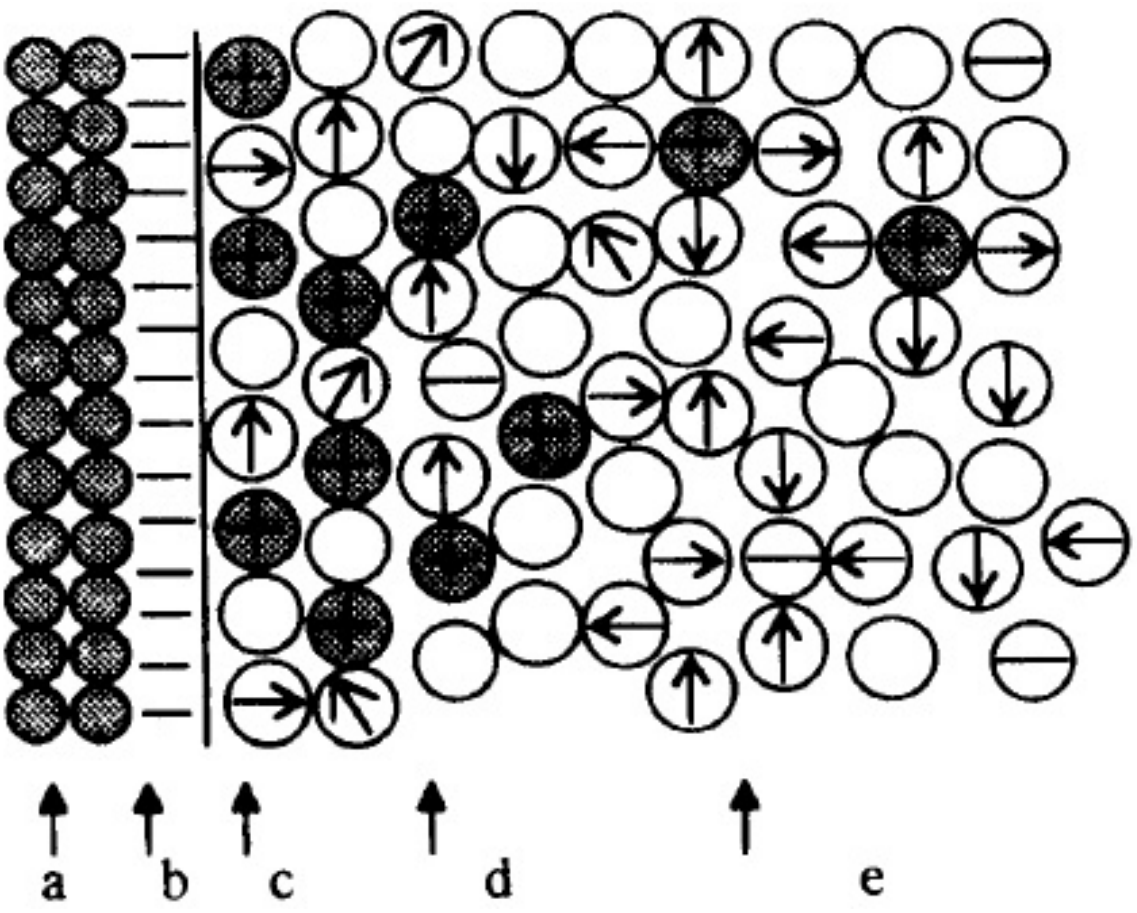

Figure 2.8.2: Electrical situation at a metal electrode-dielectric interface, the 2 electrical layers[1].

A metal electrode-dielectric interface showing (a), positive metal cores; (b), the outer electron cloud of the metal; (c), the structured inner Helmholtz layer of molecules and ions; (d), the outer Helmholtz layer and (e), the Gouy-Chapman diffuse space charge layer. In this illustration the net charge in the dielectric (-q) is shown as positive and the image charge in the metal (q) is negative. The Lewis model serves as visualisation of the impact of nanoscale fillers on macroscopic material.

- **Tsagaropoulos' model**: The nanoparticles incorporation in a polymer creates interactions between the nanoparticles and the polymer chains, which are located in the nanoparticles vicinity. These interactions cause regions with restricted chain mobility around the nanoparticles, and these restricted mobility regions can have their own glass-transition temperature[62,73].(T_g) The glass transition temperature (T_g) is one of the most important properties of any epoxy and is the temperature region where the polymer transitions from a hard, glassy material to a soft, rubbery material. However, this model does not specifically focus on space charge accumulation behaviour for nanocomposites.

- **The Tanaka model**: The multi-core model proposed by Tanaka[15] is one that extends the idea of an electrical double layer model further, by assuming that when a spherical inorganic nanoparticle is embedded in a polymer matrix, three layers are formed around it, as far as the chemical aspect is concerned. These three layers are the:

  - The bonded first layer which consists of molecules, forming a layer of 1 nm thickness. These molecules are physically bound to the particle surface by coupling agents, and the layer is formed by covalent, van der Waals or hydrogen bonds.
  - The bound second layer consisting of strongly bonded polymer chains which also interact with the first layer. Due to the strong interactions, the structure of the polymer is changed in this region, because chains/parts of

chains are aligning perpendicular to the particle surface. Therefore this layer influences the chain mobility, and is assumed between 2 and 9 nm in thickness.

– The loose third layer that interacts with the bound second layer, consists of polymer chains that see morphological changes due to the filler material. These changes can materialize in changes of chain formation, chain mobility, free volume or crystallinity. This layer can be several tens of nm thick.[55]

This model explains some properties related to nanocomposites like free volume, permittivity, loss tan δ, low field conduction, high field conduction, space charge, thermally simulated current, electroluminescence, photoluminescence, dielectric breakdown strength, partial discharge resistance, glass transition temperature, thermal conductivity, carrier trapping and treeing phenomena.

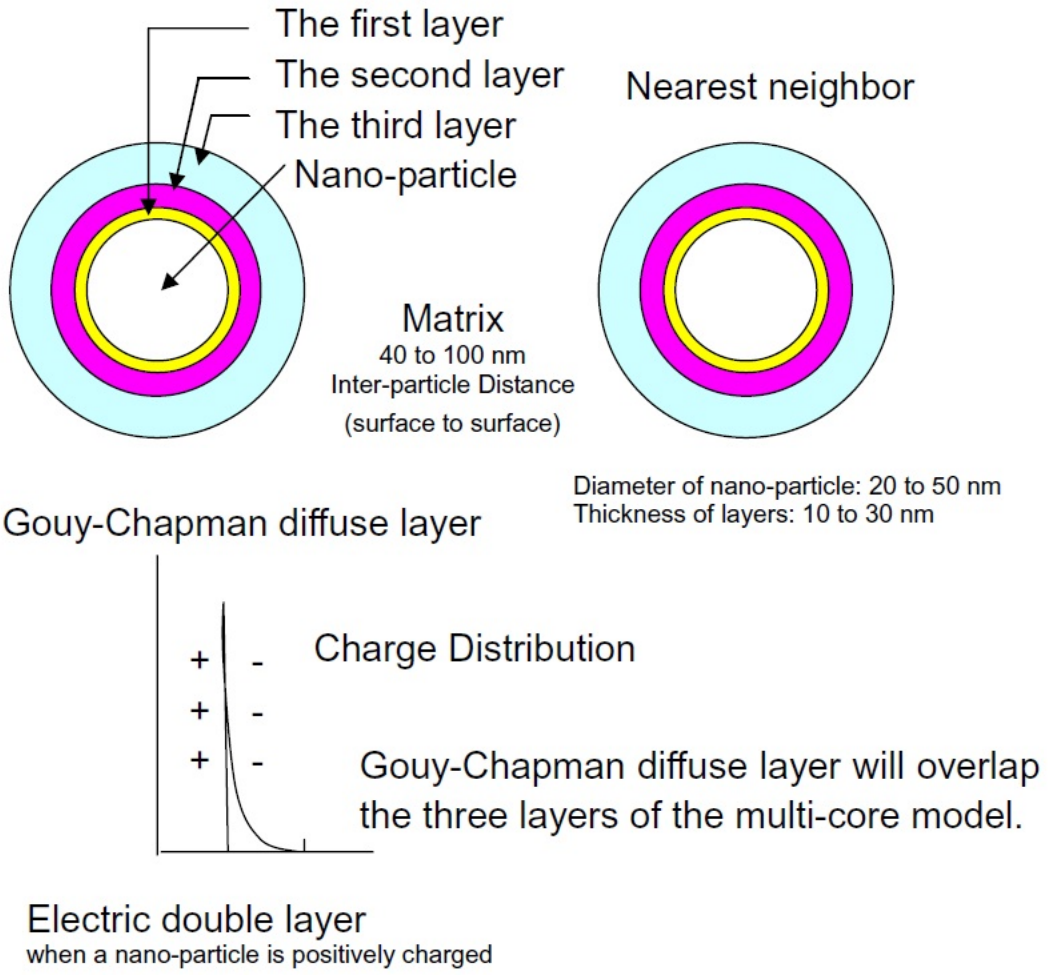

Figure 2.8.3: Multi core model for nano-particle and polymer interfaces(Tanaka)

- **The Polymer Chain Alignment Model(PCAM)**: It has already been previously suggested by the various PNC models that the surface area, thus interfaces between host material and filler particle, have a profound effect on the intrinsic and functional properties of a nanocomposite. The PCAM assumes that surface functionalized nanoparticles can lead to an alignment of polymer chains[55]. This chain alignment in combination with the filler material leads to a restructuring of the host polymer[55]. The space charge behaviour in PNC depends on the particle distribution and filler material. It has been suggested by the PCAM that with an even distribution of surface modified nanoparticles, the nanoparticles may act as recombination centres[55].

Thus, these are some of the popular theoretical constructs for describing nanocomposites and their behavioural properties.

2.9 Space charge analysis parameters

The space charge analysis parameters applicable for this research work are listed below:

- Amount of space charge accumulated in specimen (if any)
- Charge distribution in specimen, whether interfacial region (the regions close to the injecting electrode) accumulation or bulk accumulation
- Charge mobility, in a qualitative fashion
- Depletion rate of space charge accumulated (if any)
- Average space charge density
- Evaluation of electrical threshold fields for space charge accumulation

The next chapter deals with the experimental methods used in this research work, to characterize the specimens.

The strongest arguments prove nothing so long as the conclusions are not verified by experience. Experimental science is the queen of sciences and the goal of all speculation.

Roger Bacon

3 Experimental procedures

3.1 Experimental techniques adopted

As befits an experimental research work, in this section an overview is taken upon the experimental methods used to obtain the space charge distributions for the nano-filler added samples. There are several techniques to measure the space charge distribution inside dielectrics. In this work the pulsed electroacoustic method (PEA) is used for the space charge measurements.

3.2 An introduction to test specimens

Samples were 50 mm in diameter and ranged in thickness between 0.4 and 0.6 mm. These plaques are circular. The hBN nanofillers measure about 70 nm in average particle size, and are present in the samples with a volume% of 0.2%, 0.5%, 0.6%, 1% and 5%. Wherein multiple instances of a filler concentration is present, therein method of production of the plaque samples differ. They are diagrammatically presented in Figure-3.1.1.
These specimens were produced by 3 different synthesis techniques, and subdivided into batches, according to filler content. Knowledge of techniques used in production was not made available *a priori*, so as to retain objectivity in classification of the samples according to space charge behavioural patterns.
In Figure-3.2.1, the specimens are arranged in order of increasing filler content, starting from neat epoxy. In the case of multiple instances of samples belonging to the same filler grade group (for example, the 3 specimens belonging to the 0.2 volume% fill grade), they are arranged under a single header.

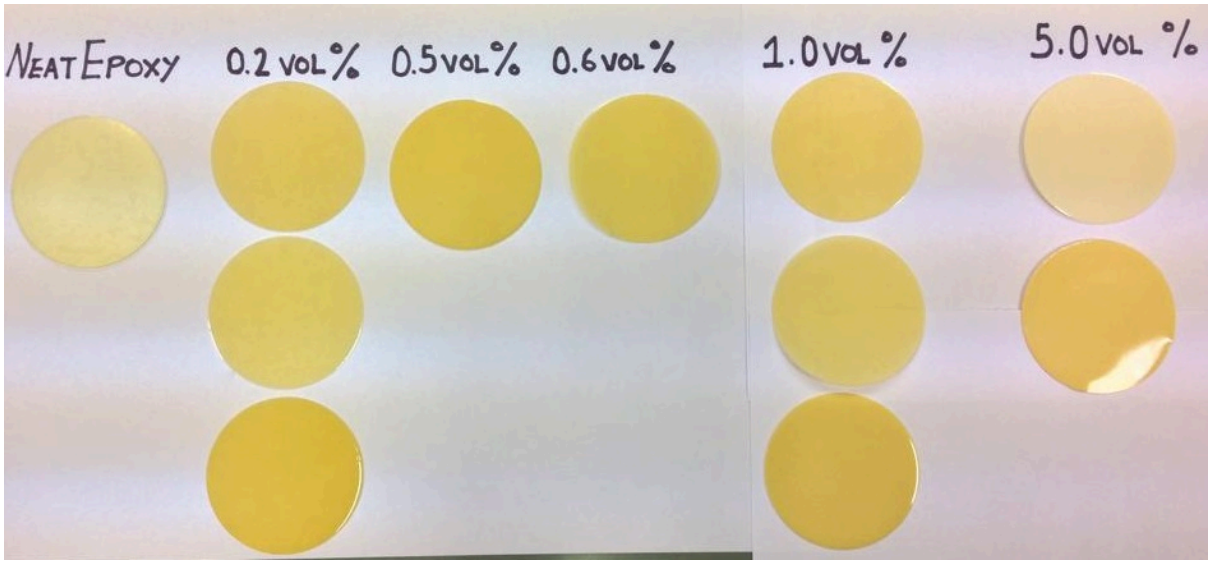

Figure 3.2.1: All test specimens, arranged by increasing fill grade.

3.3 Space charge measurements

There are several techniques to measure the space charge distribution inside dielectrics. They are namely, the Piezoelectric Induced Pressure Wave Propagation (PIPWP) method, Laser Induced Pressure Propagation (LIPP) method, Thermal Step Method (TSM), TPM (Thermal Pulse Method), LIM (Laser Intensity Modulation) method, EBM (Electron Beam Method). In this work the pulsed electroacoustic method (PEA) is used for the space charge measurements. Space charge inside an insulator distorts the electric field and can cause significant field enhancements. Therefore, the magnitude and location of the space charge in a dielectric is a matter of major importance. In earlier days, destructive methods to measure space charge were used such as field mills and capacitive probes. These methods are, in fact, surface charge measurements as the test object has to be cut into slices in order to arrive at the site of the charge. The disadvantage of destroying the sample has been overcome by the use of a new generation of space charge measurement methods.

All these methods use a common principle. An externally applied physical quantity interacts with the charge inside the sample. The charge in its turn interacts with, or generates a second physical quantity that can be externally measured. The physical quantities differ per method and they can be pressure, temperature, electric voltage or current. Nowadays, pulsed methods are widely used and the most popular method used to determine the charge profile in dielectrics is the acoustic pulsed method. If the acoustic wave is internally generated by the space charge and propagates through the dielectric with the space charge information, it is known as the PEA method. In practice, the relative movement of the charge with respect to the electrodes can be controlled by a non-uniform expansion of the medium induced by a local temperature elevation on one of the sample sides (*methods known as thermal[95,96]*) or by the generation of a pressure wave (*methods known as acoustic[97].*) These methods can take different names depending on the type of stimulation applied, thermal or acoustic, and its shape.

Finally, there is a third method known as the **PEA technique** based on a different principle[94]. Here, a voltage pulse is applied to the sample to provide stimulation. The induced electric field produces on each existing charge a Coulomb force. Acoustic waves are thus engendered by the exchange of momentum between the electrical charges, bound to the atoms of the dielectric, and the medium. These waves are then detected by a piezoelectric sensor, converted into an electrical signal, and recorded as function of time to provide the basis for the reconstruction of a one-dimensional distribution of the space charge bulk density.

In the 1990's, these techniques matured and were routinely used in labs and industrial sites[98]. Among them, pressure wave propagation (acoustic) and thermal methods became popular in Europe and North-America, whereas the pulsed electro acoustic technique was preferred in Japan. In spite of the fact that the situation is currently undergoing a change, the PEA method is still less well-known in Europe.

3.3.1 General theory behind the PEA method

The PEA technique, alternatively called the electrically stimulated acoustic wave (ESAW) technique, is a non-destructive method which has been developed to measure the dynamic net charge density in solid insulating materials under an applied voltage as a function of time. The technique was originated in Japan some 15 years ago by Maeno, Takada and coworkers[31,92]. The PEA method was developed in 1987, and it was shown theoretically that this method can be used to measure the space charge profile. But due to the limited frequency band of the ceramic piezo-electric transducer used by that time, the detected signal did not directly indicate the space charge profile. The ceramic piezo-electric transducer was then replaced by a PVDF transducer. Certain properties of the polymer piezoelectric transducer, such as high sensitivity, a wide frequency range, a broad dynamic response, and a low acoustic impedance, make it possible to overcome the disadvantage of the ceramic transducer in frequency characteristics. The PEA technique is more common than other techniques due to its simplicity in structure, low cost and easy to implement for both plaque and cable samples.

Until recently, charge storage effect was only probed using techniques capable of yielding information about integral quantities of charges such as thermally stimulated discharge studies. During the 1980's, a new class of techniques was developed with the ability of disclosing differential data such as the charge distribution along the thickness direction. In most of these methods, a displacement of charges is imposed relatively to the measuring electrodes in a capacitor where the dielectric is placed between two metallic electrodes[99]. The influence charge on the electrodes is thus modified and this variation is measured in the external circuit. This signal is transformed into a voltage variation across the sample terminals in case of the measurement being performed in open circuit or into a current variation in the case of a short-circuit measurement. The charge displacement is induced by an external perturbation applied to the sample in such a way as to modify its transversal dimension in a non-uniform manner, this last condition being necessary to obtain an electrical response by the deformation of a charged material. In addition, the form and the evolution of the perturbation as a function of time must be known during the measurements.
Figure-3.3.1 depicts the simplified diagram of a generic PEA system sample cell and detector. The sensor-amplifier response necessitates the deconvolution of recorded data, in order to obtain the space charge profile in the specimen under test. The acoustic pulse is measured using a piezoelectric transducer. In the PEA method, the minimum duration of the acoustic pulse is equal to the duration of the applied electric pulse. In order to obtain a high relative spatial resolution (2 - 5%), firstly a narrow pulse should be selected, and secondly a thin transducer should be used.

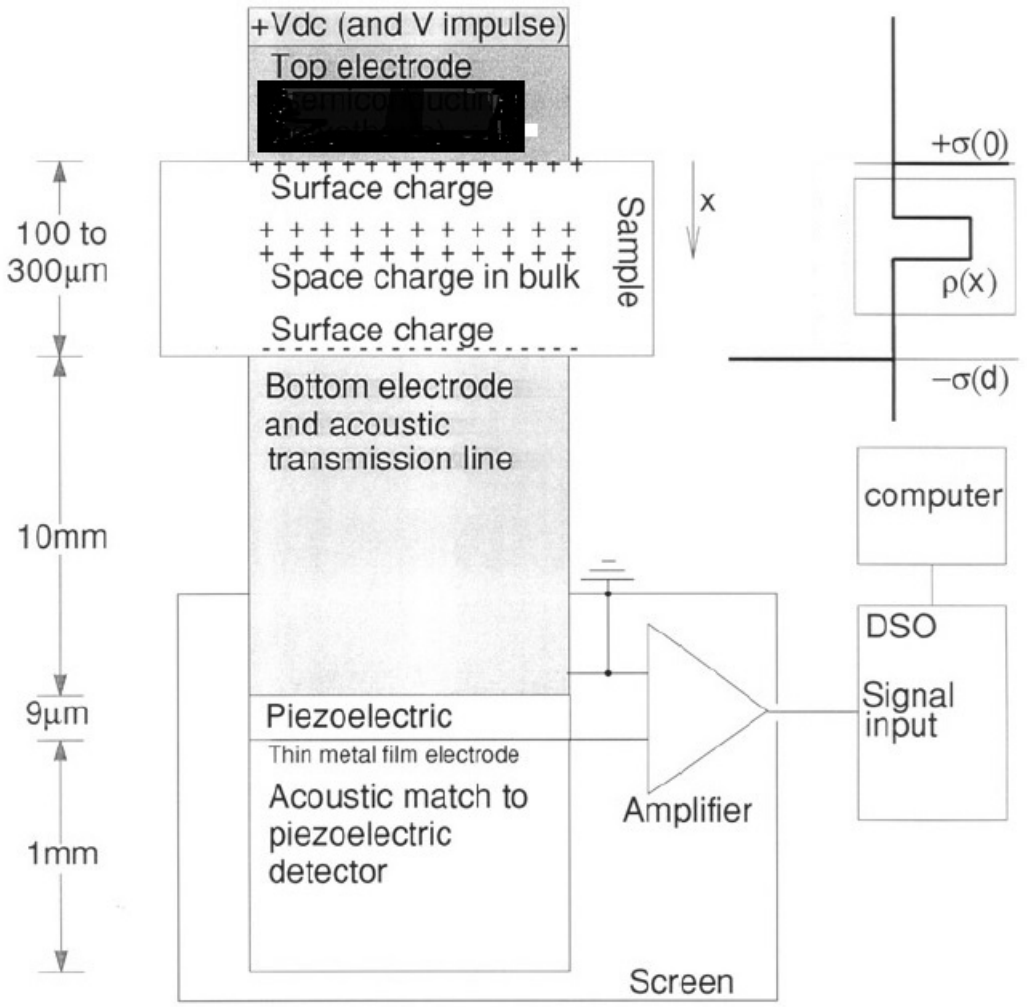

Figure 3.3.1: A simplified diagram of a generic pulsed electro-acoustic system sample cell and detector, ©J.M. Alison, 1998[93]

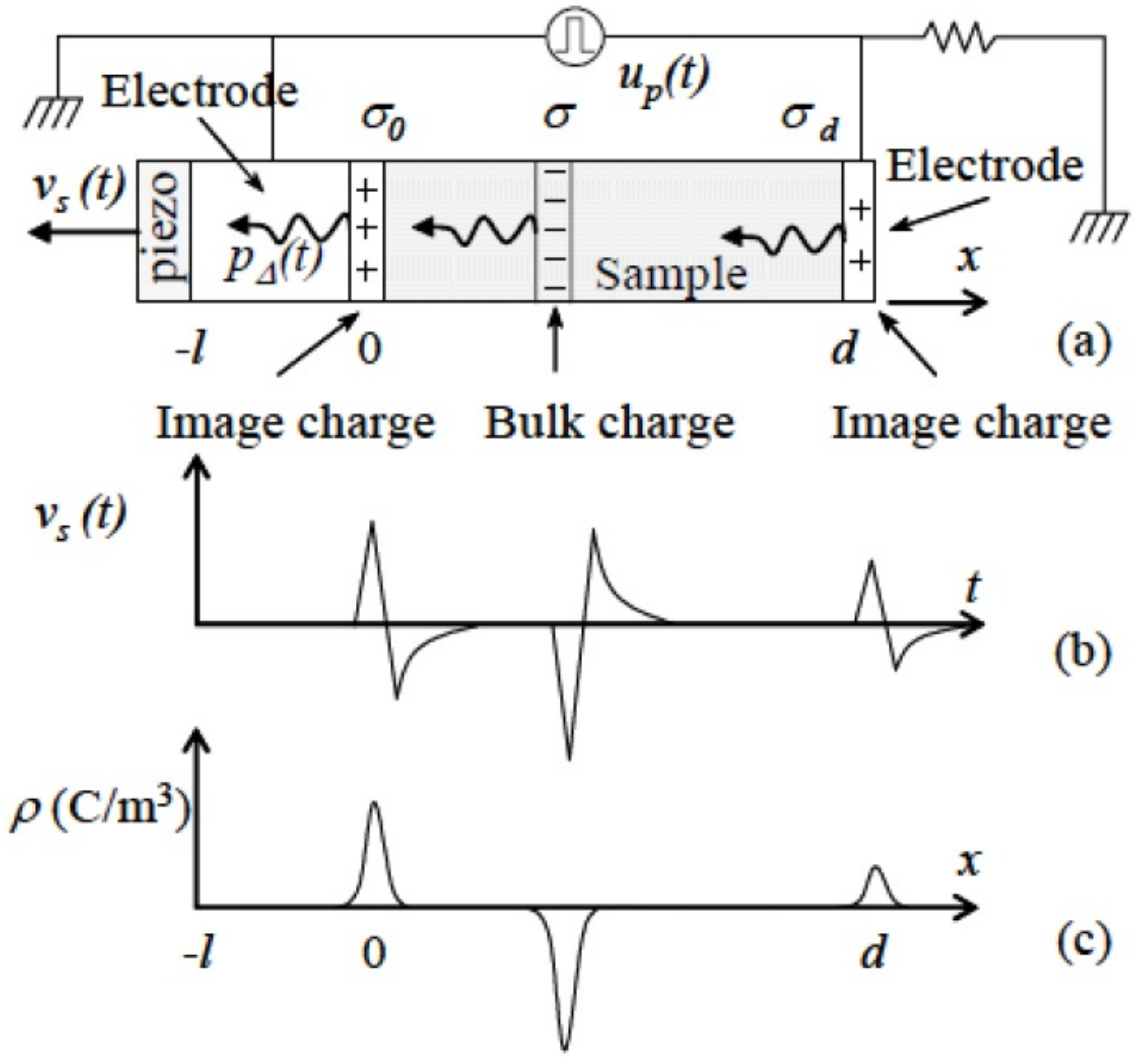

Figure 3.3.2: Principle behind the PEA method[19].

The PEA measurement principle is presented in Figure 3.3.2. Let us consider a sample having a thickness d presenting a layer of negative charge at a depth x. This layer induces on the electrodes the charges σ_d and σ_o by total influence so that:

$$\sigma_d = -\frac{x}{d} * \sigma, \sigma_o = \frac{x-d}{d} * \sigma \tag{3.1}$$

The diagrammatic representation in Figure 3.3.2 gives rise to a clearer comprehension of the equation(3.1) presented, and the development of charge.

The measurement setup schematic for the PEA method is depicted in Figure 3.3.2- Part (a) demonstrates the fact that charged regions give rise to acoustic waves under the effect of a pulsed field. Then, Part (b) shows that as a consequence the piezoelectric sensor delivers a voltage $V_s(t)$. Part (c) depicts that an appropriate signal treatment then gives the spatial distribution of image and internal charges. Application of a pulsed voltage $U_p(t)$ induces a transient displacement of the space charges around their positions along the x-axis under Coulomb effect. Thus elementary pressure waves $P_\delta(t)$, issued from each charged zone, with amplitude proportional to the local charge density propagates inside the sample with the speed of sound. Under the influence of these pressure variations, the piezoelectric sensor delivers a voltage $V_s(t)$ which is characteristic of the pressures encountered. The charge distribution inside the sample becomes accessible by voltage signal treatment.

A schematic diagram concerning the setup used to investigate the samples is presented in Figure 3.3.3.

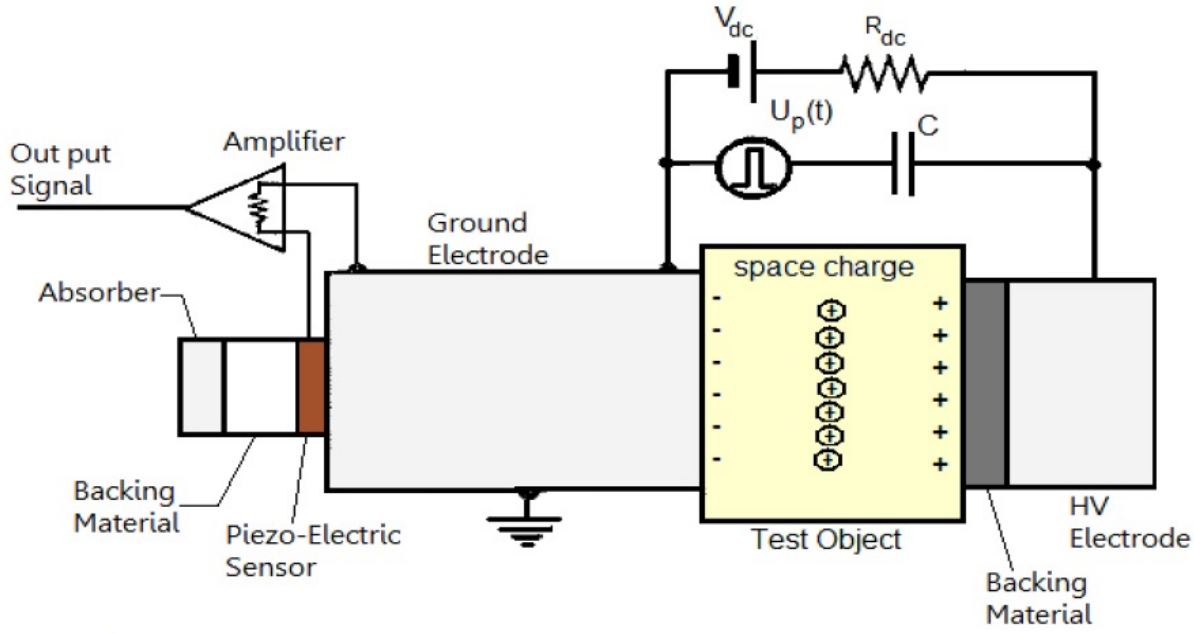

Figure 3.3.3: The PEA measurement setup schematic

The DC source, V_{dc}, is the voltage applied to initiate charge injection from the electrodes. When the short duration pulse, $U_p(t)$, is applied, the resulting electric field, E(t), acts both on the space charges and charges at the electrodes and they experience a force. This force causes the charges to move slightly in their position. This perturbation causes a pressure pulse, P(t), that is proportional to the charge distribution in the sample. The pressure pulse moves in both directions to the HV electrode and ground electrodes. The ground electrode is thick and delays the acoustic waves until the disturbances caused by the firing of the impulse generator have died away. At the back of the ground electrode, a piezo-electric transducer is located that converts the acoustic wave to an electric signal which is then amplified and fed to an oscilloscope. The backing material, having the same acoustic impedance as the piezoelectric transducer but lacking piezoelectric properties, is added to suppress the reflections of the acoustic wave which might disturb the measurement. The sensor converts the acoustic signal P(t) into a voltage V(t). This conversion is frequency dependent giving favour to the higher frequency signals. Besides, the sensor has a certain capacitance which acts a high pass filter together with the input resistance of the amplifier.

To account for the cumulative effects, a deconvolution process is implemented in the signal processing. In effect, this process does the following; a transfer function is obtained for a signal of a known shape. The transfer function is then used to calculate the processed signal from a received signal using the deconvolution process. This deconvolution in time domain is equivalent to division of the output signal by the transfer function in frequency domain. As the acoustic signals travel through the sample, energy is dissipated due to elastic losses. The acoustic wave is, therefore, attenuated. The attenuation is seen in the decreasing amplitude of the signal as it travels through the sample. The signal is also dispersed; where, high frequency components are attenuated more than the low frequency components. The dispersion affects the signal such that it gets broader as it travels along the sample. These two effects should therefore be accounted for during the mathematical processing.

3.3.2 The Pulsed Electroacoustic Method for thin plaques

A presentation of the general schematic for the test bench is shown in Figure 3.3.4. Transient field excitation is provided by a short pulse (8 ns) voltage generator. A HVDC supply (maximum voltage, typically 20 kV, being limited by the geometry of the cell), is used to apply DC electric stress to the sample during measurement. A piezoelectric sensor (PVDF 9 μm) detects the incident acoustic waves, and then provides a characteristic voltage.

The specifications of our PEA setup are presented herein. The setup was built indigenously at the High Voltage Laboratory, TU Delft.

Test unit	Technical specifications
Amplifier:	Gain=60 dB, Bandwidth=0.1-500 MHz, Input impedance=50Ω
Sensor:	PVDF foil thickness=9μm
Pulse generator:	Amplitude= 0-1 kV, pulse width= 8 ns
Max. temperature attainable:	70 degrees Celsius
Maximum voltage:	20 kV

Table 3.3.1: Specifications of the PEA setup used for plaque sample investigation.

The top electrode is made of aluminium and a semi-conducting material (carbon black reinforced polymer) is placed in contact with the sample in order to have a good acoustic impedance matching. The bottom electrode is made of stainless steel. It has a large thickness and so acts as delay line between the acoustic signal and the electrostatic noise provided by the pulse generator. A PMMA sample is used to hold the piezoelectric sensor on the lower electrode with a good acoustical impedance matching. The polyvinylidene fluoride PVDF sensor is a polymeric piezoelectric transducer with certain properties that make it suitable for detecting acoustic signals generated by space charge and converting them into voltage signals. The magnitude of the signal is proportional to the space charge density and the sign of the signal coincides with the sign of the space charge. This means that positive charges will cause a positive voltage and vice versa. Such kind of properties that favor the use of PVDF sensors are: high levels of piezo-activity, an extremely wide frequency range, a broad dynamic response and a low acoustic impedance. In order to avoid reflections of acoustic waves, a proper acoustic termination is required at the sensor. For this purpose, a material (PVDF non-polarized) with the same acoustic properties of the sensor is used in combination with a material (absorber) able to absorb the acoustic waves. The electrical signal provided by the sensor is amplified and fed into an oscilloscope, where it is displayed and stored.

3.3.3 General measurement procedure

Measurements can be performed in two different ways. The first case is voltage-on measurements where space charge within the test object is measured while a DC voltage is applied. The space charge present in the bulk of the insulation and the charges at the electrodes are detected. Electrode charges consist of two types of charges. The first type is a result of the presence of the DC voltage and the second type is induced by the space charge in the sample.
Furthermore, voltage-off measurements can be carried out where space charge is measured while the DC voltage is absent and the test object is short-circuited. The space charge present in the bulk of the insulation is detected. Charges at the electrodes are also detected but they are only induced by the space charge. These charges at the electrodes are called *"mirror charges"*.

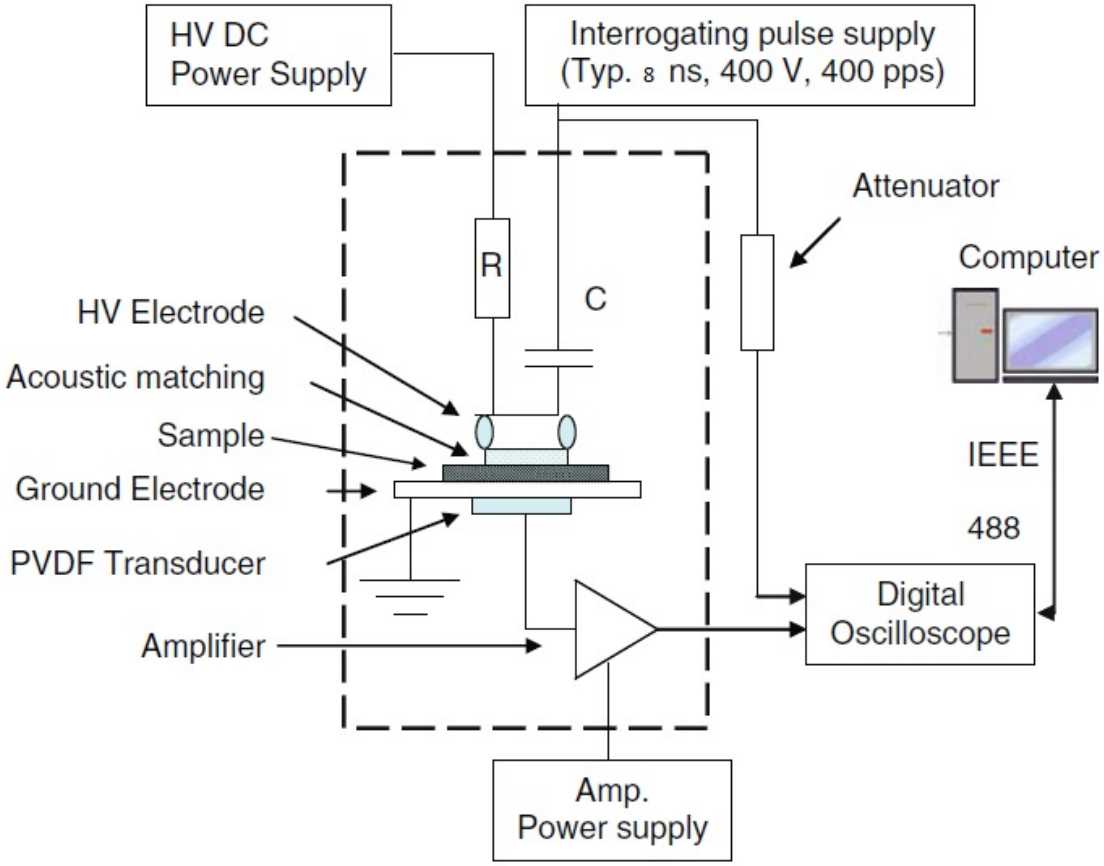

Figure 3.3.4: General schematic of the PEA test bench

Photographs of the test setup, as present in the High Voltage Laboratory of TU Delft, can be found in Appendix-II. In Figure-3.3.4, the general system schematic of a PEA test setup is presented. An important feature to be pointed out is the selection for the series resistance to be used in the PEA test setup. The pulse voltage cannot be applied to the sample if the series resistance is not present in the circuit.If the series resistance is not present in the circuit, the capacitance of the specimen under consideration (for neat epoxy as used in this work, the sample capacitance was determined to be 17 pF) and the equivalent capacitance of the DC power source (around several mF) result in parallel connection, and the total capacitance is several mF. This leads to most of the pulse voltage being applied to the coupling capacitor (around several nF), and not being applied to the sample. If a suitable resistance is inserted into the circuit between the sample and the DC voltage source, the pulse voltage will be shared by capacitance of the sample and coupling capacitance. Therefore, the pulse voltage can be applied to the sample as the value of the coupling capacitance is much larger than that of sample capacitance.

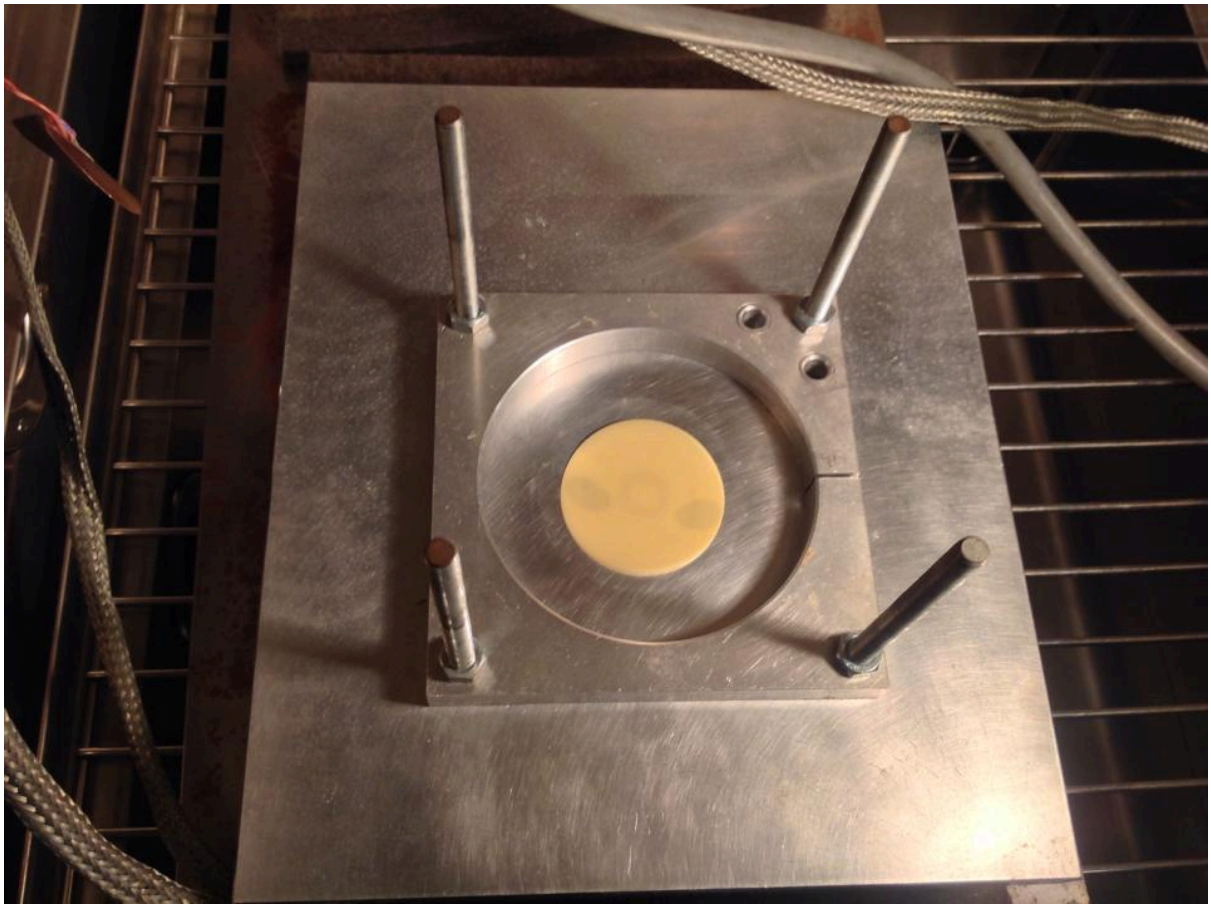

Figure 3.3.5: Setup photograph-3 (Plaque sample loaded on PEA base)

Before performing the measurements, the electrodes, the sample, and the PEA cell underlying the sample were thoroughly cleaned using alcohol and they were allowed to dry for some time. The base of the PEA cell, as seen here, needs to be cleaned since presence of foreign particles, as well as unwanted protrusions and aberrations affect the measurement, as well as show up as spurious observations (artifacts) during the space charge profile processing.

The silicone oil is applied to the base (1-2 drops), and the sample is placed carefully on it. Care is taken to ensure that there is no sudden mechanical movements to the setup, so as not to disturb the alignment of the sample at the central region of the base.

Figure-3.3.6 shows the HV electrode and the circular semicon strip which remains in tight contact with the sample during test duration. It is securely fastened with wingnuts onto the PEA base, to ensure proper mechanical contact with the sample at all times of testing.

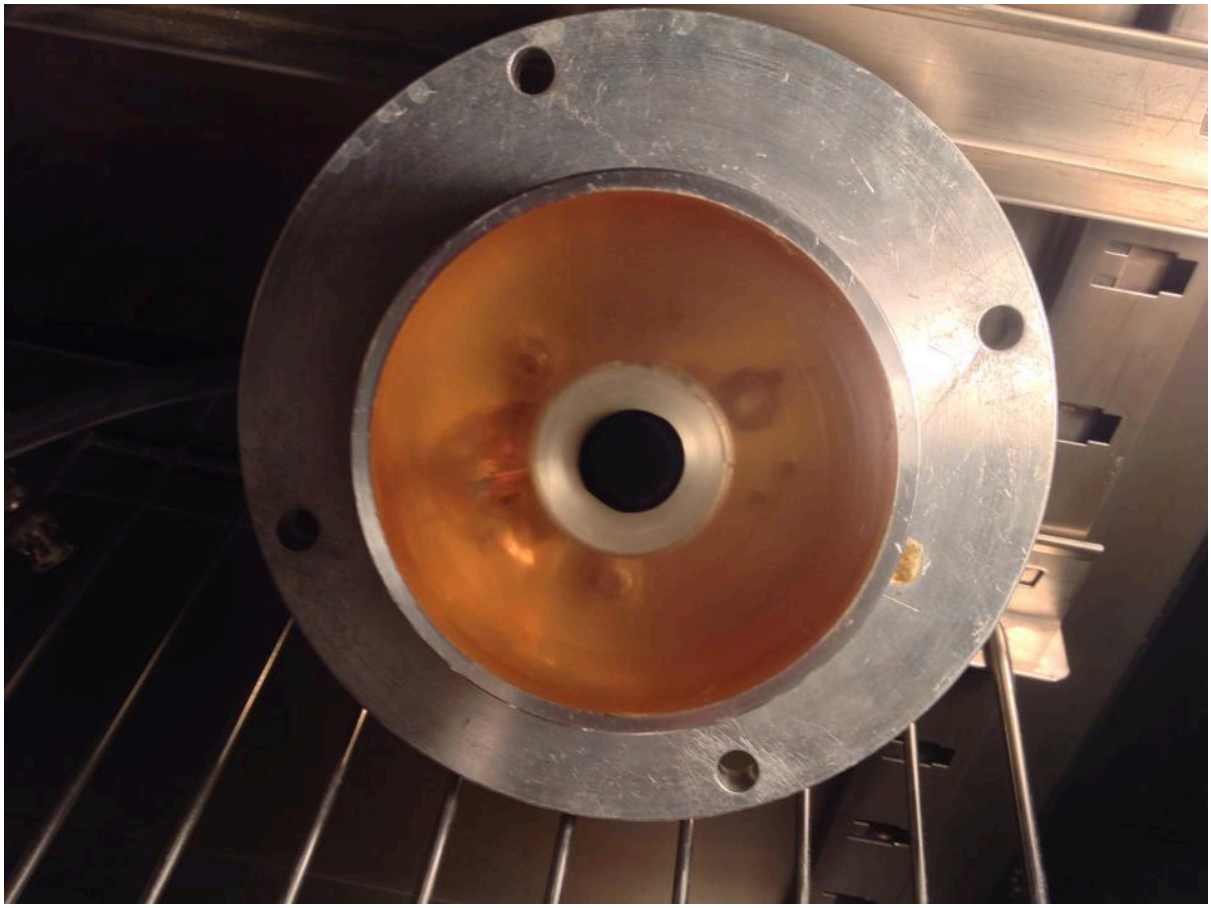

Figure 3.3.6: Setup photograph-4 (HV electrode, with circular carbon-black semicon)

3.3.4 Correction of the detected signal

Generally, the electrical signal detected at the scope does not directly represent the acoustic signal at the sensor. This is mainly due to the fact that the sensor-amplifier system acts as a high-pass filter[28]. In order to correct the detected signal, deconvolution techniques [28] have been adopted in this work. Moreover, acoustic waves are attenuated and dispersed, while traveling through lossy media. So, the acoustic signal detected at the sensor does not directly correspond to the space charge distribution within the test specimen.

3.3.5 Attenuation & dispersion

Acoustic waves are attenuated and dispersed while travelling through lossy media. Therefore, the acoustic signal detected at the sensor does not directly correspond to the space charge distribution within the test specimen.
In a lossy medium, the amplitude of a pressure wave due to space charge decreases while the wave travels through the test object. Attenuation is a frequency dependent phenomenon which causes high frequency components to be more attenuated than lower frequencies. Therefore, the charge peak in the detected signal results not only smaller but also wider if compared to the peak that would be detected if the medium was ideal. In a dispersive medium, the shape of a pressure wave due to space charge changes while the wave travels through the material. This is due to the fact that the speed of sound in a material is frequency dependent.

3.3.6 Calibration of the recorded signal

Finally, calibration of the measuring system must be performed in order to convert the detected signal at the scope [**mV**] into a space charge density signal [$\frac{C}{m^3}$]. This procedure can be carried out on the basis of a known charge distribution at the earth electrode. To convert a voltage signal v(t) into a calibrated space charge profile $\rho(t)$, a calibration factor K_{cal} is defined according to the equation 3.2 provided.

$$K_{cal} = \frac{v_{pr}(t)}{\rho(t)} \tag{3.2}$$

Where $v_{pr}(t)$ is the processed signal after deconvolution, attenuation and dispersion correction.
In order for the calibration factor to be calculated, a certain DC voltage V is applied to an initially space charge free sample. **This is an essential condition for proper calibration and measurement: The sample should be free of space charge at the beginning of the measurement.** The calibration factor can be calculated according to equation 3.3.

$$K_{cal} = \frac{\int_{x_1}^{x_2} v_{pr}(x)dx}{\sigma_e} \tag{3.3}$$

Where x_1 and x_2 denote the starting and the ending point of the earth electrode respectively, σ_e is the earth electrode surface charge density and for a known applied voltage V it can be calculated according to equation 3.4.

$$\sigma_e = \varepsilon_o \varepsilon_r E_e = \varepsilon_o \varepsilon_r \frac{V}{d} \tag{3.4}$$

Where d is the sample thickness and ε_r is the relative permittivity of the sample.
Once the calibration factor has been determined, the space charge profile can be obtained according to equation 3.3.
In order to verify that the calibration procedure is correctly done, the electric field distribution E(x) across the sample can be calculated according to equation 3.5.

$$E(x) = \frac{1}{\varepsilon_o \varepsilon_r} * \int_o^d \rho(x)dx \tag{3.5}$$

Afterwards, the voltage distribution V(x) across the sample can be calculated according to equation 3.6.

$$V(x) = -\int_o^d E(x)dx \tag{3.6}$$

The electric field strength distribution calculated from Equation (3.5) should match the value (known *a priori*) the experimenter wishes to apply, via the DC voltage applied across the sample- to ensure that the recovered space charge profile is reasonably similar to the original space charge distribution.

3.3.7 Test conditions (electrical & temperature based)

The electrical field values applied were 8 $\frac{kV}{mm}$ and 30 $\frac{kV}{mm}$ respectively.
The two temperatures used for the experimental measurements were 25 degrees Celsius & 45 degrees Celsius respectively. Relative humidity was set constant at 35% by usage of the climate control chamber at the High Voltage Laboratory, TU Delft.

3.3.8 Specific details about signal processing in this work

A brief overview of the process used to obtain the space charge profile after experiments is discussed herein, with a specific focus on the research work presented.
Since neat epoxy is our baseline sample for all subsequent filler comparisons, the recorded signal is primarily presented here, along with an explanation of what mathematical processing was performed on the signal. The same procedure was henceforth consistently performed upon all the other signals recorded, and the resulting trends are compared. Neat epoxy was

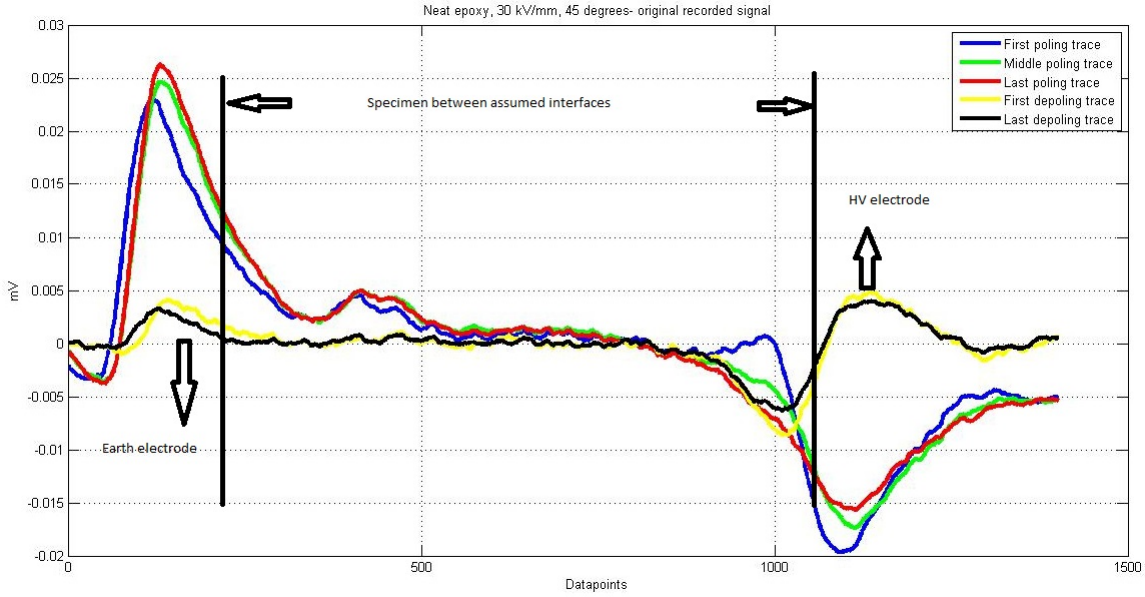

Figure 3.3.7: The preliminary observations from raw data.

measured at $8\,\frac{kV}{mm}$ and $30\,\frac{kV}{mm}$ at the temperatures of $25°C$ & $45°C$, respectively. The data processing was an arduous task, and it has been explained in a brief fashion subsequently.

Primarily, the data obtained from the LeCroy DSO is in the form of numerical column vectors- a single column representing the spatial charge distribution across the specimen corresponds to a single trace, and a single trace is the average of many sweeps, carried out by a customized software[32]. Since the number of traces is too voluminous in magnitude to handle in terms of computer disk space prevalent upon the digital storage oscilloscope- many traces are averaged together in time by the software[32], as well as extension of spatial length of information contained by the matrix obtained, with the electrical response in space and the traces across the datapoints in time. The optimum software[32] settings are programmatically set & recalled each time a new measurement is performed. 3000 sweeps of the DSO, with an optimum trigger level ensures proper fidelity of signal. A visual check is performed each time to ensure the absence of any anomalies in recording. It has been observed that for a sweep level of 1000, the noise level is reduced by a factor of 32- after extensive trial & error, the best signal-to-noise ratio factor was corresponding to a setting of 3000 sweeps of the DSO. It was observed that the further averaging of the obtained traces after the software[32] had preliminarily averaged them in real-time & was extremely beneficial in reducing scatter in obtained data as well as ensuring consistency of information obtained. These traces are processed in MATLAB, and 2 files are averaged further into one- since this has been noticed to decrease the noise related scatter in the obtained data. The "unprocessed" traces are plotted in MATLAB, to gain a preliminary idea of the charge developments in the specimen after complete testing. A diagrammatic representation in Figure-3.3.7 makes the situation clearer. The purpose of juxtaposing the first & final depoling traces along with selected poling traces in the Figure-3.3.7 is to gain an idea about the nature of charge accumulated in the specimen (if any), and whether at the end of the depoling period, all charges have been successfully removed or not. The observations about the "*mirror charges*" induced at the electrodes provides us important & vital information about the nature of charge accumulation, and polarity. Since the presence of space charge accumulation (if present) distorts the Laplacian electric field distribution, the nature of charge accumulation (as well as

the location) either leads to an increase (or decrease) in the electric field distribution inside the specimen. Homocharges lower the local electric field at the location of accumulation around the electrodes, whilst heterocharges increase the local electric field. An integration of the space charge profile (obtained in Figure-3.3.10) according to equation (3.5) can provide us with an idea of the electric field distribution inside the specimen. The next step is to process the obtained matrix data via MATLAB, using a customized program developed indigenously[100]. Even though we apply positive polarity DC voltage at the HV electrode, the polarities in the Figure-3.3.7 appear inverted, due to the inverted placement of the sensor foil in the PEA setup.

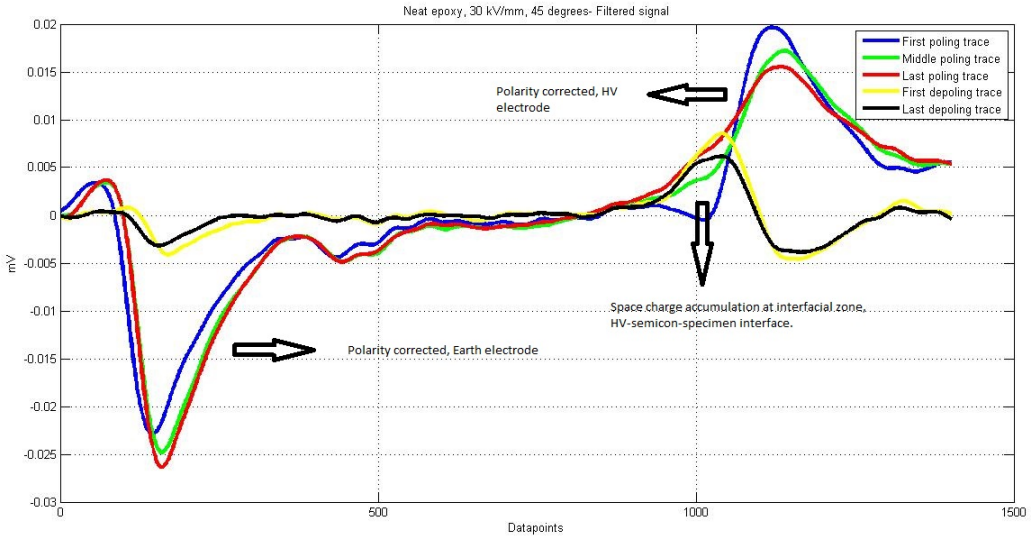

Figure 3.3.8: Signal filtered by Butterworth & Gaussian filtering, polarity corrected.

The diagram depicted in Figure-3.3.8 shows the effect of 2 filter applications (5th order low-pass Butterworth filter & Gaussian filter) carried out on data obtained, and the polarity correction of the signal. The succeeding step involves a good selection of the interfaces at the Earth-specimen zone & the HV-specimen zone. Another Gaussian filter application is made therein to obtain a proper signal height, while minimizing oscillations in data.

The next step is deconvolution of the de-noised data. The amplified electrical signal detected at the scope does not directly represent the acoustic signal at the sensor. This is mainly due to the fact that the sensor itself has a certain capacitance which in combination with the input resistance of the amplifier acts as a high pass filter. Therefore, the higher frequencies are gained in favor of the lower frequencies. In order to correct the detected signal a deconvolution technique is adopted.

To obtain the space charge profile from the convoluted signal, the ideal signal from the electrode charge is used. (So, it is a signal without the response of the sensor and the amplifier. This ideal signal is represented by a pulse which has approximately the same width as the earth electrode in the detected signal, and has a height of 1.00) The ideal signal & the measured signal are converted into the frequency domain.Then the former is divided by the latter and the inverse response function is calculated.

The following steps involve the exposition of specifics used in the customized MATLAB code developed for data pro-

cessing. The width of the ideal input pulse signal is defined by an 'indent'- a specific number of datapoints, with the central axis passing through the midpoint of these datapoints if connected, and the peak point of the Earth electrode surface charge as represented by the signal. In all cases of signal analysis, calibration of the space-charge free (safely assumed) reference signal depends upon the Earth electrode surface charge density- also, the fact remains that being closer to the sensor at the PEA system base, the impulse response at the Earth electrode is much less distorted than at the HV electrode. Hence, mathematically it makes perfect sense to base our reference calculations upon a determinable quantity- as a result of which, the deconvolved signal is shaped upon the originally obtained system response, adhering to the shape of the Earth electrode as faithfully as possible. The accuracy of the deconvolution procedure primarily depends upon the best fitting of the deconvolved signal to the mean value of the original signal, but keeping a trade-off involved between the Gaussian filter applied to signal processing (a Gaussian filter G(t) is used during the deconvolution process to reduce the amplification of the higher frequency noise components which would otherwise cause computational problems) and interface selection. The selection of interfaces in mathematical calculations for obtaining a reasonably accurate space charge profile is a vital step, and in the course of this work, it was observed- the strike-off between applied Gaussian filter values (too high magnitude values introduce more high frequency oscillations into the signal) and choosing interfaces as close as possible to the assumed interfaces, which is data derived from the depoling traces, provided there has been space charge accumulation in the specimen- and there is some remnant magnitude of space charge accumulation close to the interfacial zone. The deconvoluted data is depicted in Figure-3.3.9.

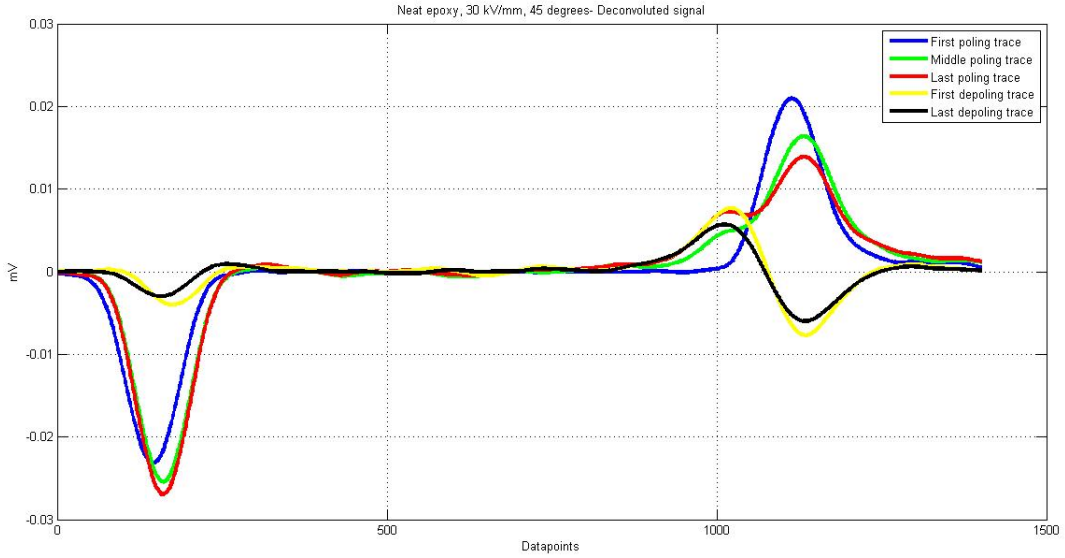

Figure 3.3.9: Deconvoluted signal

After deconvolution has been successfully carried out, calibration of the signal (conversion of the trace data from mV to C/m^3, this determination is done by a calibration procedure based on the known charge distribution at the earth electrode) is a vital step in obtaining the space charge profile, as depicted in Figure-3.3.10. The relation between the measured voltage signal at the output of the sensor and the charge distribution in the sample is defined by a factor K_{cal}, as defined in equation (3.3) To calculate the calibration factor K_{cal} a known charge distribution is needed. The signal without space charge can provide a known charge distribution which in this case corresponds to the earth electrode surface charge. The applied voltage is known therefore the charge distribution at the earth electrode can be calculated. Another important step in processing remains the attenuation & dispersion corrections- a necessary step, since while propagation through a lossy dielectric, waves get attenuated and dispersed in the medium. This correction is carried out by the indigenous program[100], and the space charge profile obtained is portrayed in Figure-3.3.10.

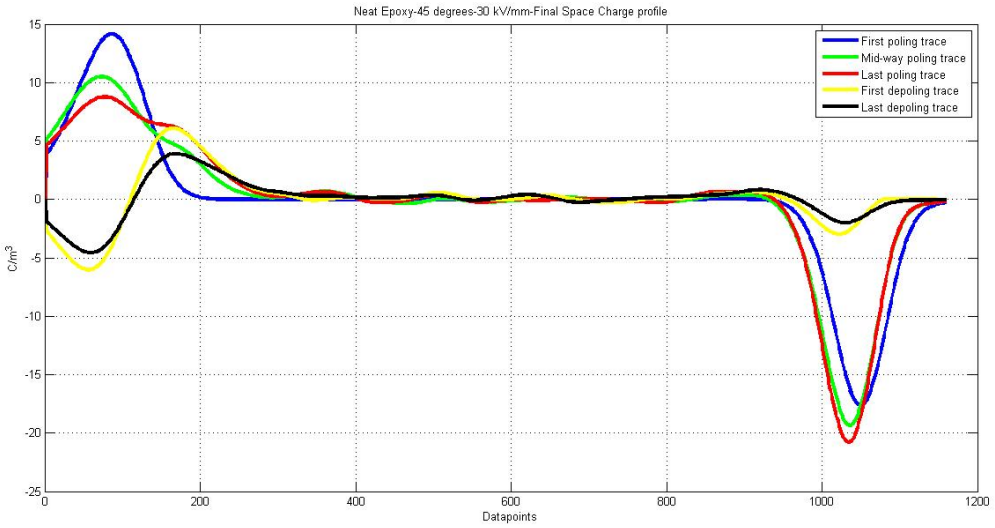

Figure 3.3.10: Obtained space charge profile

The relevant parameters of interest are saved for future use, and the relevant contour plots are generated via MATLAB, consistently maintaining the same colour scale level for easy visual comparison. The contour plots are of special importance, since space charge dynamics is relatively simpler to comprehend among different fill grades upon application of the relevant contour plots. An example is demonstrated in Figure-3.3.11.

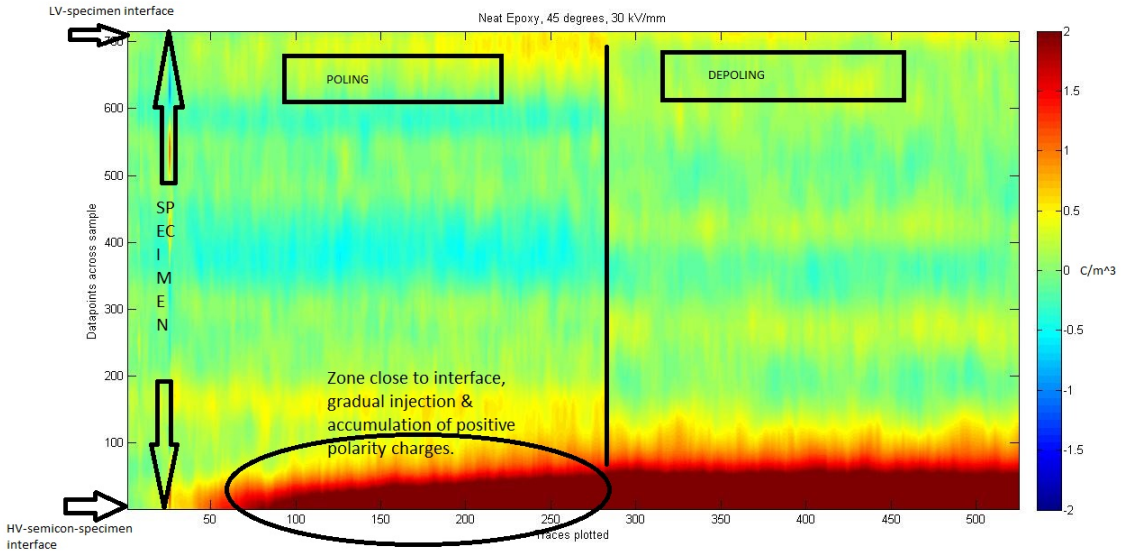

Figure 3.3.11: Obtained Contour Plot, space charge dynamics investigated.

Figure-3.3.11 clearly demonstrates injection of positive polarity charges from the HV electrode at a temperature of $45°C$ into the neat epoxy material. They are mostly trapped close to the interfacial region as pointed out, and do not penetrate into the sample bulk.

If the presented contour plots are observed closely, it is determined that between the datapoints 100 till 600, there are random, successive positive & negative oscillations observed in the sample bulk- these *should not* be considered as developed charges over the poling period, since these oscillations are only noise (generated from the imperfect termination of the pulse signal, noise from cable sources). This can be understood from the fact that they are constant throughout the measurement. (From the beginning of poling period till the end of test, including depoling) Thus, these oscillations (which can also be observed in unprocessed data) are attempted to be nullified/reduced during the deconvolution procedure, wherein a pulse signal is mathematically defined to obtain the charge distribution in the test specimen, from the convoluted signal. (An ideal pulse signal is assumed, but in reality, that is not the case)

To resolve this problem mathematically, 2 zones were defined within the processed space charge profile:

- **The interfacial zones**: In principle, the surface charge densities σ_o & σ_d at the earth and HV electrodes should be delta functions if expressed in coordinates of volume space charge density. However, because the measurement system has a finite resolution and the pulse a finite width, it is not possible to obtain this ideal result. Consequently, the induced surface charges are expressed as a negative and positive peaks and the widths of the peaks directly reflect the resolution of the measurement system. The interfacial zones are defined for our measurements as a zone of 80-100 datapoints corresponding to the bounding electrode- this helps in quantifying with a certain degree of accuracy the amount of space charge developed during the poling period, and charge dynamics across various fill-grades.
- **The sample bulk zone**: The region between 100-600 datapoints is defined as the sample bulk zone- hence these datapoints are mathematically set to null values, thus effectively processing out the distortion introduced by the sensor-amplifier completely.

Thus, the entire manner in which the signal is processed for the research work presented herein, is depicted in the previous pages.
A final example plot of the steady growth and subsequent trapping of charges in neat epoxy material is presented with the help of an average charge density vs time scatter plot in Figure-3.3.12. The 'poling' section of the average charge density plot in Figure-3.3.12 depicts the gradual & steady accumulation of space charge in neat epoxy- while the 'depoling' section of the average charge density plot depicts the portion of the 'voltage off' measurement. Interestingly, the charges accumulated in neat epoxy material during the 'poling' period do not seem to experience subsequent removal, since they are trapped- and thus the level of charge accumulation does not drop down in the depoling period. This trapped space charge accumulation can also be observed from the contour plot in Figure-3.3.11.

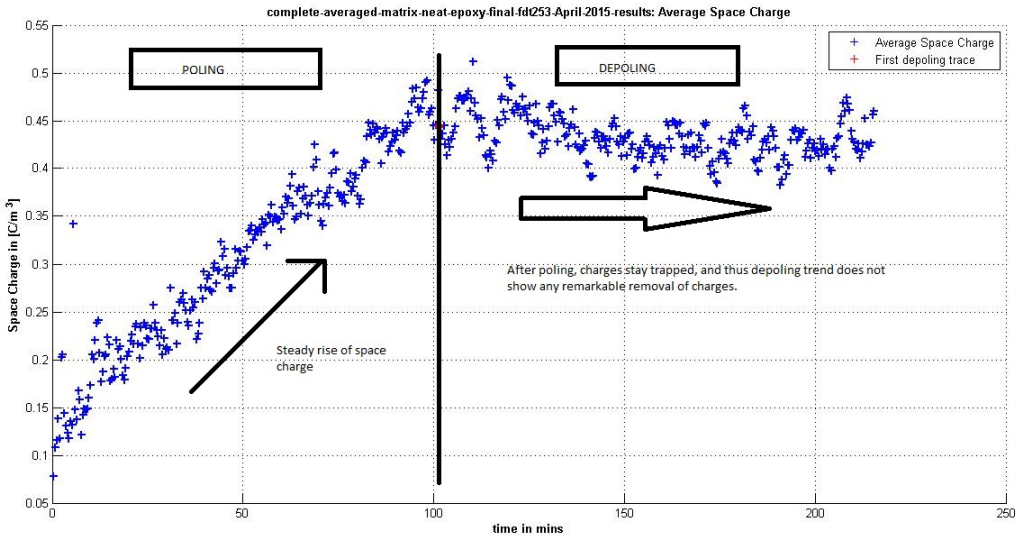

Figure 3.3.12: Obtained Average charge density plot.

Thus, with the aid of all this information, the measurement results are processed, and trends observed across fill-grades- the discussion of which is present in the next chapter.

One final check after obtaining the corrected signal is to check the ratios of the surface areas between the Earth electrode and the HV electrode spatially, since ideally, after all corrections have been performed- this ratio should be 1.00. This concludes the chapter.

I may not have gone where I intended to go, but I think I have ended up where I needed to be.

Douglas Adams

4

Experimental results & analysis

Since the stage has been set for a discussion about the research work performed, this chapter deals with the presentation of the performed space charge measurements & subsequent analysis.

It is now time to examine the first of the two important questions this research work seeks to address. The two questions are stated herein.

- **What is the effect of incorporation of the nanoparticles upon space charge behaviour of the epoxy composite in general, and how does filler content loading affect relevant electrical behaviour?**
- **What is the effect of synthesis techniques used in this work upon space charge behaviour, and can there be a possible correlation between filler content loading effects & the technique(s) under consideration, for corresponding specimens?**

4.1 The effect of fill grade upon nano-filler incorporation in host material

In order to explore the effect of hBN fill-grade in increasing order of magnitude, it is important to explore the space charge developments in neat epoxy, the dynamics of accumulation & removal, and characterize it as the baseline reference sample.

4.1.1 Characterization of neat epoxy

Neat epoxy behaviour is primarily presented at $8\frac{kV}{mm}$ and $30\frac{kV}{mm}$ to portray the effect of elevated electric field upon charge dynamics. It is observed that at an applied electric field of $8\frac{kV}{mm}$, at the temperature of $25°C$(Figure-4.1.1), significant charge injection is not noticed in the sample. Figure-4.1.2 demonstrates the effect of electric field upon injection of charge carriers across the interfaces between the sample & the electrodes. An interesting observation is made henceforth. Secondarily, neat epoxy behaviour is presented at $25°C$(Figure-4.1.3) and $45°C$(Figure-4.1.4) at an applied electric field of $30\frac{kV}{mm}$ to portray the effect of elevated temperature upon charge dynamics.

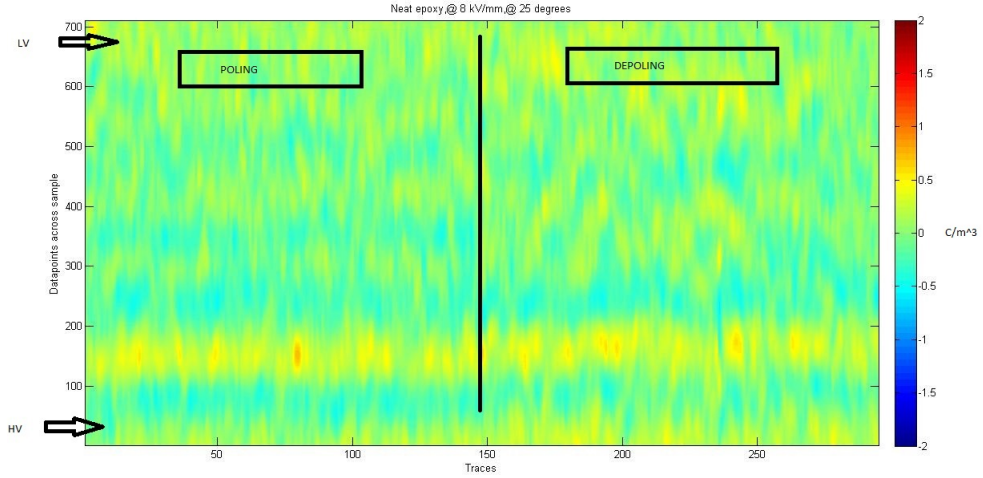

Figure 4.1.1: Neat epoxy processed signal contour plot, $8\frac{kV}{mm}$, 25 degrees

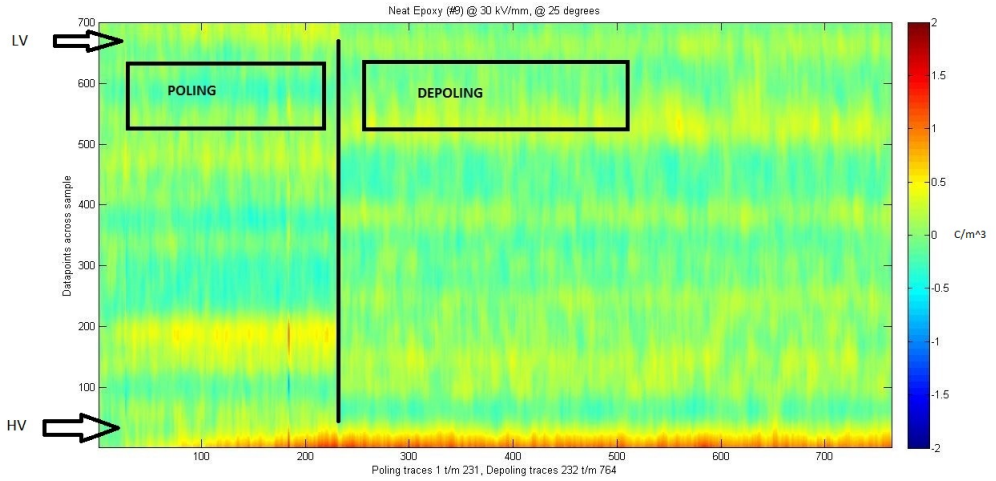

Figure 4.1.2: Neat epoxy processed signal contour plot, $30\frac{kV}{mm}$, 25 degrees

It is of particular interest herein to note that the interface at the HV-sample side consists of a semiconductive layer in contact with the electrode material, whilst the interface at the Earth-sample side consists of the metal in contact with the sample, and a thin film of silicone oil in between them. The silicone oil at the Earth-sample interface helps in improving acoustic contact, whilst the semicon strip at the HV-sample interface ensures tight and good contact, and homogeneous electric stress distribution. The electrodes are constructed of aluminium. The sign of the injected charge does not only depend on the sign of electrode, but also is related to the material of electrodes, the injection time, the injection field and

the properties of material itself[58]. In the recent two decades, many results about the injection and migration of space charge in polymers have been reported, including the behavior of space charge near the interface between polymer and metal or between two different polymers[81]. The basic definition of an interface energy barrier is given by the energy offset between the band-edge or molecular orbital in the insulator and the Fermi-level of the metal. The applied electric field at $30\frac{kV}{mm}$ provides relatively greater energy to the charge injection process at the HV-sample-semiconductive layer interface. Charge injection at metal/insulator interfaces is usually described by Schottky emission, and the barrier height for electron injection is determined by the difference between the work function of metal and the electron affinity of semiconductor which is modified by an applied field. Carbon black being a p-type semiconductor, the movement of holes as the majority charge carriers takes place. This is also why more holes are injected into the insulation, interfacially. Also, aluminum can easily inject more holes than electrons[82,60].

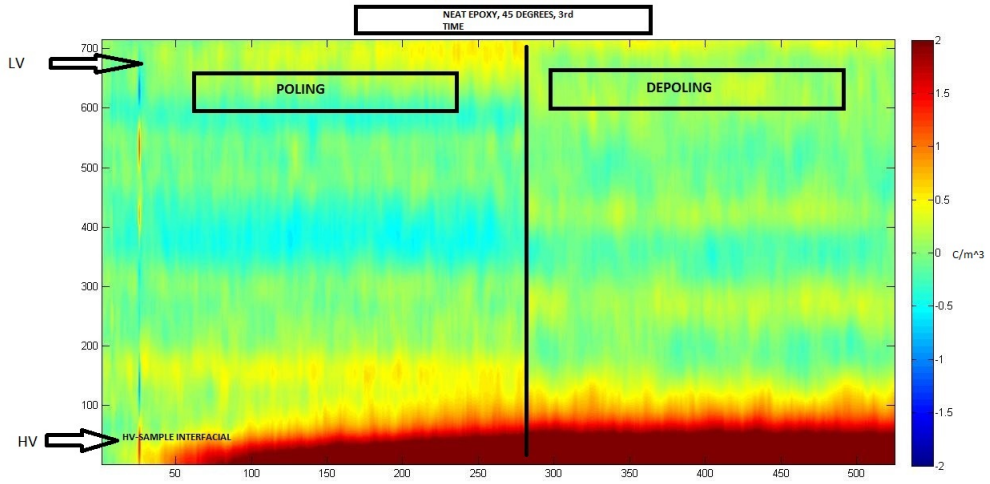

Figure 4.1.3: Neat epoxy processed signal contour plot, $30\frac{kV}{mm}$, 45 degrees

The effect of temperature on space charge development(noticeably greater amount of charge injection occurs at an elevated temperature) is very clearly observable from the contour plots presented in Figures 4.1.2 & 4.1.3 respectively. There is strong positive charge development at the HV-sample interfacial region. Several literature reports support homocharge injection in epoxy resins. Bipolar injection combined to slow polarization has been reported by *Griseri et al* [83] in a somewhat different epoxy resin. *Iizuka et al* [84] have reported similar behaviour in an epoxy resin, with some effect of relative humidity. Besides, aluminium electrodes appear to be more efficient for injection than gold electrodes: this has been observed experimentally (*Chen et al, 2001*)[85] and this is an expected result given the difference in work function for other metals with higher work-functions and aluminium (4.08 eV) [86]. Thus, the elevated temperature of 45° leads to enhanced injection of holes at the HV-sample interfacial region, and what is apparent from the depoling trends as well, the charges are trapped close to the interfacial region- It seems that deep traps are involved as a result of which, not many charges are removed during the 'depoling' period. In depletion period, there is a stabilization of rate of depletion at $45°C$ temperature, after which charges are not removed further. This can be attributed due to the release of trapped charges from comparatively 'shallower' traps. The effect of temperature is also well demonstrated by the average charge density scatter plot in Figures 4.1.5 & 4.1.6.

The difference in development of space charge accumulation, at the applied electric field of $30\frac{kV}{mm}$ is clearly demonstrated

by the figures 4.1.2 & 4.1.3- they were presented to prove that charge injection is not solely based on electric field application, but that temperature plays a vital role as well. However, these are two competing factors- since the diagrams, now presented, depict the effect of temperature at the lower field of $8\frac{kV}{mm}$ and how no significant charge injection is still observed. This also leads us to another important conclusion: **The threshold field for charge injection processes for neat epoxy at $45^{\circ}C$ is greater than $8\frac{kV}{mm}$, a fact which proves to be significant in all later comparisons. Figure-4.1.1 & 4.1.4 demonstrate that at the lower applied electric field of $8\frac{kV}{mm}$, even elevated temperature of 45° C is not enough to initiate significant charge injection. Thus, it can be stated that the applied electric field, along with the temperature are 2 significant factors in the initiation of charge injection across metal-semicon-insulator surfaces.**

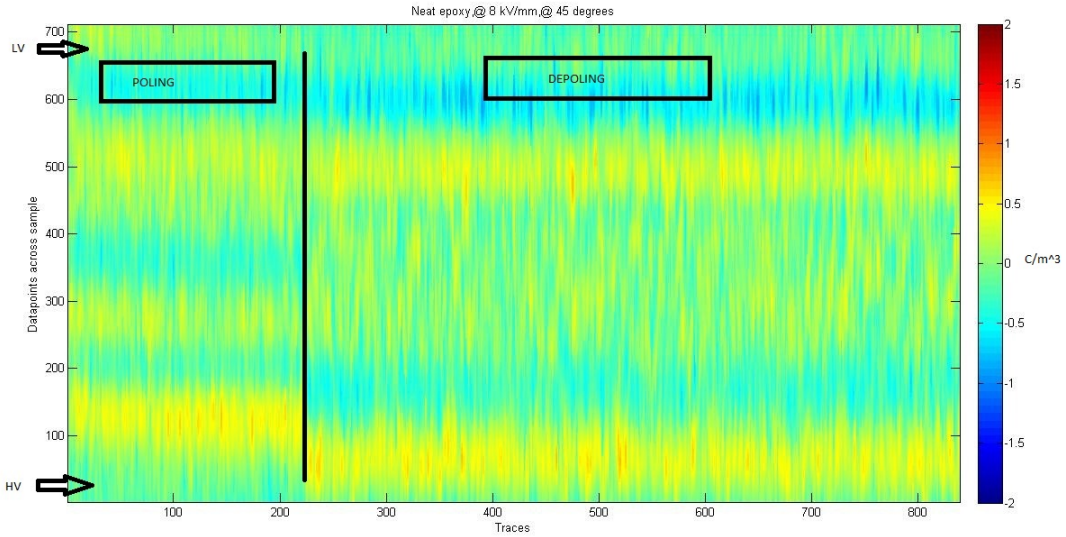

Figure 4.1.4: Neat epoxy processed signal contour plot, $8\frac{kV}{mm}$, 45 degrees

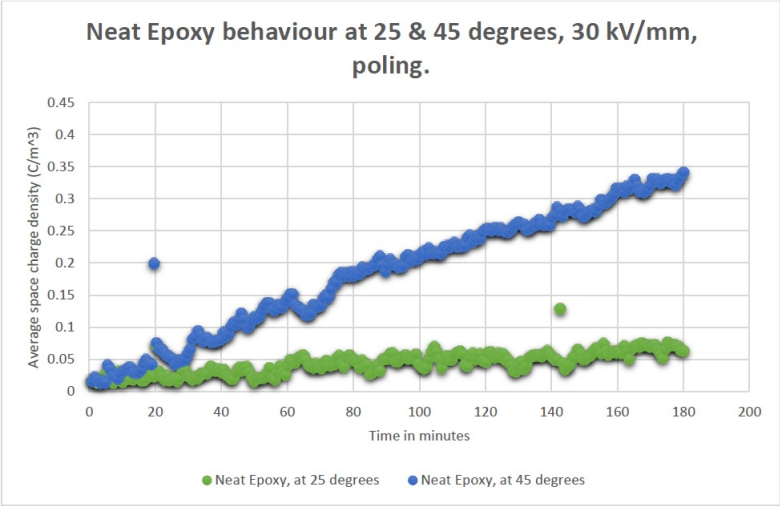

Figure 4.1.5: Neat epoxy processed average charge density plot, $30\frac{kV}{mm}$, 25 & 45 degrees

Neat Epoxy at 45 degrees accumulates charge 5 times faster than at 25 degrees.(Figure-4.1.5)

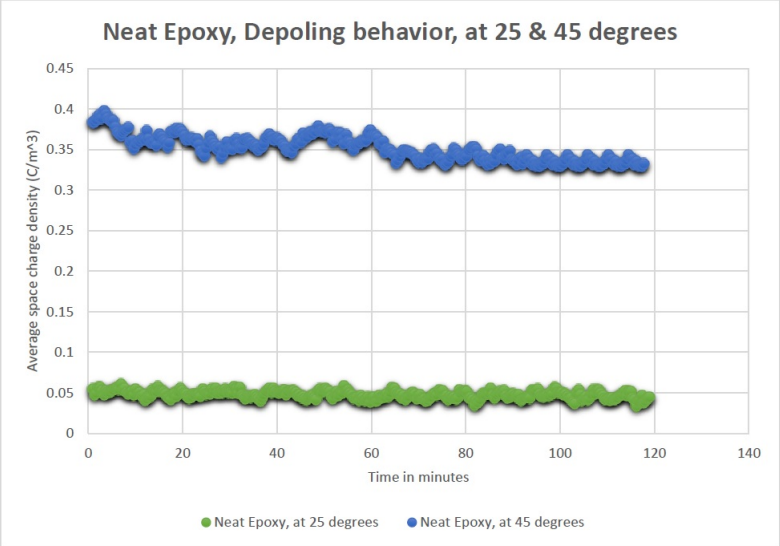

Figure 4.1.6: Neat epoxy processed average charge density plot, $30\frac{kV}{mm}$, 25 & 45 degrees

Neat epoxy depoling behaviour reveals the existence of traps in the material, since the depoling trends do not depict extensive removal of charges.(Figure-4.1.6)

A summary of neat epoxy behaviour

- *Amount of space charge*: At 45 degrees, 0.34 $\frac{C}{m^3}$; at 25 degrees, 0.06 $\frac{C}{m^3}$.(observable from Figure-4.1.5)
- *Charge distribution*: Interfacial positive polarity homocharge accumulation near HV-sample regions; effect pronounced at 45 degrees.
- *Charge mobility*: Restricted to interfacial region of HV-sample zone in all cases; this is due to the trapping of charges.
- *Depletion rate*: Neat epoxy accumulates charge faster at 45 degrees. However, the depletion rate is very nominal as compared to acquisition rate of charge.
- *Rate stabilization*: In depletion period, there is a stabilization of rate of depletion at 45° C, after which charges are not removed further.

Outline of methodology of specimen nomenclature & comparison

The samples are henceforth named as, in the following manner-
E-hBN-[Fill grade concentration]-[Alphabet in case of multiple instances of same fill grade]
For instance, there are 2 samples with the 5 volume% concentration of hBN, where the synthesis method differs. They are named as:
E-hBN-5-A, E-hBN-5-B
This similar methodology is used for the rest of the samples. All fill grades are analysed, starting from the relatively low fill grade of 0.2 volume% till the highest fill grade of 5 volume%. For comparison purposes, as demonstrated earlier on, the electrical applied field value of $30\frac{kV}{mm}$ is primarily investigated, at both temperatures.

4.1.2 The 0.2 volume% fill grade group

This fill-grade is represented by 3 samples, named as E-hBN-0.2-A, E-hBN-0.2-B, E-hBN-0.2-C. The contour plots for E-hBN-0.2-A are presented in Figures-4.1.7 & 4.1.8, and observations are made pertaining to charge accumulation behaviour and general dynamics.

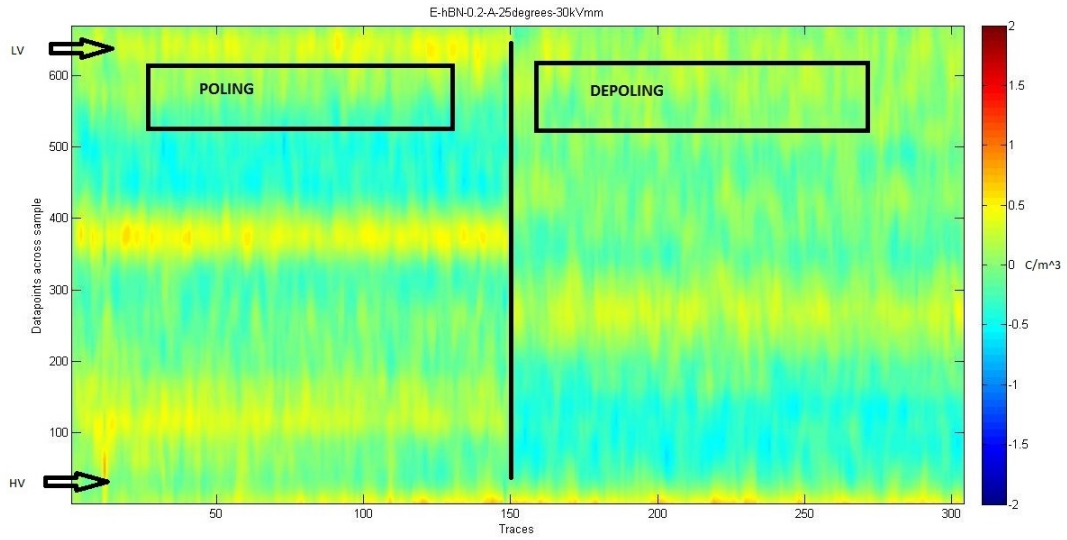

Figure 4.1.7: E-hBN-0.2-A processed signal contour plot, $30\frac{kV}{mm}$, 25 degrees

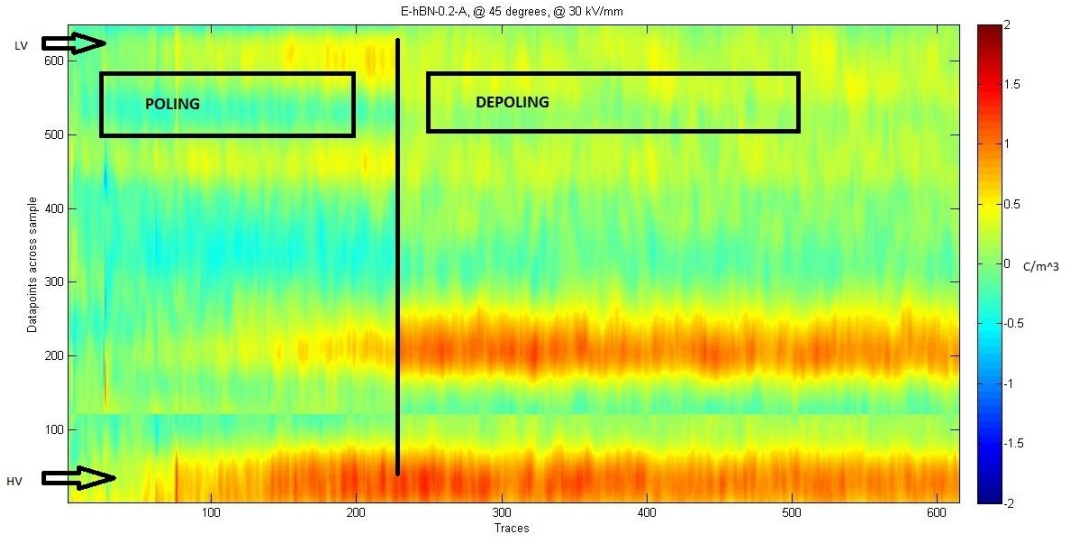

Figure 4.1.8: E-hBN-0.2-A processed signal contour plot, $30\frac{kV}{mm}$, 45 degrees

The effect of temperature is noticed clearly from the Figures-4.1.7 & 4.1.8. Extensive accumulation of positive polarity charge is noticed at an elevated temperature.

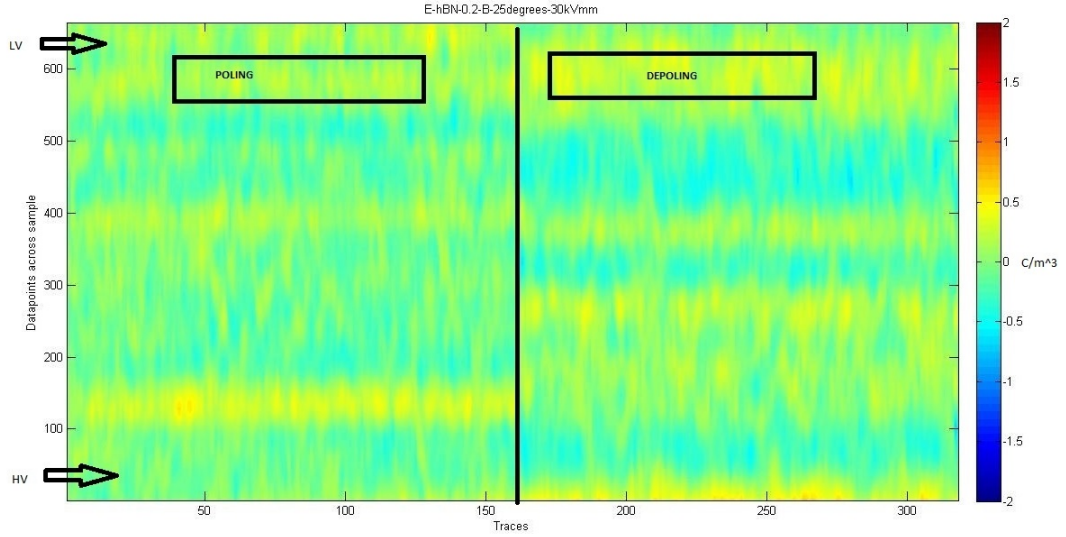

Figure 4.1.9: E-hBN-0.2-B processed signal contour plot, $30\frac{kV}{mm}$, 25 degrees

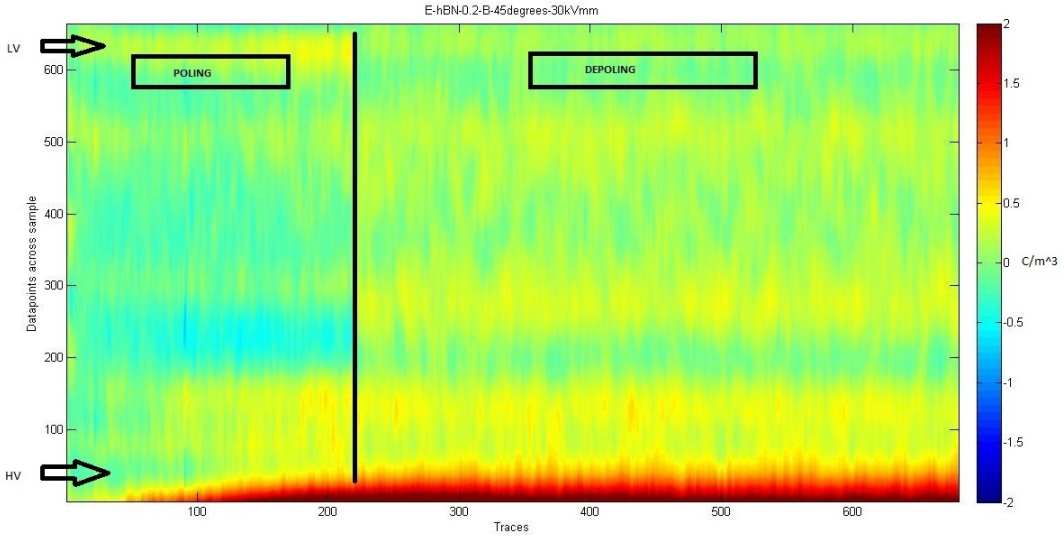

Figure 4.1.10: E-hBN-0.2-B processed signal contour plot, $30\frac{kV}{mm}$, 45 degrees

In figures- 4.1.9 & 4.1.10, the effect of elevated temperature upon charge injection process is clearly noticed.

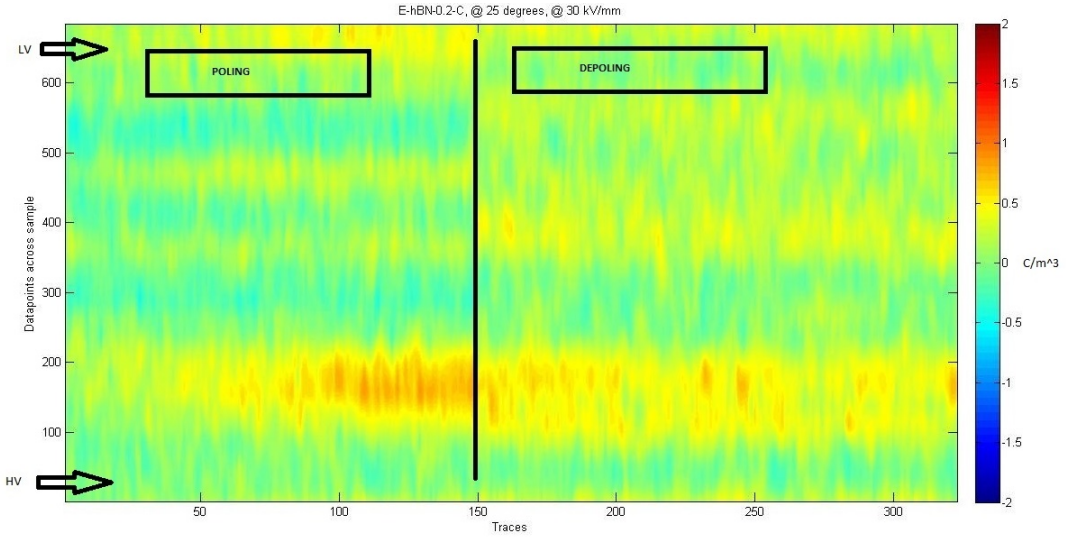

Figure 4.1.11: E-hBN-0.2-C processed signal contour plot, 30$\frac{kV}{mm}$, 25 degrees

Figures-4.1.11 & 4.1.12 depict a different behaviour for sample E-hBN-0.2-C, than the previous 2 samples presented earlier from this filler content group (E-hBN-0.2-A & E-hBN-0.2-B)- since no significant charge injection & accumulation is noticeable even at 45 degrees, though E-hBN-0.2-A & E-hBN-0.2-B having the same filler content depicted noticeable charge injection & subsequent accumulation. (Figures-4.1.7, 4.1.8, 4.1.9 & 4.1.10)

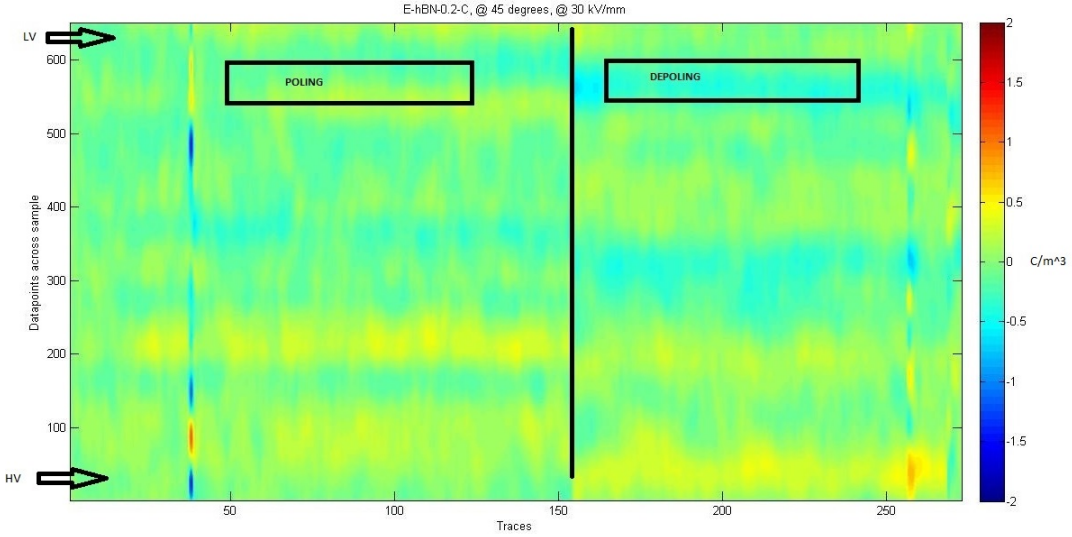

Figure 4.1.12: E-hBN-0.2-C processed signal contour plot, 30$\frac{kV}{mm}$, 45 degrees

At 45 degrees, there is no remarkable space charge development in the sample. In terms of charge accumulation, this be-

haves the best in this group. Detailed graphs depicting charge accumulation & removal characteristics for each test specimen are now presented. The fill-grade group behaviour is summarized finally.

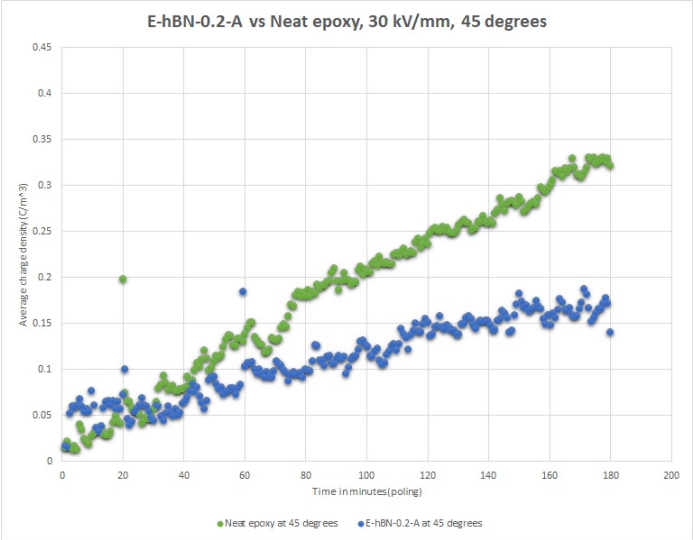

Figure 4.1.13: E-hBN-0.2-A average charge density vs time plot[poling], 30 $\frac{kV}{mm}$, 45 degrees

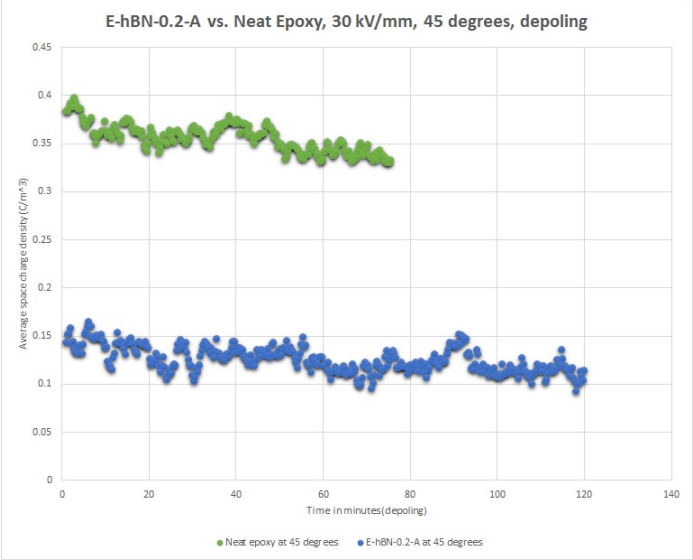

Figure 4.1.14: E-hBN-0.2-A average charge density vs time plot[depoling], 30 $\frac{kV}{mm}$, 45 degrees

Figures-4.1.13 & 4.1.14 preliminarily depict the effect of addition of 0.2 volume% nanofiller to neat epoxy- by a clear reduction in both the accumulation of space charge at the end of the poling period, and the reduced rate of growth of the amount of space charge accumulated by the sample. Of particular interest in Sample E-hBN-0.2-A is the fact, that even at a temperature of 45 degrees, charge injection is gradually suppressed. This is a possible pointer towards the fact that probably the nanoparticles' interaction with the polymer alters trap distribution & trap depth. (especially noticeable around HV-sample interfacial region in Figure-4.1.8, which shows the accumulation of charges after some time of poling, which possibly prevents the further injection of charges)

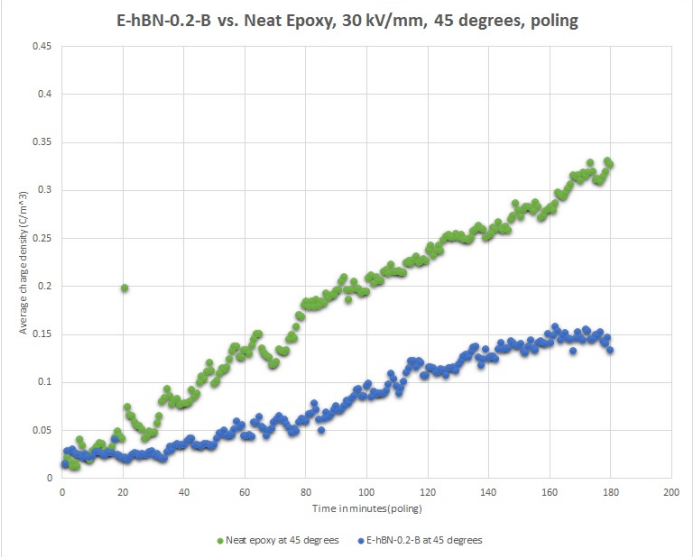

Figure 4.1.15: E-hBN-0.2-B average charge density vs time plot[poling], 30$\frac{kV}{mm}$, 45 degrees

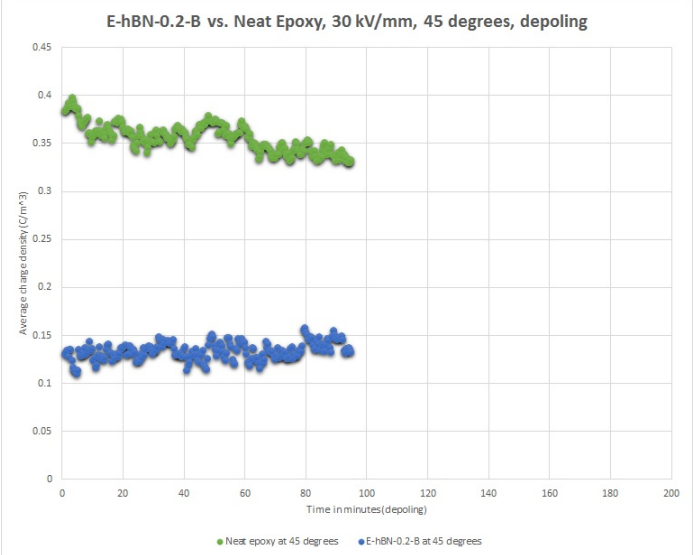

Figure 4.1.16: E-hBN-0.2-B average charge density vs time plot[depoling], 30$\frac{kV}{mm}$, 45 degrees

Figures-4.1.15 & 4.1.16 depict broadly the same situation as E-hBN-0.2-A (Figures-4.1.13 & 4.1.14), but with a difference- The rate of charge growth in the sample is slow, but steady- even though at the end of the poling period, it accumulates lesser charge than neat epoxy. However, it must be mentioned that the rate of charge accumulation in the sample is significantly lesser than the rate of charge accumulation in neat epoxy.

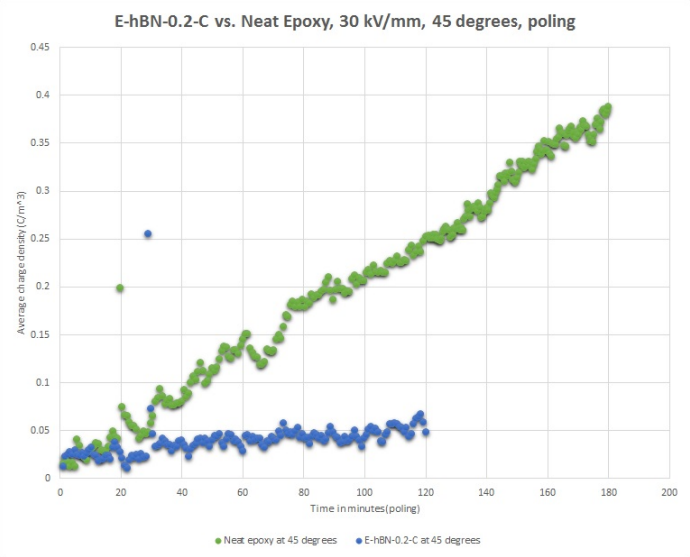

Figure 4.1.17: E-hBN-0.2-C average charge density vs time plot[poling], 30$\frac{kV}{mm}$, 45 degrees

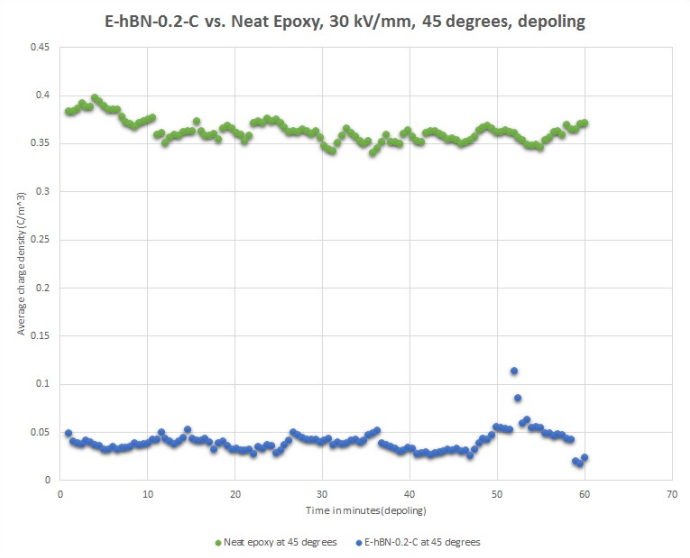

Figure 4.1.18: E-hBN-0.2-C average charge density vs time plot[depoling], 30$\frac{kV}{mm}$, 45 degrees

Figure-4.1.17 & 4.1.18 depict the growth of average space charge density as a function of time for the sample E-hBN-0.2-C; as was previously observed from Figure-4.1.11 & 4.1.12, there is no remarkable charge accumulation in the sample during the poling period- and this fact is corroborated by the very low amount of charge accumulation in the sample with respect to neat epoxy.

A summary of 0.2 volume% filler group behaviour

- *Amount of space charge*: Amount of space charge accumulated the least in Sample E-hBN-0.2-C at 45 degrees, even lesser than other 2 samples of the group. Behaviour of each sample is better at an elevated temperature, w.r.t space charge accumulation in neat epoxy, in the sense that much less amount of charge is accumulated at the end of the poling period. The best performing sample accumulates charge equalling 0.05-0.06 $\frac{C}{m^3}$.
- *Charge distribution*: Interfacial positive polarity homocharge accumulation- nature of charge accumulation is of positive polarity, interfacial in region distribution, for samples E-hBN-0.2-A & E-hBN-0.2-B (HV-Sample interfacial re-

gion). However, sample E-hBN-0.2-C shows no interfacial region charge accumulation at both temperatures. Charge distribution is negligible in sample bulk.

- *Charge mobility*: Restricted to interfacial region of HV-sample zone in all cases; points to introduction of traps close to the interface region.
- *Depletion rate*: The amount of charge accumulated is not very significant with the amount of charge accumulated by neat epoxy during the poling period, hence the depletion rate is not observably rapid.

Sample E-hBN-0.2-C is the best performer from this group, a fact that gains significant importance later on in the text, wherein the dispersion techniques are discussed.

4.1.3 The 0.5 volume% fill grade group

This fill-grade is represented by the solitary sample, E-hBN-0.5. The contour plots are presented in Figures-4.1.19 & 4.1.20, and observations are made pertaining to charge accumulation behaviour and general dynamics.

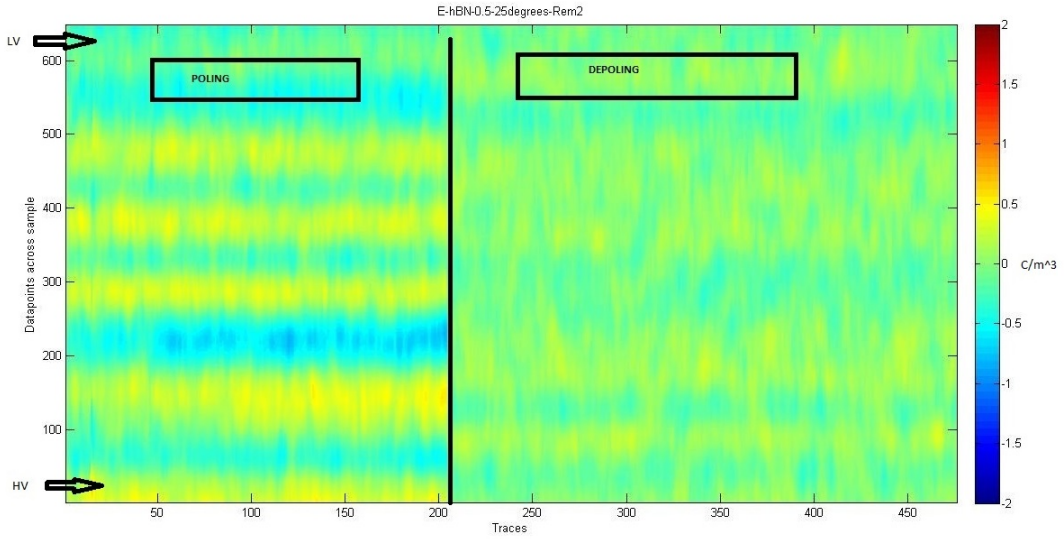

Figure 4.1.19: E-hBN-0.5 processed signal contour plot, 30$\frac{kV}{mm}$, 25 degrees

Figures-4.1.19 & 4.1.20 show an interesting observation, with respect to the increase in the fill-grade from 0.2 volume% till 0.5 volume%- there is no noticeable space charge development in sample E-hBN-0.5 at either 25 or 45 degrees. Even the growth rate of charge in the sample (as can be seen from Figure-4.1.21) is uniformly low (any increase in growth rate is almost negligible) in the poling period. It may be that due to the increase in fill grade, the charge injection suppression mechanism became more effective- charges possibly had to have a higher level of energy to be injected into the sample across the metal-semicon-insulator interface. However, it must be clarified that the charge injection process is not completely nullified- it is more probable that between the two competing mechanisms of charge injection and charge injection suppression, gradually the charge injection suppression mechanism prevails.

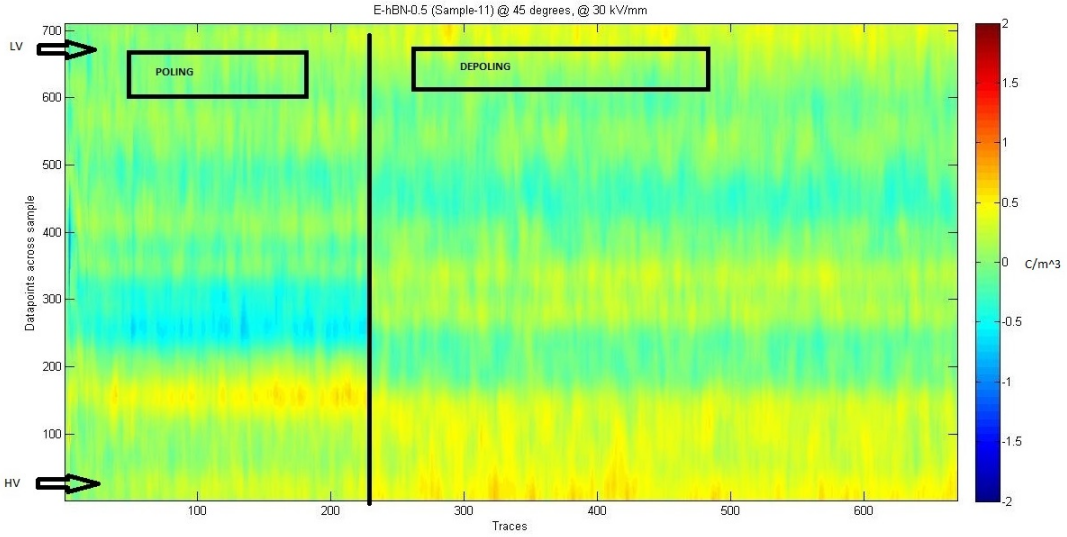

Figure 4.1.20: E-hBN-0.5 processed signal contour plot, $30\frac{kV}{mm}$, 45 degrees

At 25 or 45 degrees, there is no remarkable space charge development in the sample. This is very comparable to the sample E-hBN-0.2-C. Detailed graphs depicting charge accumulation & removal characteristics for the test specimen are now presented in Figures-4.1.21 & 4.1.22. The fill-grade group behaviour is finally summarized.

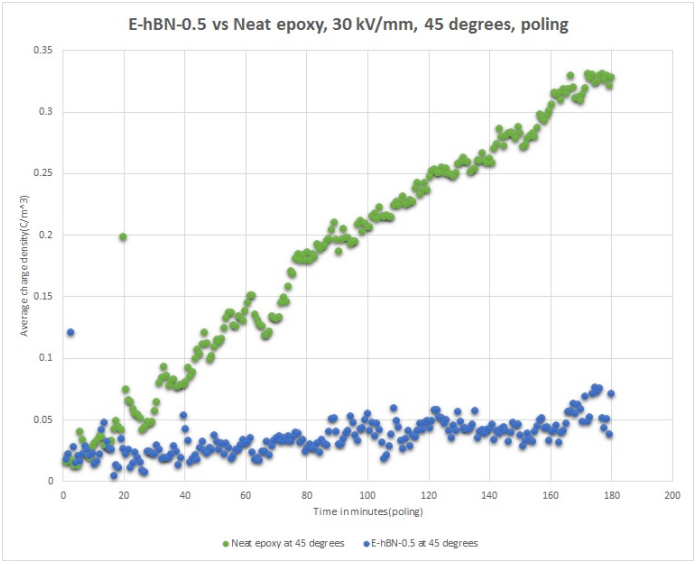

Figure 4.1.21: E-hBN-0.5 average charge density vs time plot[poling], $30\frac{kV}{mm}$, 45 degrees

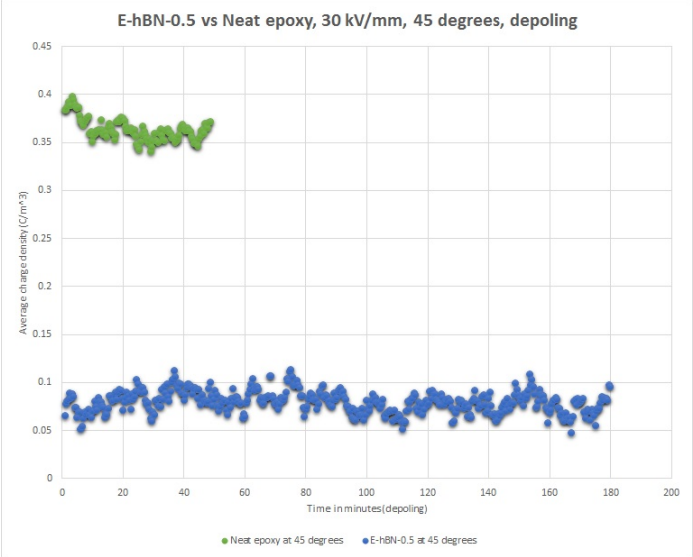

Figure 4.1.22: E-hBN-0.5 average charge density vs time plot[depoling], 30$\frac{kV}{mm}$, 45 degrees

Figures-4.1.21 & 4.1.22 show the poling and depoling trends for the sample E-hBN-0.5- they reveal an interesting fact related to the increase in filler content from 0.2 volume%, with respect to the stabilization of rate of charge accumulation around the midway time mark of poling. (Figure-5.2.11 & 5.2.12, Appendix III, depict this more clearly)

A summary of 0.5 volume% filler group behaviour

- *Amount of space charge*: In terms of charge accumulation, 0.05-0.06 $\frac{C}{m^3}$ at both temperatures. This is very comparable to the sample E-hBN-0.2-C. The behavior enhancement is particularly noticeable at 45 degrees.
- *Charge distribution*: Charge distribution is not really observable near the HV-sample interface, or the LV-sample interfacial region. Negligible in sample bulk.
- *Charge mobility*: Due to the charge accumulation in E-hBN-0.5 being very less as compared to neat epoxy, and also no clear zone of visible accumulation- much cannot be commented on the mobility of charges. However, it is assumed that they are possibly close to the interfacial region, mainly at the HV-sample interface.
- *Depletion rate*: Depletion rate is not very significant in this case, since the amount of charge accumulated at the end of the poling period is very less, as compared with neat epoxy.

The noteworthy fact is that at 25 degrees, charge growth rate stabilizes for the sample E-hBN-0.5 between 40-60 minutes, unlike neat epoxy. The sample behavior is comparable to E-hBN-0.2-C.

4.1.4 The 0.6 volume% fill grade group

This fill-grade is represented by the solitary sample, E-hBN-0.6. The contour plots are presented in Figures-4.1.23 & 4.1.24, and observations are made pertaining to charge accumulation behaviour and general dynamics.

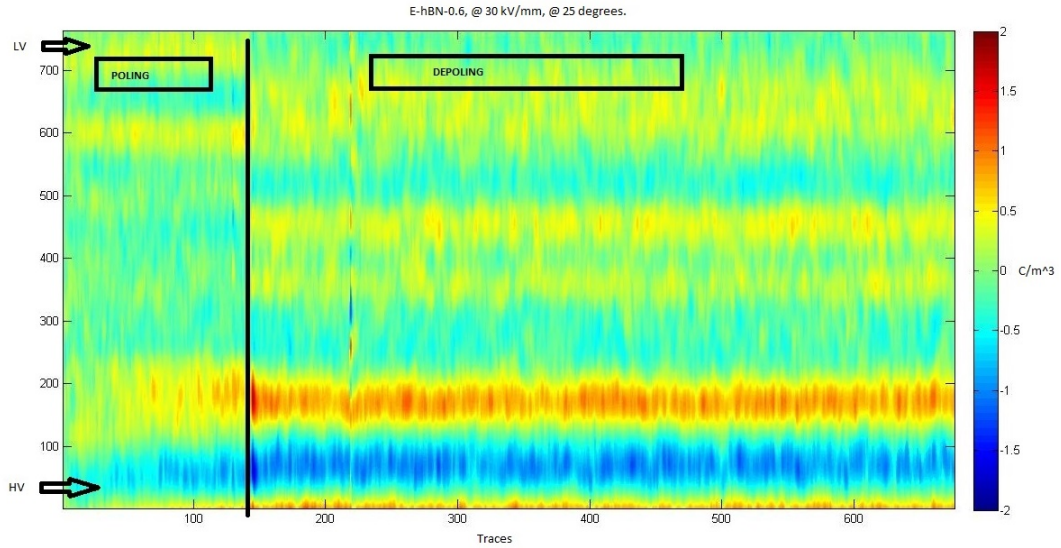

Figure 4.1.23: E-hBN-0.6 processed signal contour plot, $30\frac{kV}{mm}$, 25 degrees

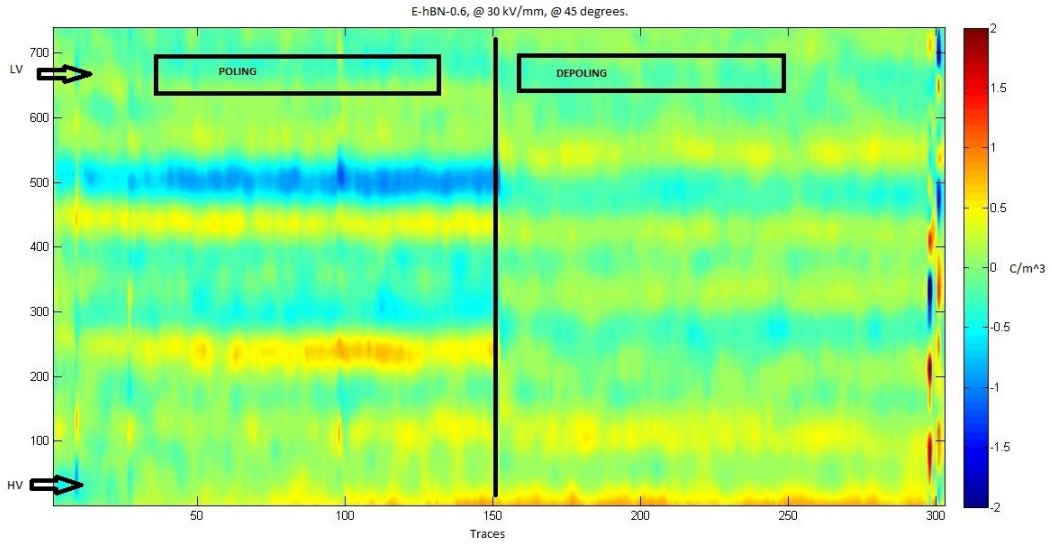

Figure 4.1.24: E-hBN-0.6 processed signal contour plot, $30\frac{kV}{mm}$, 45 degrees

The oscillations (especially at 25 degrees) is mathematically completely processed out while calculating charge accumulated. All over, there is an extremely slight degree of positive charge injection at the HV-sample interfacial region, in both cases. Detailed graphs depicting charge accumulation & removal characteristics for the test specimen are now presented. The fill-grade group behaviour is finally summarized.

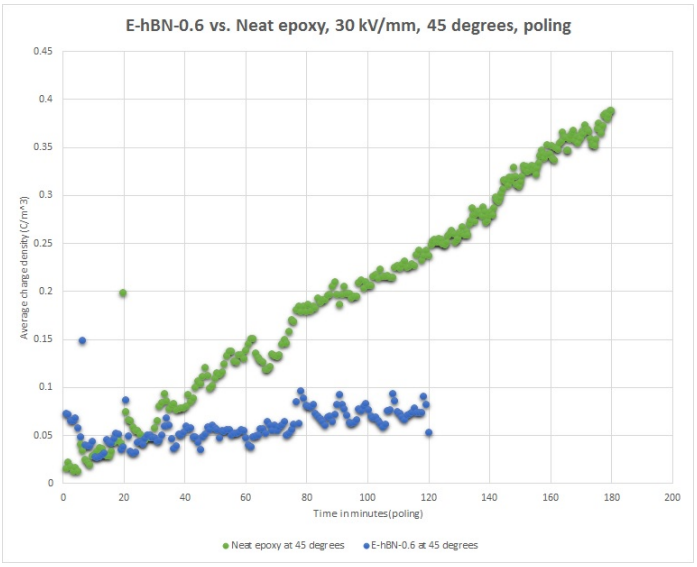

Figure 4.1.25: E-hBN-0.6 average charge density vs time plot[poling], 30$\frac{kV}{mm}$, 45 degrees

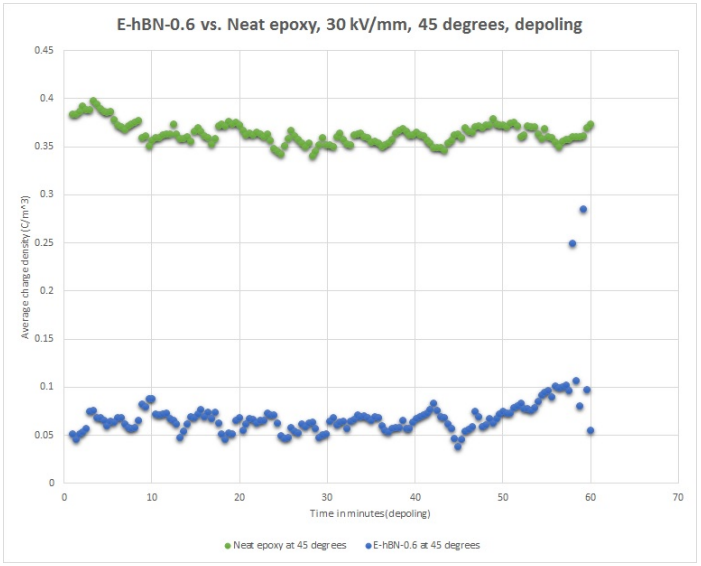

Figure 4.1.26: E-hBN-0.6 average charge density vs time plot[depoling], 30$\frac{kV}{mm}$, 45 degrees

Figures-4.1.25 & 4.1.26 depict the charge accumulation & charge removal characteristics for the sample E-hBN-0.6. It is interesting to note that the slight increase in fill-grade content from 0.5 volume% to 0.6 volume% does not appreciably change space charge dynamics to a great extent.

A summary of 0.6 volume% filler group behaviour

- *Amount of space charge*: In terms of charge accumulation, 0.05-0.1 $\frac{C}{m^3}$ at both temperatures. This is slightly higher than the sample E-hBN-0.5. The behaviour enhancement is particularly noticeable at 45 degrees.
- *Charge distribution*: Charge distribution is again not clearly visible (which, quantitatively is almost negligible as well, with respect to charge accumulation in neat epoxy) at the HV-sample interface. Negligible in sample bulk.
- *Charge mobility*: Due to such low accumulation of charges, and no noticeably visible region of accumulation- conclusion about charge mobility is not feasible. However, it is probably located close to the interfacial region, closer to

the HV-sample interface, since an accumulation therein would explain the subsequent charge injection suppression, due to the presence of homocharge.

- *Depletion rate*: Depletion rate is not very significant, but charge accumulation at end of poling period is lesser when compared to neat epoxy charge behaviour.

Sample behaviour is comparable to E-hBN-0.5 fill grade specimen. However, noteworthy fact is that charge rate stabilization, as was noticed in E-hBN-0.5, is not observed.

4.1.5 The 1.0 volume% fill grade group

This fill-grade is represented by 3 samples, named as E-hBN-1-A, E-hBN-1-B, E-hBN-1-C. The contour plots for E-hBN-1-A are presented in Figures-4.1.27 & 4.1.28, and observations are made pertaining to charge accumulation behaviour and general dynamics.

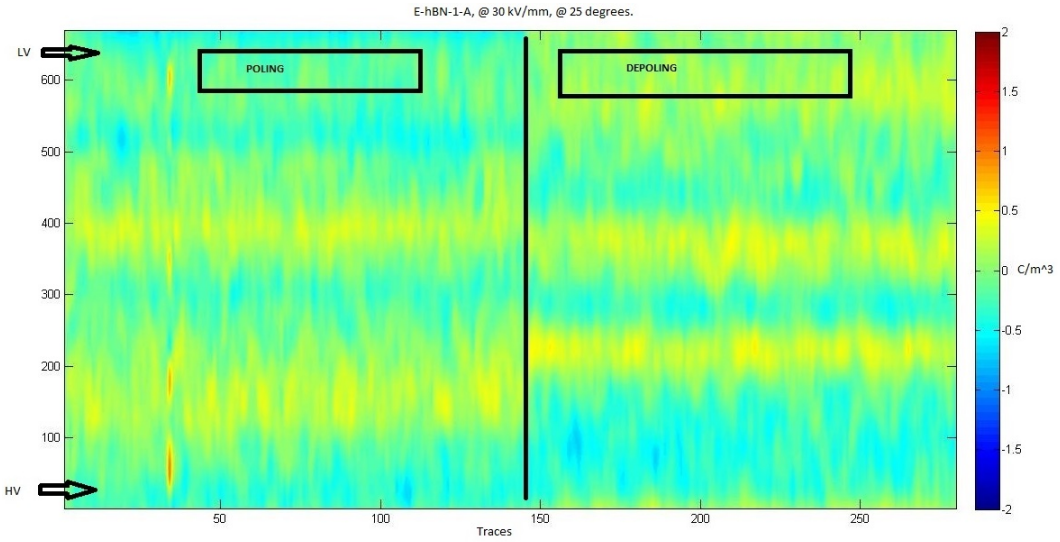

Figure 4.1.27: E-hBN-1-A processed signal contour plot, $30\frac{kV}{mm}$, 25 degrees

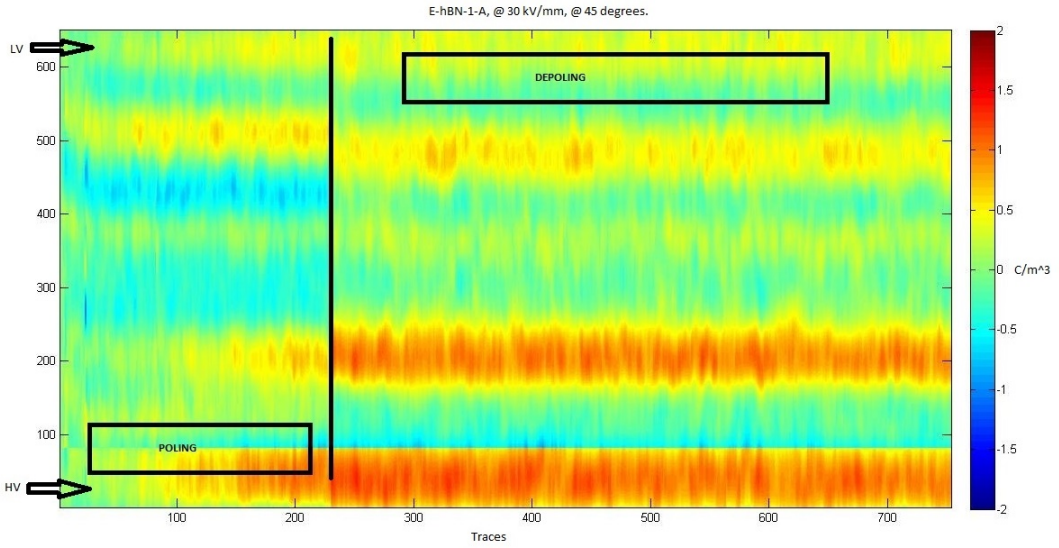

Figure 4.1.28: E-hBN-1-A processed signal contour plot, $30\frac{kV}{mm}$, 45 degrees

The effect of elevated temperature on charge injection process is clearly observed from Figure-4.1.28, with pronounced injection of positive polarity charge from the HV electrode into the sample, with charge accumulation close to the interfacial region. There is no observable charge injection at 25 degrees, as shown in the Figure-4.1.27.
The contour plots for E-hBN-1-B are depicted in Figure-4.1.29 & 4.1.30.

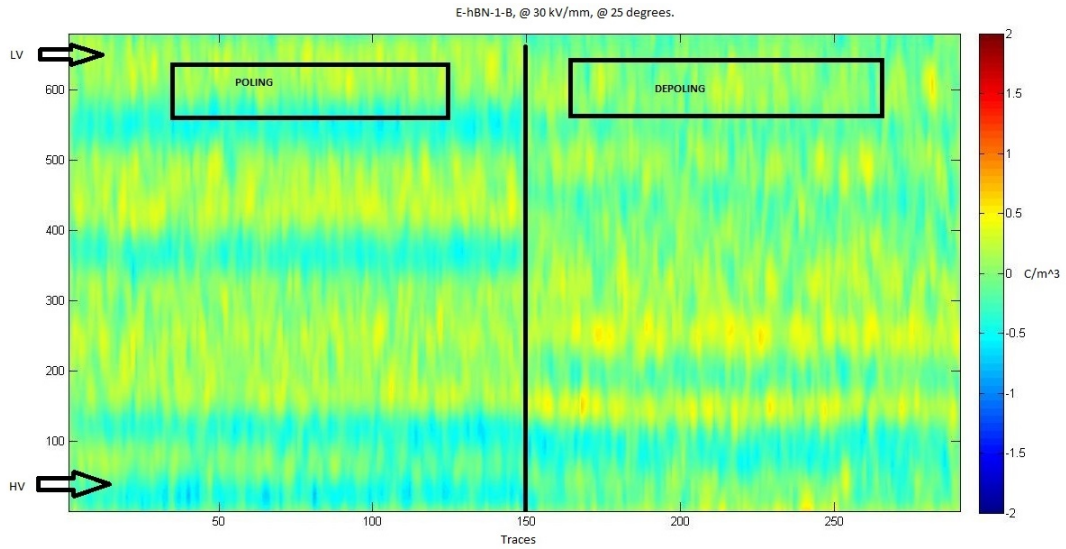

Figure 4.1.29: E-hBN-1-B processed signal contour plot, $30\frac{kV}{mm}$, 25 degrees

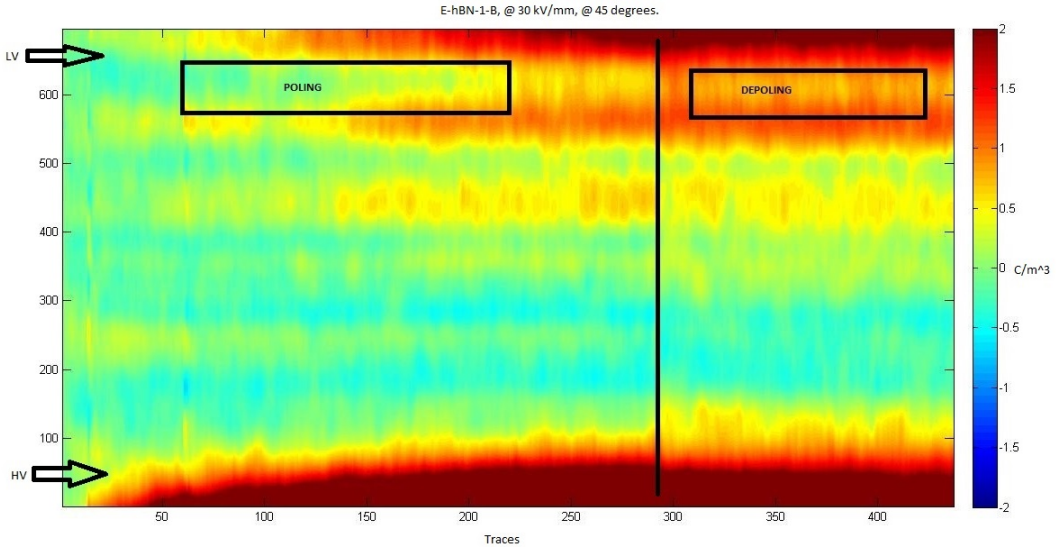

Figure 4.1.30: E-hBN-1-B processed signal contour plot, $30\frac{kV}{mm}$, 45 degrees

Once again, the effect of elevated temperature on charge injection processes is clearly noticed in Figure-4.1.29 & 4.1.30, with pronounced charge injection of positive polarity at HV-sample interface. This specimen was measured thrice at 45 degrees, clearly shows enhanced migration of positive charges towards Earth-sample interfacial zone. This effect cannot be fully explained without further investigation, since this same observation is not present for the other specimens in this fill-grade group.

The contour plots for E-hBN-1-C are depicted in Figure-4.1.31 & 4.1.32.

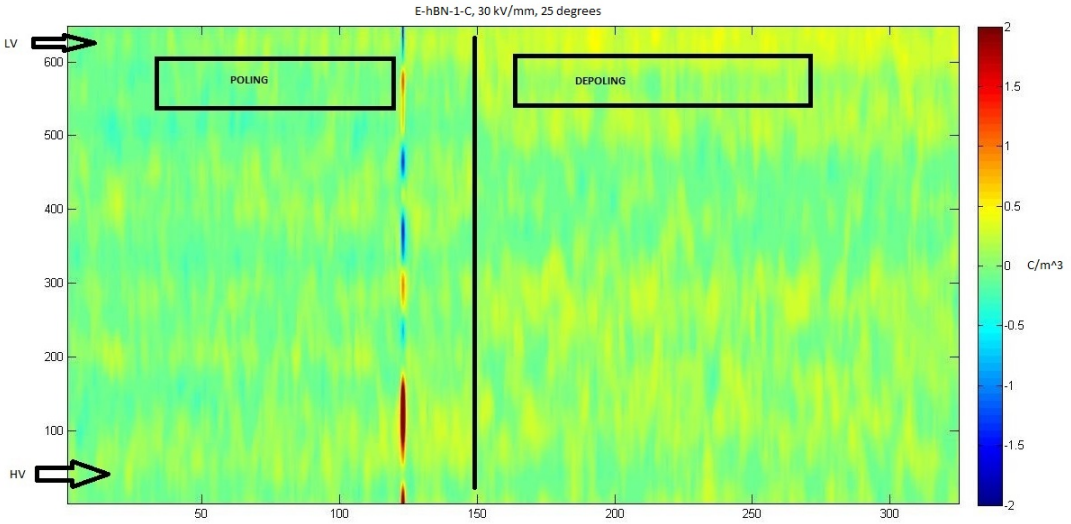

Figure 4.1.31: E-hBN-1-C processed signal contour plot, $30\frac{kV}{mm}$, 25 degrees

If the set of figures (Figures-4.1.19 & 4.1.20 with Figures-4.1.31 & 4.1.32) are compared, it is seen that charge dynamics is similar at both temperatures. This is an important observation, since it reveals an important fact: Even the fill-grade increased across 0.5 volume% till 1 volume% (double), the charge suppression mechanism was observable even at the lower fill grade effectively. The increase in fill grade did not drastically change accumulation behaviour, and in both cases, charge accumulation behaviour was improved. The slight difference in amount of charge finally accumulated at the end of the poling period is observable from Figures-4.1.21 & 4.1.37), wherein it is noticed that in case of the sample E-hBN-1-C, slightly higher amount of charge is accumulated.

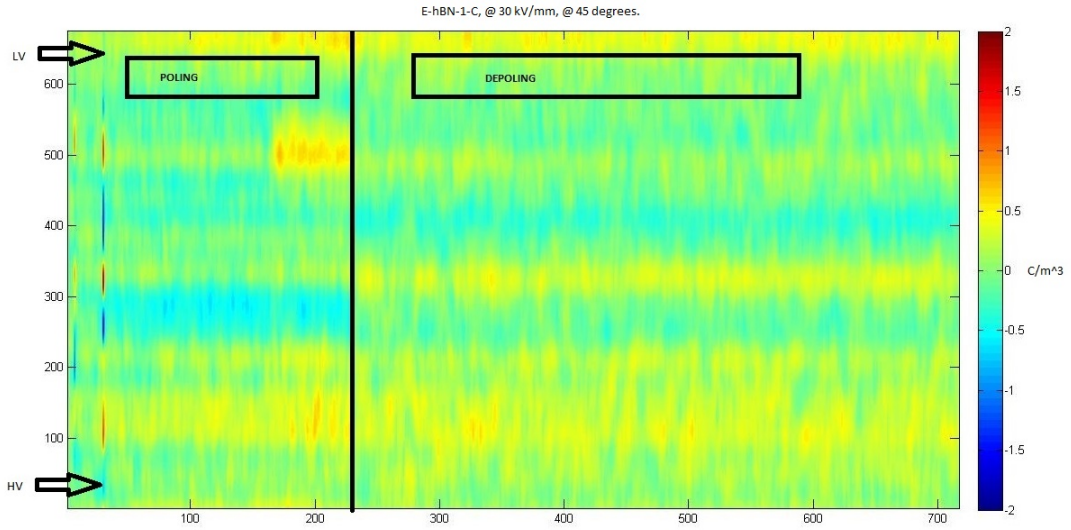

Figure 4.1.32: E-hBN-1-C processed signal contour plot, $30\frac{kV}{mm}$, 45 degrees

At 25 or 45 degrees, there is no remarkable space charge development in the sample, since charge injection seems to be suppressed to a great extent. In terms of charge accumulation, this behaves the best in this group. Detailed graphs depicting charge accumulation & removal characteristics for each test specimen are also presented here. The fill-grade group behaviour is summarized finally.

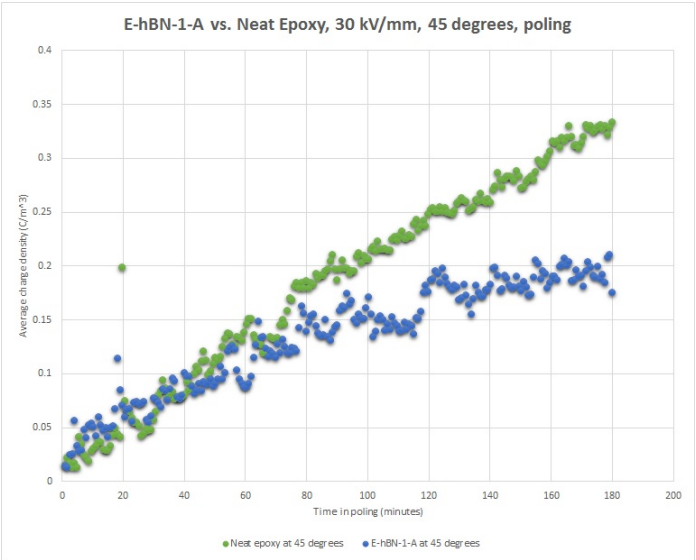

Figure 4.1.33: E-hBN-1-A average charge density vs time plot[poling], $30\frac{kV}{mm}$, 45 degrees

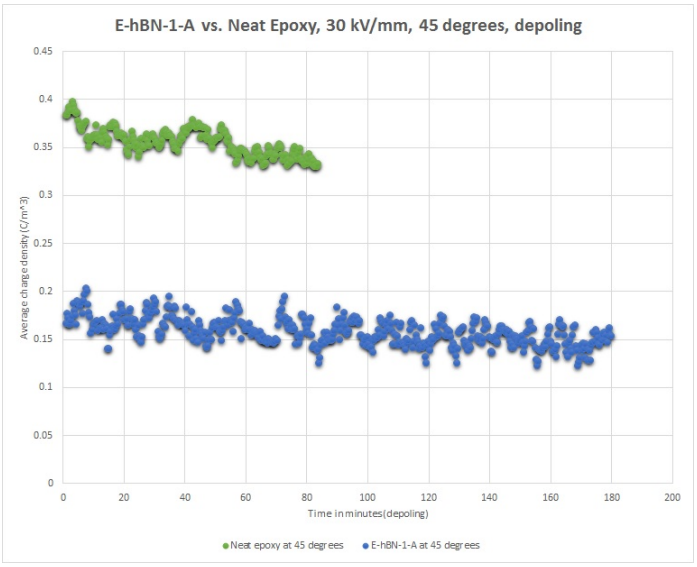

Figure 4.1.34: E-hBN-1-A average charge density vs time plot[depoling], 30$\frac{kV}{mm}$, 45 degrees

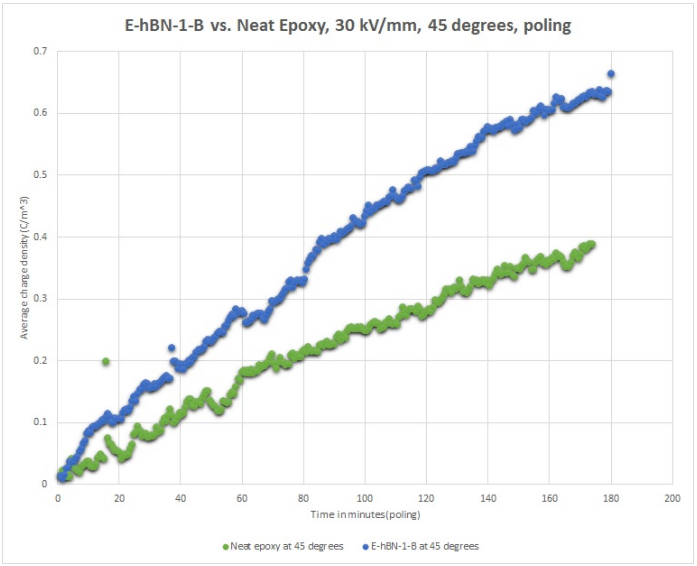

Figure 4.1.35: E-hBN-1-B average charge density vs time plot[poling], 30$\frac{kV}{mm}$, 45 degrees

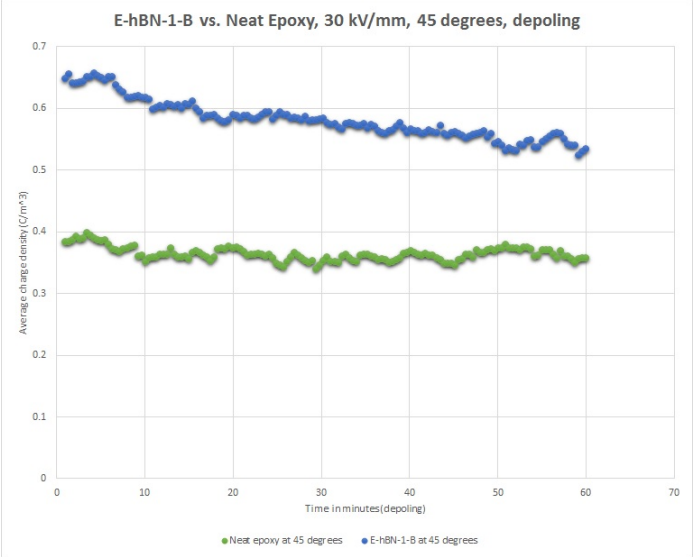

Figure 4.1.36: E-hBN-1-B average charge density vs time plot[depoling], 30$\frac{kV}{mm}$, 45 degrees

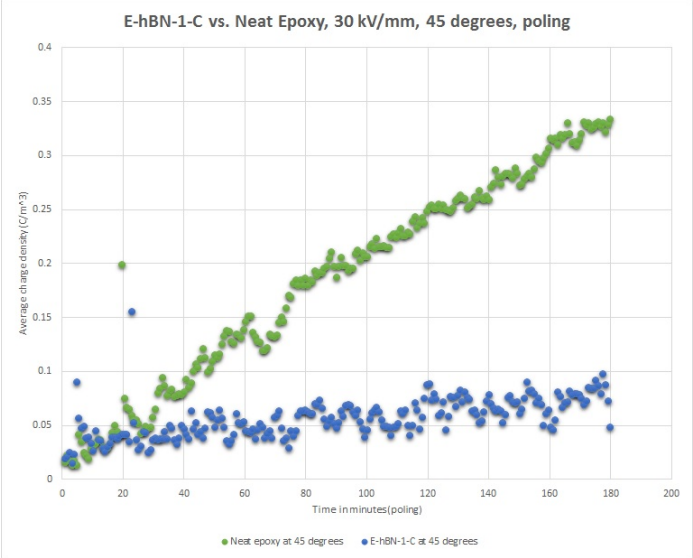

Figure 4.1.37: E-hBN-1-C average charge density vs time plot[poling], 30$\frac{kV}{mm}$, 45 degrees

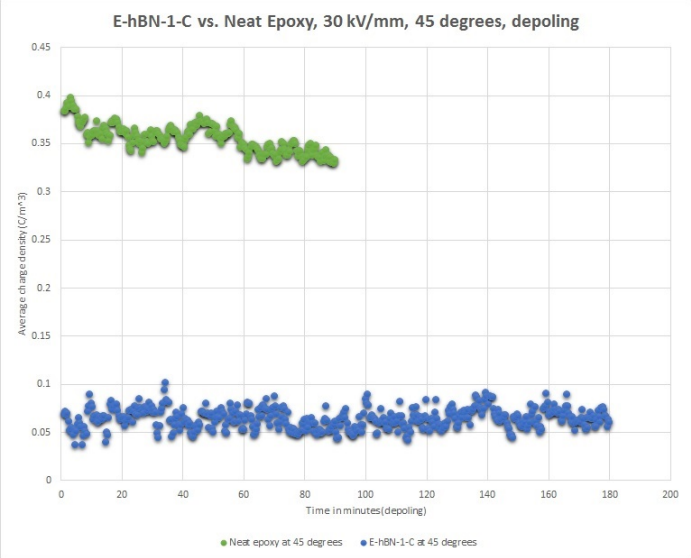

Figure 4.1.38: E-hBN-1-C average charge density vs time plot[depoling], $30\frac{kV}{mm}$, 45 degrees

Figures-4.1.33 & 4.1.34 depict the charge accumulation and removal characteristics for sample E-hBN-1-A. It is interesting to note that a subsequent increase in fill-grade from 0.6 volume% previously presented no longer results in as low a space charge accumulation as that of E-hBN-0.6 (it is however still lower than the space charge amount accumulated for neat epoxy). Figures-4.1.35 & 4.1.36 depict the charge accumulation & removal characteristics for sample E-hBN-1-B, and this presents some rather unexpected results, both in terms of charge accumulation and charge dynamics. Figures-4.1.37 & 4.1.38 depict the charge accumulation & removal characteristics for sample E-hBN-1-C- a behaviour which is once again strikingly similar to the similar characteristics exhibited by samples E-hBN-0.5 & E-hBN-0.6. (Figures-4.1.21 & 4.1.25)

A summary of 1 volume% filler group behaviour

- *Amount of space charge*: In terms of charge accumulation, 0.05-0.6 $\frac{C}{m^3}$ at both temperatures. The amount of space charge differs in all 3 cases- with the highest for E-hBN-1-B at 45 degrees $(0.6\frac{C}{m^3})$ to the lowest for E-hBN-1-C at 45 degrees $(0.05\frac{C}{m^3})$.
- *Charge distribution*: Charge distribution is predominantly positive interfacial charge at the HV-sample interface, for specimens E-hBN-1-A & E-hBN-1-B.
- *Charge mobility*: Charge mobility appears to be increased in case of specimen E-hBN-1-B, especially noticeable in the migration of positive polarity charges towards the Earth electrode, from the HV electrode. The accumulation of homocharges at the interfacial region is still noticeable for specimens E-hBN-1-A & E-hBN-1-B. However, sample E-hBN-1-C does not demonstrate any noticeable charge accumulation.
- *Depletion rate*: Depletion rates are improved than Neat epoxy at 45 degrees, for specimens E-hBN-1-A & E-hBN-1-B, with reference to Figure-4.1.34 & Figure-4.1.36.

4.1.6 The 5 volume% fill grade group

This is the highest fill-grade and final group. This fill-grade is represented by 2 samples, named as E-hBN-5-A & E-hBN-5-B. The contour plots for E-hBN-5-A are presented in Figure-4.1.39 & 4.1.40, and observations are made pertaining to charge

accumulation behaviour and general dynamics.

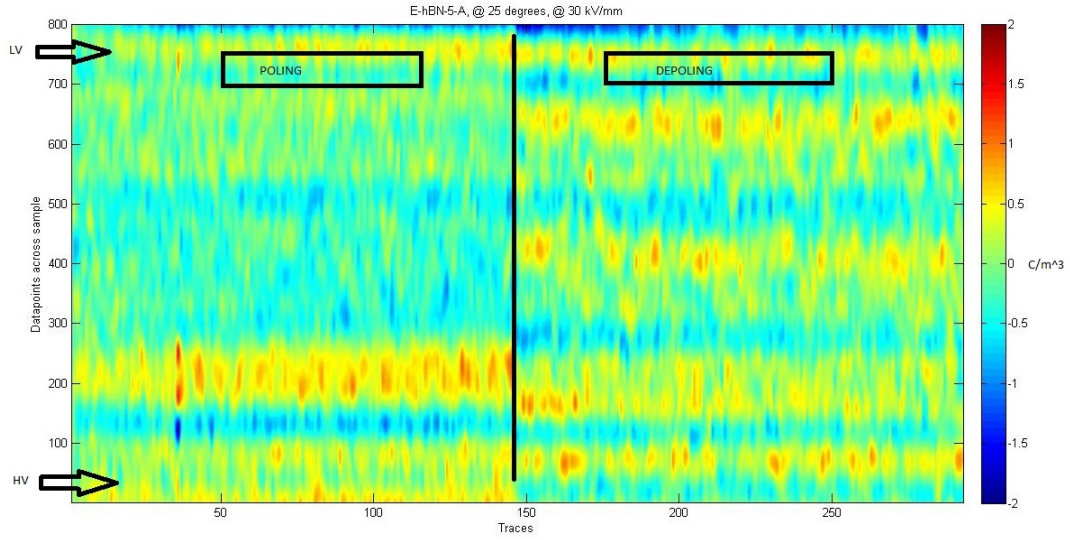

Figure 4.1.39: E-hBN-5-A processed signal contour plot, $30\frac{kV}{mm}$, 25 degrees

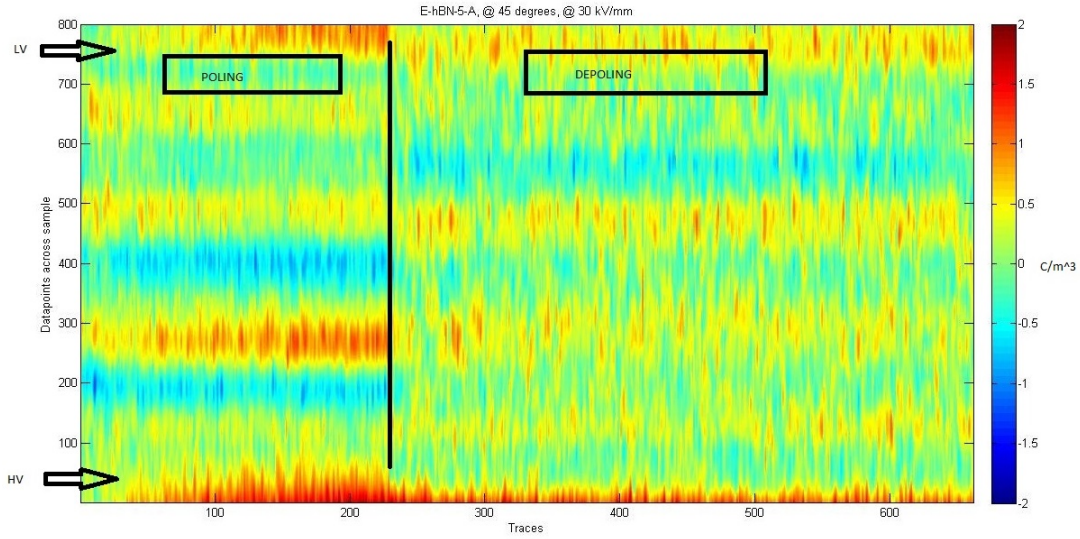

Figure 4.1.40: E-hBN-5-A processed signal contour plot, $30\frac{kV}{mm}$, 45 degrees

Once again, from Figure-4.1.40, it can be observed that there is a higher degree of charge injection from the HV electrode at an elevated temperature and subsequent accumulation close to the interfacial region of the HV electrode.
The contour plots for E-hBN-5-B are presented in Figure-4.1.41 & Figure-4.1.42 respectively.

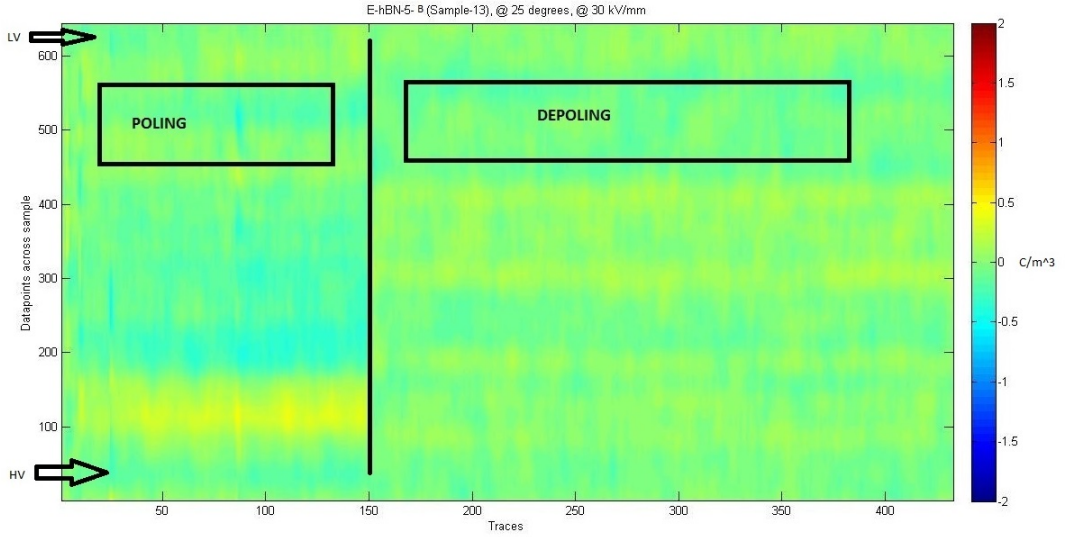

Figure 4.1.41: E-hBN-5-B processed signal contour plot, $30\frac{kV}{mm}$, 25 degrees

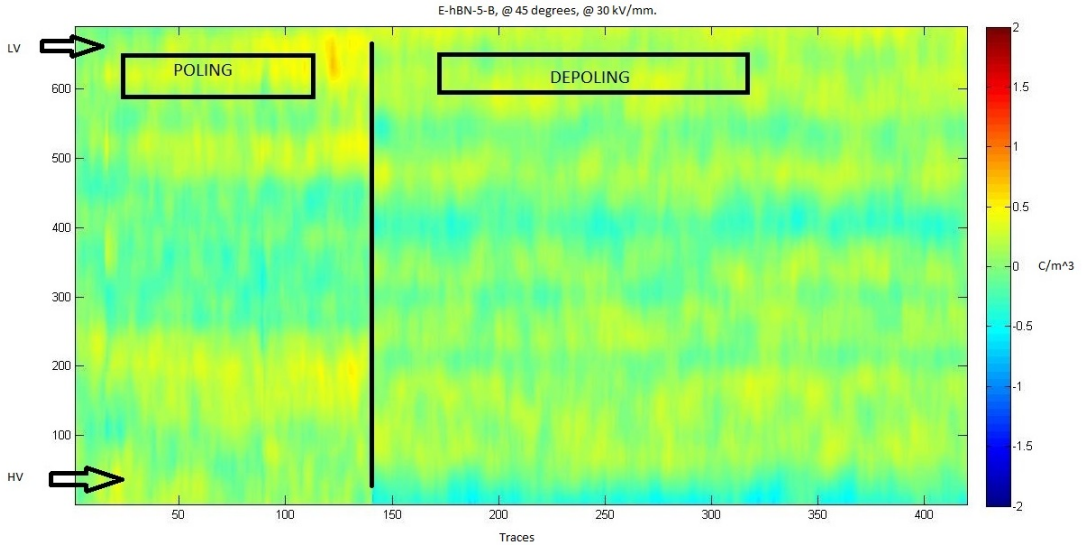

Figure 4.1.42: E-hBN-5-B processed signal contour plot, $30\frac{kV}{mm}$, 45 degrees

Interestingly, amount of space charge accumulated is exactly similar to E-hBN-0.2-C, $0.05\frac{C}{m^3}$. This is the superior performer from the 5 volume% group. This sample shows improved performance even at 25 degrees, as well as 45 degrees (the contour plots in Figures-4.1.41 & 4.1.42 reveal effective charge injection suppression at both temperatures)- superior to Sample E-hBN-5-A, from the 5 volume% filler group.

Detailed graphs depicting charge accumulation & removal characteristics for each test specimen are also presented in Figures-

4.1.43, 4.1.44, 4.1.45 & 4.1.46. Figures-4.1.43 & 4.1.44 depict the charge accumulation & removal characteristics for sample E-hBN-5-A. It is observable from the presented figures in 4.1.43 and 4.1.44 that the charge accumulation characteristics do not change significantly over the rapid increase in fill grade from 1 volume% till 5 volume%. (though, for sample E-hBN-5-A, the final charge accumulation seems to be higher in magnitude than E-hBN-0.5 and E-hBN-0.6, but considerably lesser than charge accumulation in neat epoxy) Figures-4.1.45 & 4.1.46 depict the charge accumulation & removal characteristics for sample E-hBN-5-B. This sample (E-hBN-5-B) shows similar charge accumulation characteristics to E-hBN-0.5 & E-hBN-0.6 (Figures- 4.1.21 & 4.1.25) The fill-grade group behaviour is summarized finally.

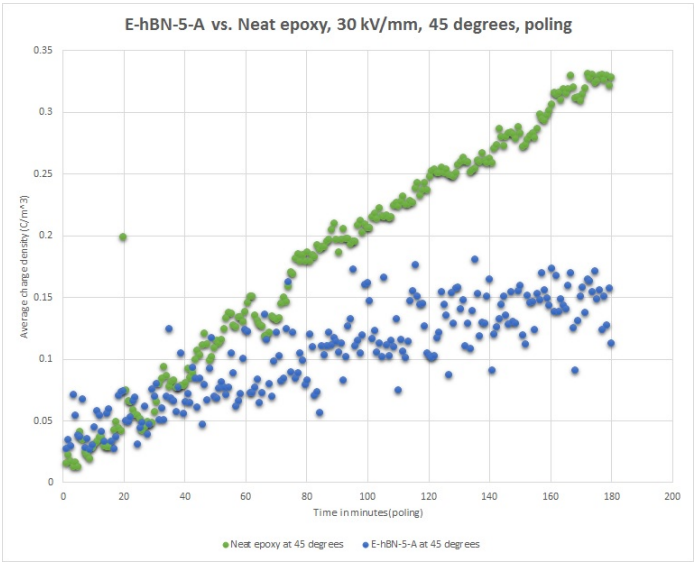

Figure 4.1.43: E-hBN-5-A average charge density vs time plot[poling], 30$\frac{kV}{mm}$, 45 degrees

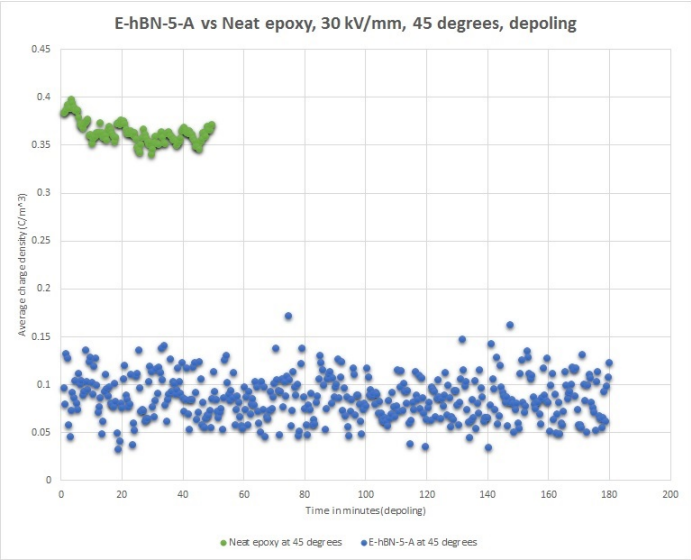

Figure 4.1.44: E-hBN-5-A average charge density vs time plot[depoling], 30$\frac{kV}{mm}$, 45 degrees

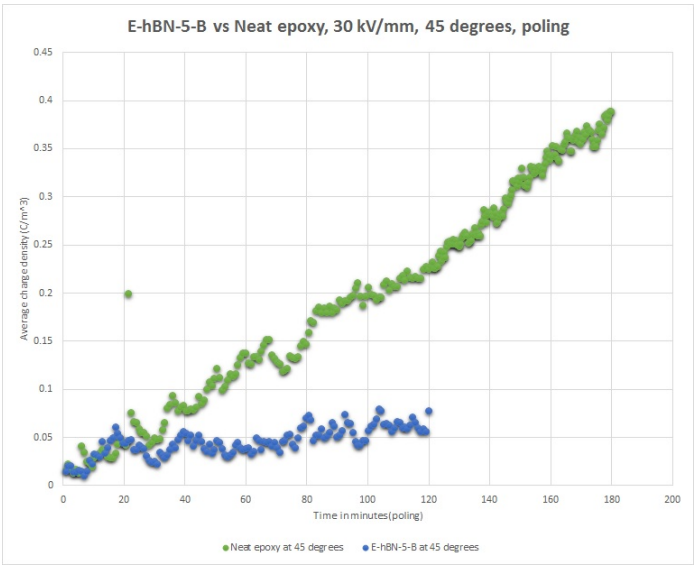

Figure 4.1.45: E-hBN-5-B average charge density vs time plot[poling], 30$\frac{kV}{mm}$, 45 degrees

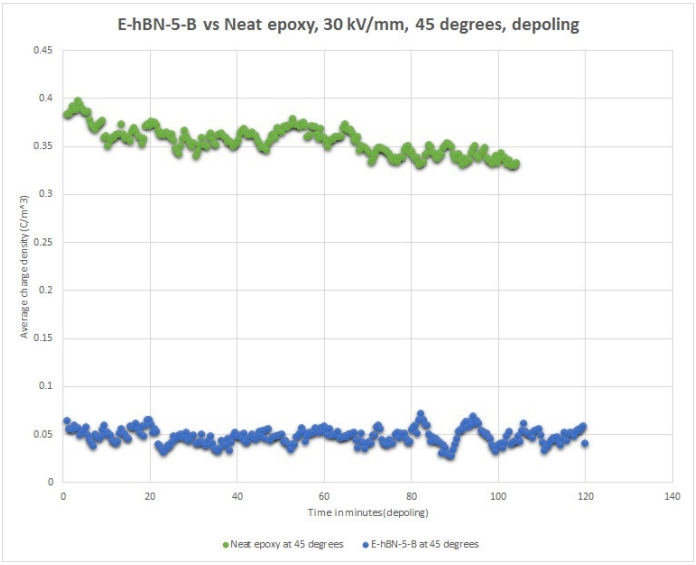

Figure 4.1.46: E-hBN-5-B average charge density vs time plot[depoling], 30$\frac{kV}{mm}$, 45 degrees

A summary of 5 volume% filler group behaviour

This group shows interesting and similar dynamics to the lower fill-grade samples. Better charge accumulation behaviour than 1 volume% filler group.

- *Amount of space charge*: Charge accumulation is between 0.02-0.05 $\frac{C}{m^3}$.
- *Charge distribution*: Charge distribution is predominantly positive interfacial charge at the HV-sample interface; very little charge injection observed in case of latter sample E-hBN-5-B.

- *Charge mobility*: Charge distribution is again negligible in the sample insulation bulk, charge mobility is not noticed in a remarkable fashion.
- *Depletion rate*: The depletion rates are not very fast, but the amount of space charge accumulation at the end of the poling period is lesser compared to neat epoxy as well. Possible introduction of traps in the material, restricts the charges from liberating themselves, since they do not possess enough energy.

Sample E-hBN-5-B shows superior performance than E-hBN-5-A. **In conclusion, it is observed that all the best performing samples have similar behavioral patterns, and even exact amounts of space charge accumulation.** A broad purview of all the filler groups presents and supports this statement.

4.2 Analysis of effect of filler content on nanocomposites

An epoxy nanocomposite system can display high permittivity at low frequencies and high electrical conductivities with low percolation thresholds when conducting fillers are dispersed[61]. Shapes and sizes of nano-fillers, their contents, inter-filler distances, interfacial morphology, and mesoscopic structures are all important parameters to characterize polymer nanocomposites. The main effect of increasing filler content (thermal conductivity being the primary reason), with superior performance exhibited by some samples in this research work, has been two-fold, broadly speaking. The primary observation has been a reduction in amount of the space charge accumulated over similar poling times, and secondarily, it has been the stabilization of the growth rate during poling period for some fill-grades.(As seen for samples E-hBN-0.2-C, E-hBN-0.5 for growth rate stabilization; Samples E-hBN-0.2-C, E-hBN-0.5, E-hBN-0.6, E-hBN-1-C, E-hBN-5-B show lesser amounts of space charge accumulation with respect to neat epoxy)
The extent of polymer chain immobility in nanocomposites is a function of the filler concentration. In the simplest situation, the bonding of a polymer to filler can be expected to give a layer of *'immobilized'* polymer. The size of this layer is critical to the global properties (electrical, mechanical and thermal) of the composite and it is this interaction zone that is key to determining the behaviour. As has been well established in research literature, [8],[6], in nanocomposite systems, there is a high probability that strong interface dynamics play a major role at relatively lower fill grades, involving the large volume fraction of interfaces and polymer chain entanglements, inhibit the motion of charge carriers, and these charge carriers injected from the metal-semicon-insulator interface are trapped close to the same zone. This results in a prevention of further charges being injected into the PNC. At higher fill grades, it is possible that the effect of the beneficial *immobilized* layers of polymer is obscured by the higher relative permittivity of the filler. Also, for nanocomposites with higher filler loading, water uptake plays a crucial role as well, since nano-particles are vulnerable to moisture, due to their high surface-to-volume ratio & hydrophilic nature[90].
Some explanations can be advanced for the findings in this research work. The depoling trends observable from the contour plots, all reveal one salient characteristic: **There is not much removal of charges during the depoling period, which can indicate trapped charges close to the interfacial zone where accumulation had taken place, with insufficient energy to liberate themselves.** Also, of interest, is the fact that neat epoxy has a relatively faster rate of depoling than most of the nanocomposites- this indicates to *possible band structure alteration by the presence of nanocomposites, and subsequently different energy levels of traps & recombination sites.* This fact is well-supported by existing literature [63,64]and several other works. Thus, this alteration of band structure can in turn necessitate the injection of higher energy-possessed charges into the insulator from the metal-semicon interface- failing to gain enough energy, lesser charges are injected, and those that are injected get trapped close to the interface, and lower the electric field distribution around that region. This in turn, leads to lesser injection across the electrode-insulator interface, and consequently, lesser amount of space charge. Many studies have pointed out that the introduction of inorganic nanoparticles into polymer would bring in a large amount of deep trap sites, which form barriers to the injection of space charge from electrodes and decrease the local electric field distortion in the bulk[64]. The results presented here support this statement.
The second of our clues consists of the stabilization of poling growth rate of space charge, observed in some of the specimens- this could have a two pronged explanation. Primarily, it can be attributed to all the accumulation of homocharges (posi-

tive polarity charges) at the injection electrode-semicon-insulator interface, after initial injection and subsequent trapping, in which low mobility of transport of charges also plays a factor. Secondarily, it can point towards the possible introduction of trap sites close to the interfacial region, which when filled up by the charges injected into the sample across the HV electrode-semicon-insulator interface, can potentially block the further injection of charges, by effectively raising the barrier potential. Authors have proposed that the filler added to base resin acts as an *"induced dipole"* under DC electric field and it works as a trap site[65]. This might explain that the introduction of such sites may lead to the alteration of band structure of the nanocomposites, as discussed in the previous paragraph.

The final of our clues lies in the fact that for all the relatively superior performers ascertained from space charge measurements, there is strikingly little difference in the electrical behaviour. As has been pointed out, an increase in filler loading from 0.2 volume% till a 5-fold increase upto 1 volume%, followed by a further increase in fill grade loading, again by a factor of 5, till the highest concentration of 5 volume% should introduce an enormous increase in effective surface area of the nanoparticles, as well as *increase interaction zones' area*[26]- an effect which should have had a remarkable effect upon the specimen behaviour. But, the observations presented herein in this research work do not reveal such a fact. It is known that the morphology of a polymer can be modifed by nano-fillers, due to the high aspect ratio, so that the mechanical, thermal, and electrical properties of the polymer could be affected significantly by the introduction of nano-fillers[66]. This points towards the fact that since the samples tested in this research work (especially the ones that come from the best performing technique, the Nanomizer technique) possess good dispersion and distribution of nanoparticles, which can lead to the re-organization of a larger volume of the polymer matrix, causing the immobilization of a larger number of polymer side chains. However, space charge accumulation behaviour and dielectric response of a nanocomposite depends on competing processes (such as interfacial polarization, effect of humidity which influences the amount of water uptake)- hence, filler concentration possibly exhibits more marked differences across different techniques for nanoparticle distribution.

Finally, it may be proposed that polymer morphology is probably altered by immobile layers formation by nano-particles in the epoxy matrix [87], hence all the processes play an important role in determining the space charge behaviour and also effective composite permittivity of the composites- research is being conducted as of present, to determine the various factors at play.

The effect of fill grade upon nanocomposites can be summarized as:

- Introduction of filler content into epoxy material, as per the fill-grades in this work, exhibits an improved performance with respect to space charge accumulation. (leading to much lesser accumulation of space charge in general; with the exception of a singular sample, E-hBN-1-B) Suppression of charge injection is one of the noticeable factors, at the elevated (with respect to 25 degrees Celsius)temperature of 45 degrees Celsius- which points to the introduction of traps close to the HV-semicon-insulator interface (noticeable from the observations presented previously), leading to the rapid accumulation of 'homocharges', and prevention of further charge being injected into the sample.

- The introduction of filler content into epoxy material affects the charge injection mechanism-for all fill-grades the rate of accumulation of space charge is slowed down appreciably.(except sample E-hBN-1-B, a point in case wherein the other two samples from the same fill grade group E-hBN-1-A & E-hBN-1-C are in agreement with the proposed statement)

- Increasing fill grade from 0.2 volume% till 1 volume% shows a minor increase in accumulated space charge within the nanocomposite, while the further increase in fill grade from 1 volume% till 5 volume% shows a decrease in accumulated space charge within the specimen. However, a point must be made that since these differences are not appreciably large, their behaviour may be considered to be qualitatively similar. It may be possible that the introduction of nanoparticles into the polymer matrix re-organizes morphology of the chains in such a fashion, that increasing filler content somehow leads to a more uniform arrangement of a 'nano-filler-layer' across the matrix, in comparison to lower fill grades. Since the filler grade groups usually exhibit similar charge dynamics & accumulation rates, even though an increase in filler grade happens steadily, the slight differences in final amounts of charge accumulation may reveal the fact that with possible increase in fill grade, the depths of the traps introduced in the material may be

more(*deeper*) than the depths of the traps(*shallower*) introduced in the material at relatively lower loadings. It may be possible that the number of traps do not significantly increase upon increase in filler loading, but the depths & distribution of the traps change. Along with the fact that polymer chain morphology, and possible alteration of band structure may happen- a multiplicity of factors influences the exact effect of increase in fill-grade. It may be interesting to conduct measurements that investigate transient phenomena that might occur during space charge accumulation across a range of samples with increasing filler grade content- growth rate stabilization time can possibly reveal a pointer towards the complex charge dynamics at play here.

However, with the advancement of these possible observations, the stage is set to move on to the next section and investigate the effect of dispersion techniques in this work.

4.3 The effect of nano-particle distribution upon space charge behaviour

"The synthesis method of nanocomposites directly influences the particle distribution and dispersion with the material, hence has a significant effect on their dielectric properties"[12,55]. It has been previously established in research literature that a good dispersion of nano-particles in the host material (the epoxy matrix herein) ensures no agglomeration of particles, and thus prevents unwanted effects upon electrical behaviour of the nanocomposite. Interfacial phenomena depend on filler dispersion in the nanocomposite, and according to various proposed theoretical models discussed earlier- agglomerated or clustered nano-filler locations due to synthesis techniques result in non-uniform distribution, with differing inter-particle distances, which result in uneven forces application- and can lead to unexpected accumulations of space charge and other related phenomena. As has been stressed earlier, interfacial effects are very important for nano-filler & polymer matrix interaction, hence the importance of this section devoted to studying the observable effects of synthesis techniques.

4.3.1 A brief study upon epoxy based nanocomposites dispersion techniques

In this research work, 3 techniques have been used for hBN nanoparticle distribution into epoxy host matrix, namely:

- *The Nanomizer Technique*: The first step is to disperse modified nanoparticles in epoxy by using an ultrasonic bath for 15 minutes[88]. Then, epoxy and the particles are stirred with a rotational speed of 2000 rpm. Afterward, the mixture is subjected to the dispersion process called Nanomizer. Nanomizer forces agglomerations to break and leads to a good dispersion and distribution of the particles in the polymer matrix due to the ultrahigh pressure of 200 LPa and the narrow aperture (170 μm). The mixture of epoxy and particles is passed through the Nanomizer ten times[88]. Then, the proper amount of hardener is added to the mixture and the material is mixed with the mixer for 15 minutes. The composite is degassed under vacuum and cast in molds. The best performing samples come from this technique.
- *The Solvent Technique*: This technique includes the dispersion of particles in a solvent (ethanol) by means of an ultrasonic bath and evaporation of ethanol before further proceeding with the synthesis process[88]. Afterward, the solution is heated to 105°C in order for ethanol to be evaporated. The evaporation of ethanol requires several hours of heating, while the weight of the solution is closely monitored to realize the completion of the ethanol evaporation. During the evaporation procedure, it is important to maintain the dispersion of particles; therefore, a magnetic stirrer is used. Then, the appropriate amount of hardener is added to the solution and a high shear mixer at 5000 rpm for 15 minutes is used. The material is cast in aluminum molds and cured at 140°C for 3 hours. Afterwards, the samples are post-cured at 120°C for 16 hours[88]. The 'worst' performer is from this group. (E-hBN-1-B)
- *The Speedmixer Technique*: In the case of the speedmixer technique, modified particles are not dispersed in ethanol but instead, they are directly mixed with epoxy. The mixing of the two materials is performed with the use of speedmixer[88]. Epoxy and dry surface-modified nanoparticles are mixed for 15 minutes. Afterward, the proper amount of hardener is added to the mixture and the material is mixed for another 5 minutes[88]. Finally, the mixture is degassed under vacuum and cast in molds. The curing and post-curing process is the same as in the solvent technique.

It shall be observed later on, that the performance of this technique lies in between the 'Nanomizer technique' & 'Solvent technique' considering terms of quality.

The samples belonging to the same production technique were chosen without *a priori* knowledge, and later verified with available data, with an excellent success rate. This is an important step, since it indicates that isolation of the samples from the same batch can be performed with the knowledge of the previously conducted space charge measurements, mostly in terms of nature of charge accumulation, similar charge dynamics. The location of charge accumulation is also a factor, however, for the specimens investigated herein, charge accumulation occurs mostly at the interfacial region close to the HV-semicon-sample interface) The next section deals with a comparative analysis of the same.

4.3.2 Comparative analysis between production techniques

The samples are first subdivided into their respective parent groups, according to dispersion technique, namely:

- **The Nanomizer group**: This group comprises of samples E-hBN-0.2-C, E-hBN-0.5, E-hBN-1-C & E-hBN-5-B. A juxtaposed compilation of contour plots has been provided herein for easier visual comparison, as to ascribed similarity of behaviour.

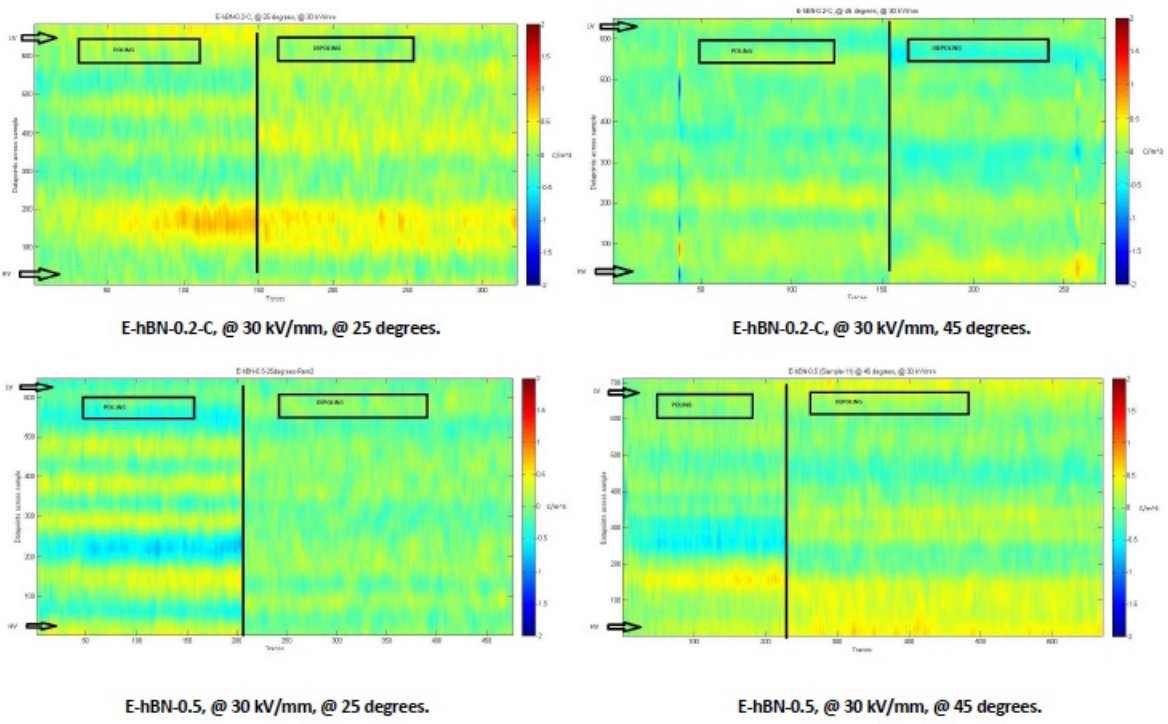

Figure 4.3.1: Samples E-hBN-0.2-C & E-hBN-0.5

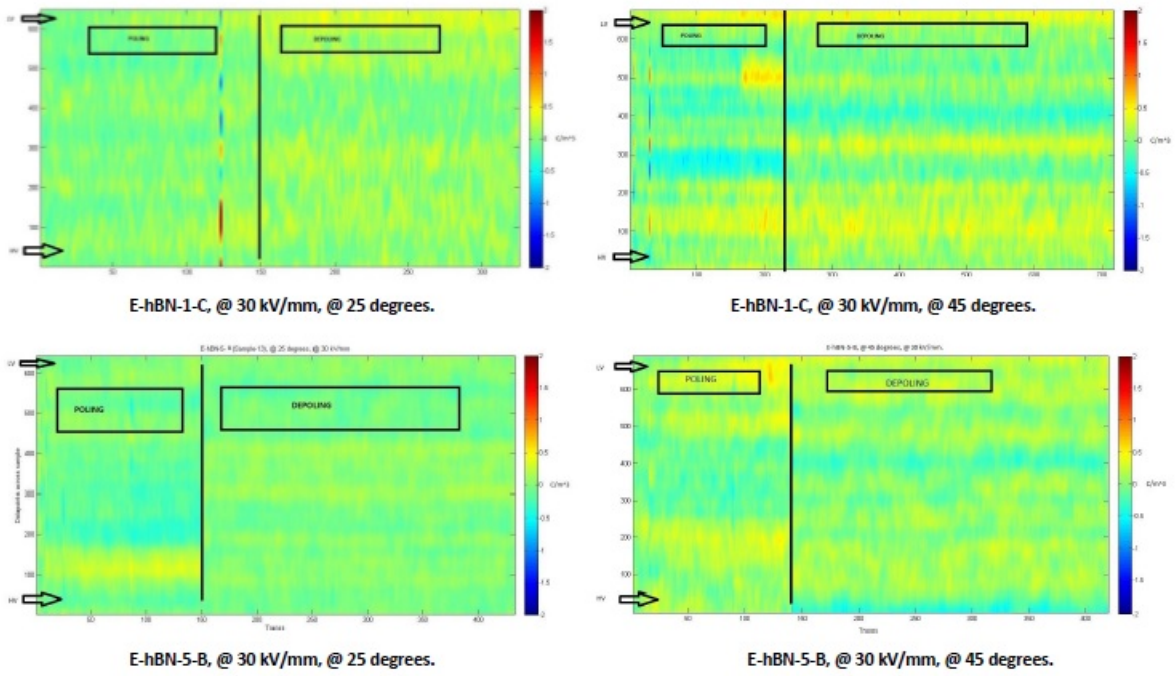

Figure 4.3.2: Samples E-hBN-1-C & E-hBN-5-B

No significant charge accumulation at 30 kV/mm, either at 25 or 45 degrees Celsius. All the best performing samples show similar space charge accumulation behaviour, and even similar amounts of accumulation. A selection of traces plotted for the sample E-hBN-0.5, at 30 kV/mm, at 45 degrees (the interested reader may refer to Appendix III) reveal that whatever little amount of charge is accumulated in this sample (similar behaviour noticed for some other samples as well), occurs in the time period from start till the midway mark of total poling time. Beyond that, charge injection is suppressed, or recombination yields in less total charge. As investigated earlier, deep trap sites are possibly introduced, however this point remains open to debate,[5]. Authors have proposed that the filler added to base resin acts as an **"induced dipole"** under dc electric field and it works as a trap site[65]. Charge injection may be suppressed due to the introduction of nanoparticles into neat epoxy after a certain time, since the increase in the number of trapping sites possibly trap the injected charges close to the interfacial region, where they accumulate as 'homocharges', and thus raise the energy barrier for charge injection, due to which this process slows down. If we assume that charge injection from the aluminium electrodes has lessened, then it means that the barrier height for injection has increased. This can occur for 2 reasons: The nanoparticles have raised or altered the band energy of the existing states, or else trapped charge around themselves, close to the electrode-insulator interfacial zone. Relatively better performance is exhibited at the higher temperature of 45 degrees for the nanocomposites.

- **The Solvent group**: This group comprises of samples E-hBN-0.2-A(Sample 5), E-hBN-1-B(Sample 4) & E-hBN-5-A(Sample 1). A juxtaposed compilation of contour plots has been provided herein for easier visual comparison, as to ascribed similarity of behaviour.

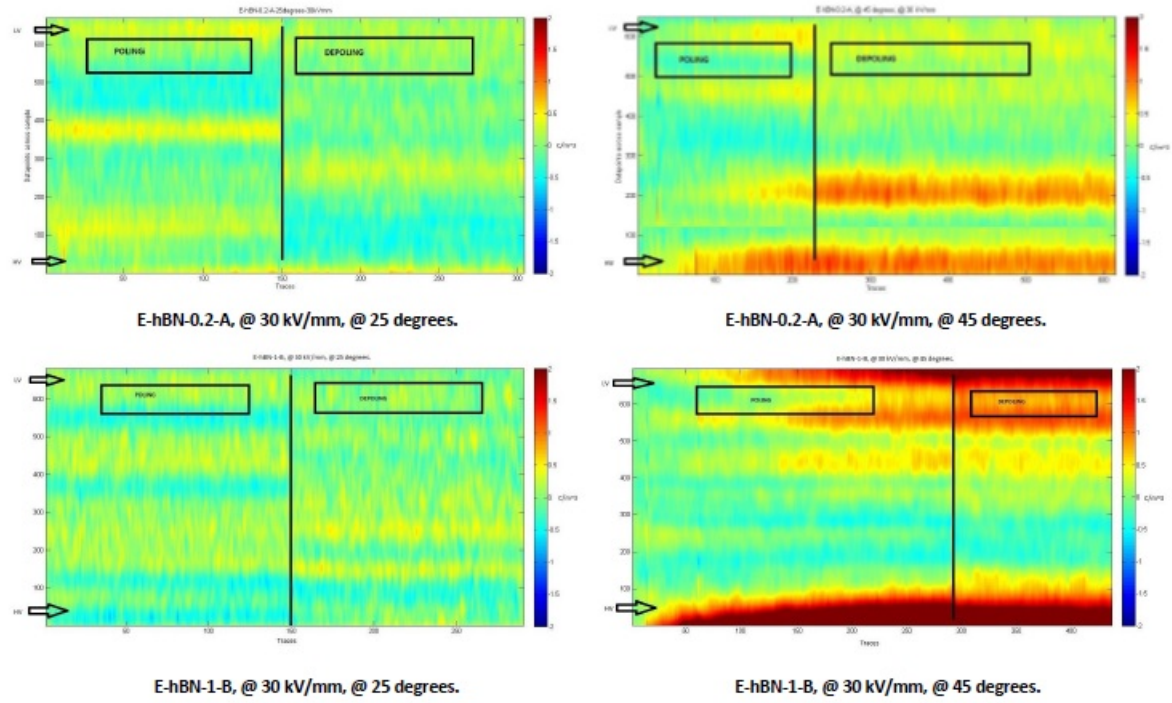

Figure 4.3.3: Samples E-hBN-0.2-A & E-hBN-1-B

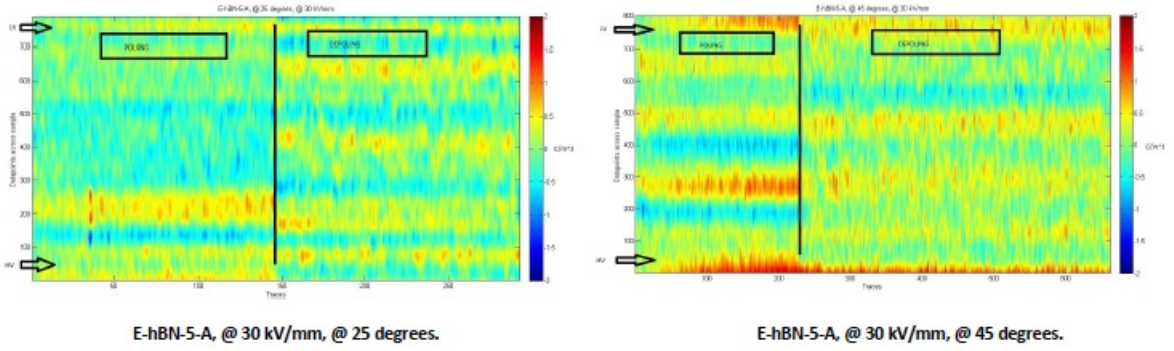

Figure 4.3.4: Sample E-hBN-5-A

The least effective synthesis technique amongst all the 3 techniques[88]. With the exception of E-hBN-1-B (Sample 4) that accumulates even greater space charge than neat epoxy at 45 degrees- the other 2 from this technique accumulated similar charge levels to that of neat epoxy.(possibly slightly less) The behaviour of E-hBN-1-B cannot be fully explained with the data available, but it is possible that E-hBN-1-B underwent a greater degree of polymer chain reorganization, or water content uptake may have been greater- 2 factors which usually influence the dielectric properties of a nanocomposite.

- **The Speedmixer group**: This group comprises of samples E-hBN-0.2-B(Sample 6), E-hBN-0.6(Sample 8) & E-hBN-1-A(Sample 3). A juxtaposed compilation of contour plots has been provided herein for easier visual comparison, as to ascribed similarity of behaviour.

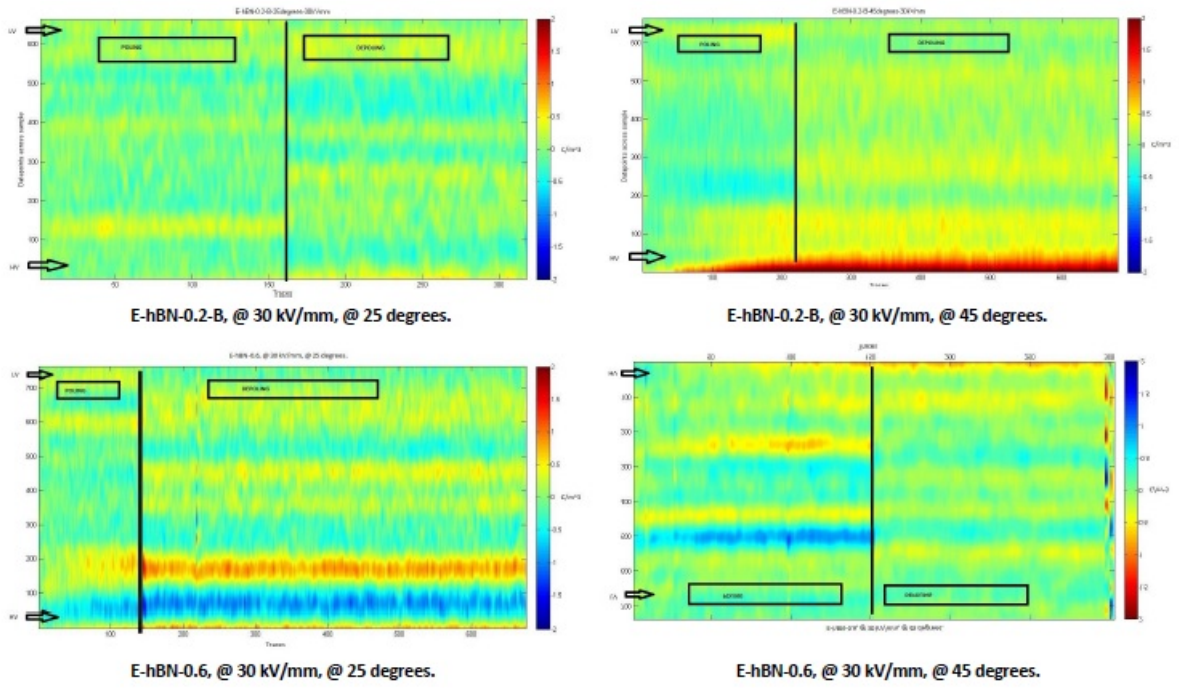

Figure 4.3.5: Samples E-hBN-0.2-B & E-hBN-0.6

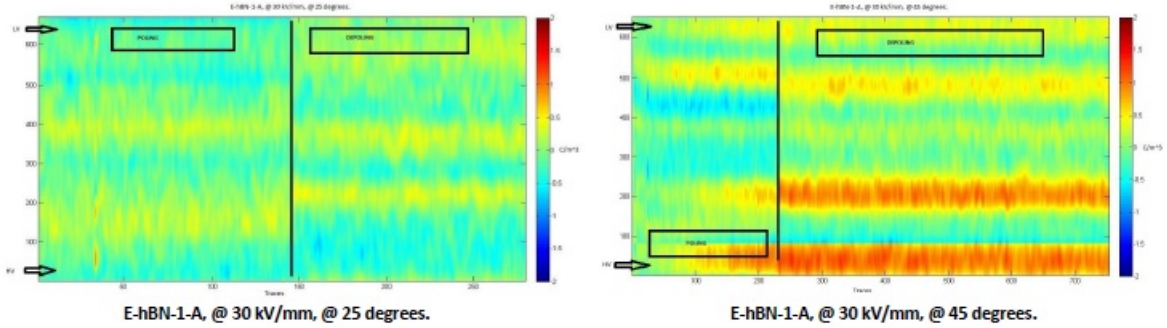

Figure 4.3.6: Samples E-hBN-1-A

This technique falls in between the 'Nanomizer' technique and the 'Solvent' technique, in terms of performance. The notable thing about this group, is one of its members- the sole sample with 0.6 vol% filler concentration. It performs in league with the relatively better performers from the 'Nanomizer' group, in terms of rate of accumulation of space charge, final amount of space charge accumulated. The depoling rates do not show any marked improvement, since it is related to the introduction of traps in the material, which is not a function of synthesis technique.

Hence, if a relative ranking of superiority (from most effective till least effective) is performed, the order list is as follows:
1) The 'Nanomizer' technique
2) The 'Speedmixer' technique
3) The 'Solvent' technique
Thus, we arrive at 2 main questions, which may serve as key tenets to the effect of particle dispersion techniques and filler content in nanocomposites. They are presented below:
1) What is the effect of fill grade then, between the same technique?
2) What is the effect of particle distribution then, between different fill grades?
Hence, it is a question of 2 factors. Each time, one factor is kept constant to investigate the other.

Investigating the effect of fill grade upon Nanomizer technique

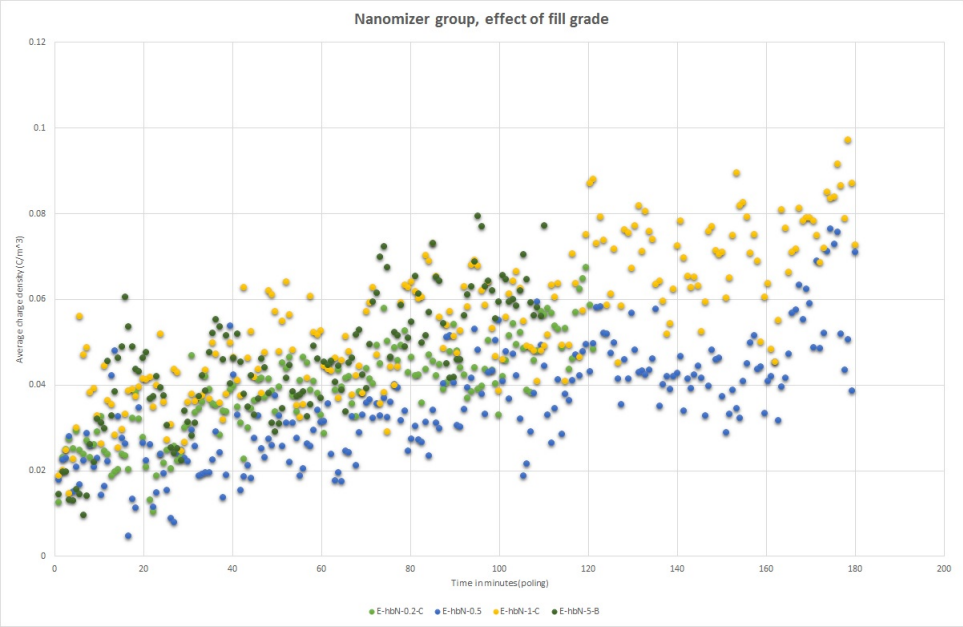

Figure 4.3.7: Comparison between average charge density plot, 30$\frac{kV}{mm}$, 45 degrees

It is interesting to see that for the nanomizer technique, all fill grades seem to be optimum performers from this chart. Another significant observation is that an increase in fill-grade does not deteriorate the performance of neat epoxy, if the technique is kept constant. This is a very significant observation, since most results in available literature reveal that usually an increase in filler grade leads to a worse electrical performance.

Investigating the effect of fill grade upon Solvent technique

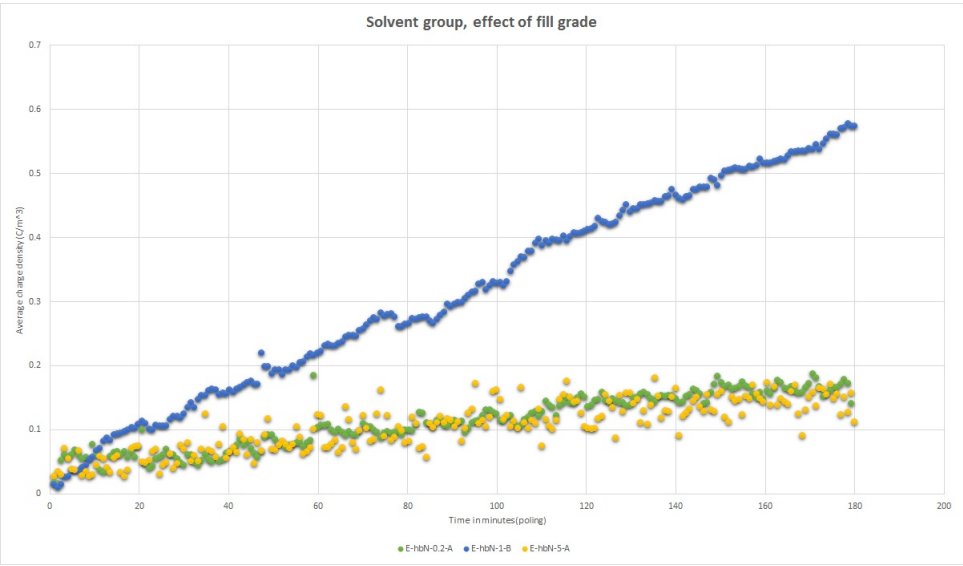

Figure 4.3.8: Comparison between average charge density plot, 30$\frac{kV}{mm}$, 45 degrees

It is quite evident here that except for the sample E-hBN-1-B, the other two behave similarly. It indicates the importance of each step of the synthesis technique- in all probability, this sample may have undergone accelerated ageing, being affected more by the processes involved in ageing. It is also possible that intrinsic changes occurred for some reason in polymer-filler morphology, and thus possibly contributed towards a change in the electrical behaviour, especially with respect to space charge accumulation.

Investigating the effect of fill grade upon Speedmixer technique

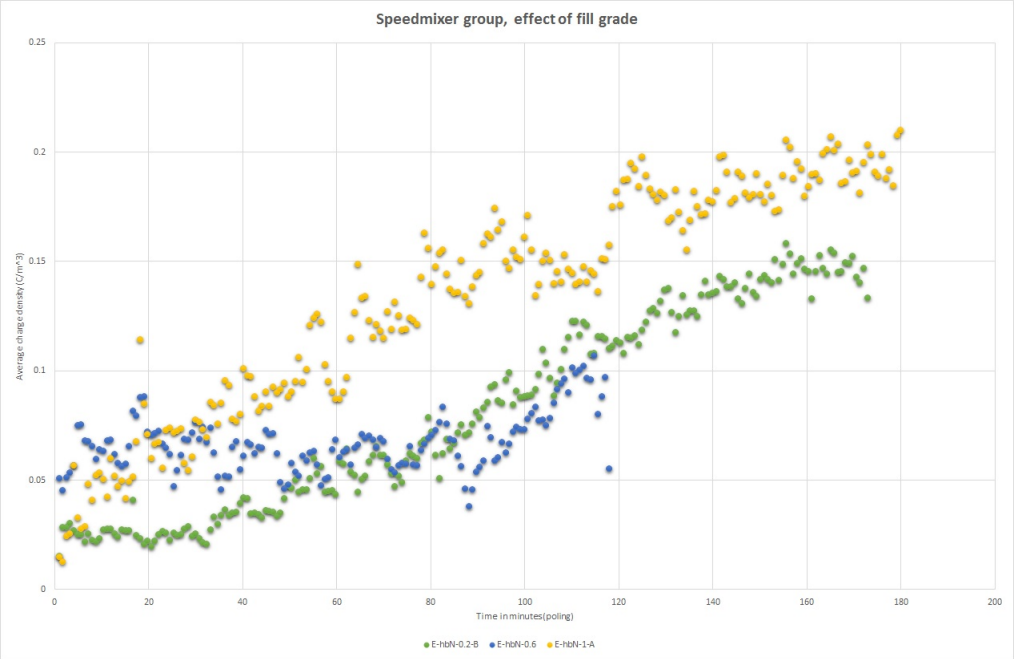

Figure 4.3.9: Comparison between average charge density plot, 30$\frac{kV}{mm}$, 45 degrees

It is highly interesting to note the effect of increasing fill grade herein. The stabilization in growth is noticed in 0.6 fill grade sample. Thus, in conclusion, we can state that:
A) The Nanomizer technique does not seem to be affected by filler content. It performs uniformly superior at all fill grades.
B) The solvent & speedmixer technique show an effect of filler content; namely that from 0.2% till 0.5%-0.6%, behaviour is optimal across all techniques, 1% and 5% filler content show similar behaviour with respect to space charge accumulation during the poling period, and removal of charge during the depoling period.

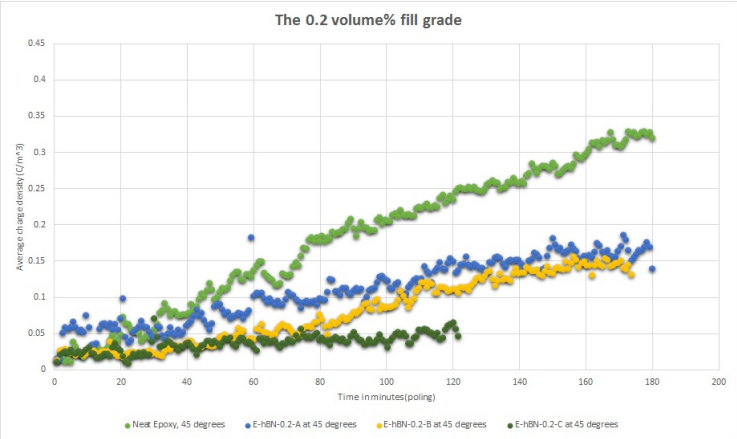

Figure 4.3.10: Comparison between average charge density plot, 30$\frac{kV}{mm}$, 45 degrees

It is clear from this graph, that the order of superiority of the techniques, and its effect on the fill grade is observable- Nanomizer is the best, followed by speedmixer, and finally the solvent method.

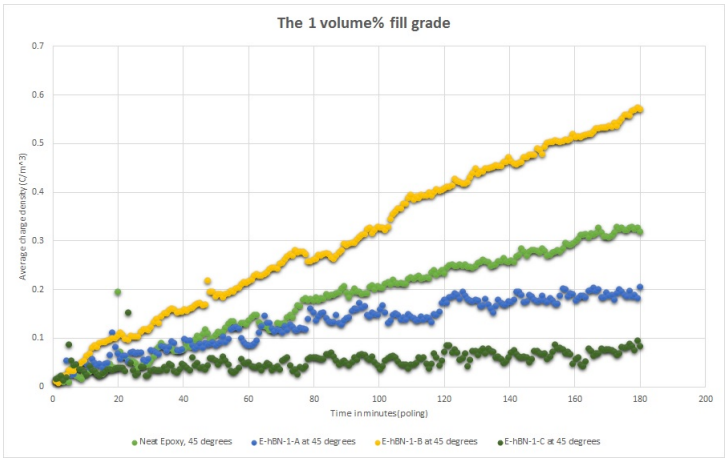

Figure 4.3.11: Comparison between average charge density plot, 30$\frac{kV}{mm}$, 45 degrees

The same observation is valid here as well- Nanomizer is the best technique, followed by speedmixer technique, and finally the solvent technique. The differences become rather stark here than the 0.2 vol%.

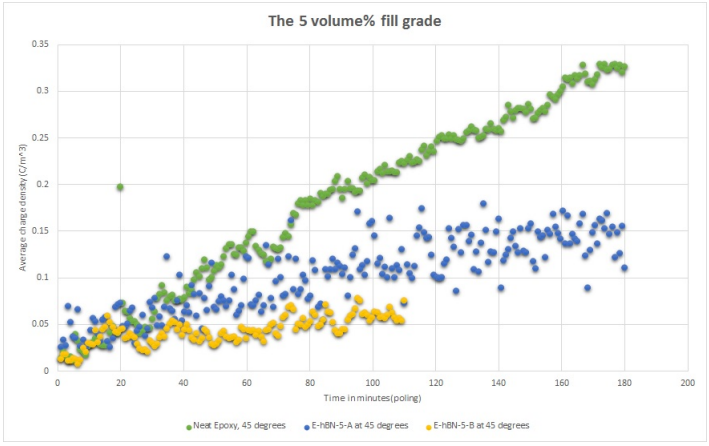

Figure 4.3.12: Comparison between average charge density plot, $30\frac{kV}{mm}$, 45 degrees

Though data for the speedmixer technique is not available here, again the sample produced with nanomizer technique exhibits better performance than solvent technique. The trend thus remains constant.
Thus, the synthesis process leads to observation of a clear difference across the 1 volume% and 0.2 volume% fill-grade, but no significant difference is observed across 5 volume% fill grade.
0.2% till 1% have lower permittivity values, 5% has higher permittivity values. The decrease in permittivity can be attributed to the surface modification of the particles. An *"interfacial layer"* is believed to be formed around the particles in which the polymer chains align perpendicular to the particle surface. The chain mobility in the vicinity of the particles is restricted resulting in the decrease of the relative permittivity. However, the beneficial effect of these layers can be obscured at high filler concentrations, by the higher relative permittivity of the filler. Also, at higher fill grades (e.g. 5 volume%), there is more probability of overlap between interfacial layers between nanoparticles, leading to more immobile layers[73]. However, the statement from [73] is unable to explain the higher ε value of 5 vol% nanocomposites with respect to neat epoxy. (An unexpected result since the relative permittivity of epoxy (3.82) is lower than BN (4)- so one might expect a composite permittivity value between that of epoxy and BN.) This phenomenon has been reported in literature[89]. However, the relative permittivity of the samples increases as the filler concentration increases. It might be said that filler content dominates from 1 till 5% than particle synthesis, and synthesis technique dominates at lower loading (0.2% till 0.6%).
Thus, this section on comparative analysis of synthesis techniques is hereby concluded.

4.4 Threshold Field measurements upon samples

The starting point of the measurements for this work is the fact that that it is often possible to define a critical field separating an ohmic type of conduction from a non-linear regime in the current-voltage characteristic of solid dielectrics. In the **SCLC** theory [44,19,22], this critical field corresponds to the start of rapid space charge accumulation. There are techniques to detect this threshold field via conduction current measurements, space charge measurements and electroluminescence measurements. As reported in [53], the authors found that when the field strength was above 15 kV/mm at 20 degrees Celsius, the average charge density tends to grow with the electric field. It was also seen that the average charge density remains around a certain value when the field strength is smaller than or equal to 10 kV/mm at 20 degrees Celsius, whatever material the electrode is. In that case, there was almost no sign of charge injection from the electrodes and thus space charge accumulation in the specimens. Al, Ag and Au electrodes were characterized during the tests carried out by the aforementioned authors.
The electrode material has a considerable effect on the space charge behavior in epoxy resin, whatever temperature the test was conducted at. The space charge accumulation in epoxy resin and the subsequent nanocomposites is mostly positive in polarity, trapped close to the interfacial region near the HV-sample interface, leading to the gradual accumulation of 'homocharges', which in turn slows down charge injection process. The easiness of charge injection is positively correlated with

the work function of the electrode material. The test results presented herein were conducted at 45°C, with the best performing samples as determined previously, to attempt and find a correlation between filler content & threshold field values. As usual, primarily neat epoxy is characterized for value of threshold field.

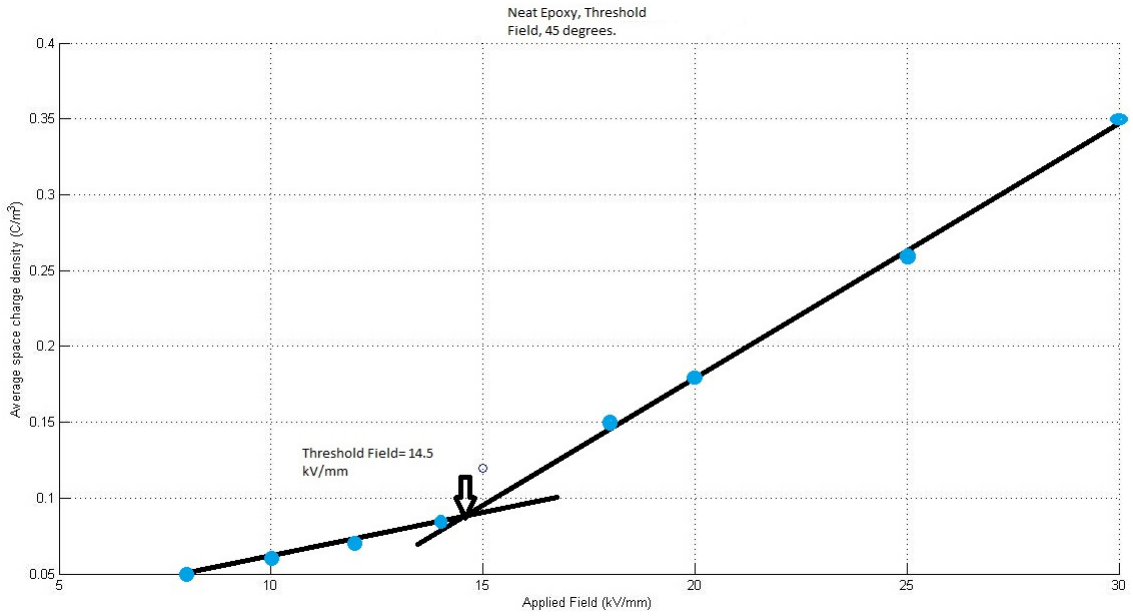

Figure 4.4.1: Neat epoxy threshold field plot, 45 degrees

Figure-4.4.1 exhibits the threshold field determination for neat epoxy, with a selection of 8 points indicating tests carried out at 8 different applied electric field values respectively. The threshold field is determined as 14.5 kV/mm-15 kV/mm. Proceeding as per increasing fill-grade, the next best performer is E-hBN-0.2-C.

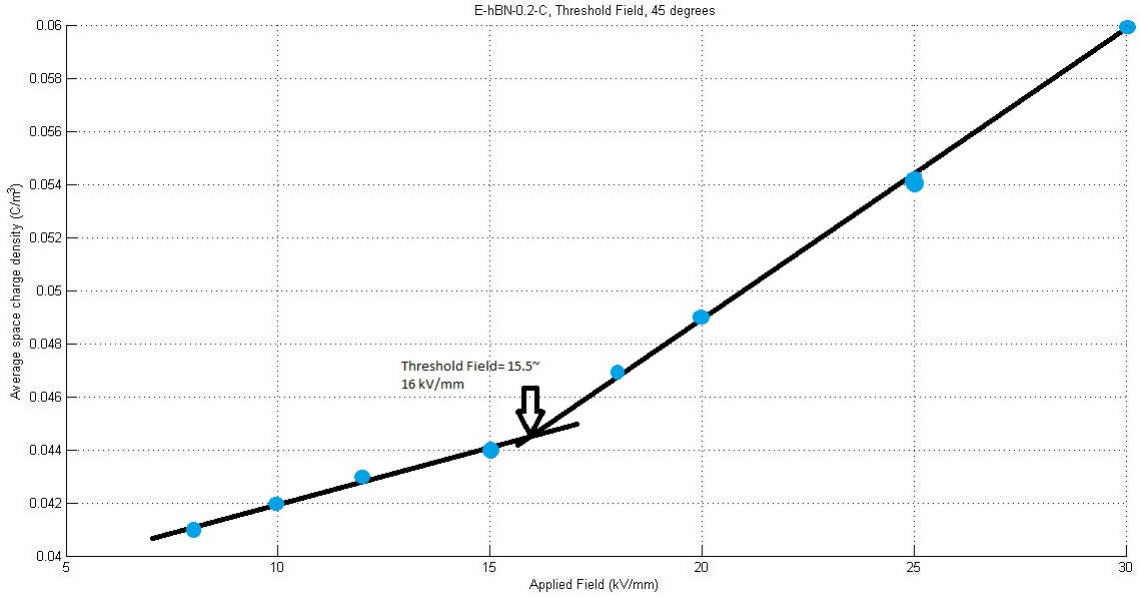

Figure 4.4.2: E-hBN-0.2-C threshold field plot, 45 degrees

It is already interesting to note the increase in threshold field value (Figure-4.4.2) with increasing filler content, an observation well supported by suppression of charge injection phenomenon investigated earlier.
Proceeding as per increasing fill-grade, the next best performer is E-hBN-0.5.

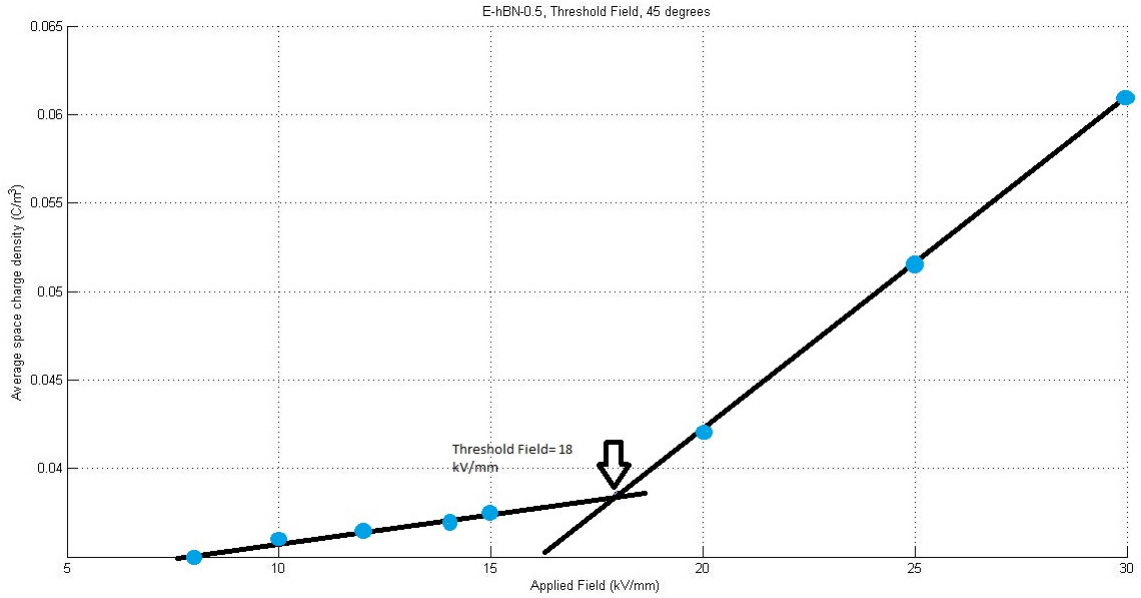

Figure 4.4.3: E-hBN-0.5 threshold field plot, 45 degrees

The previously studied trend of increase in the threshold field continues, from the increase in filler grade from 0.2 volume% till 0.5 volume%. Figure-4.4.3 depicts the determination for the threshold field value for sample E-hBN-0.5 as 18 kV/mm.

Proceeding as per increasing fill-grade, the next best performer is E-hBN-0.6.

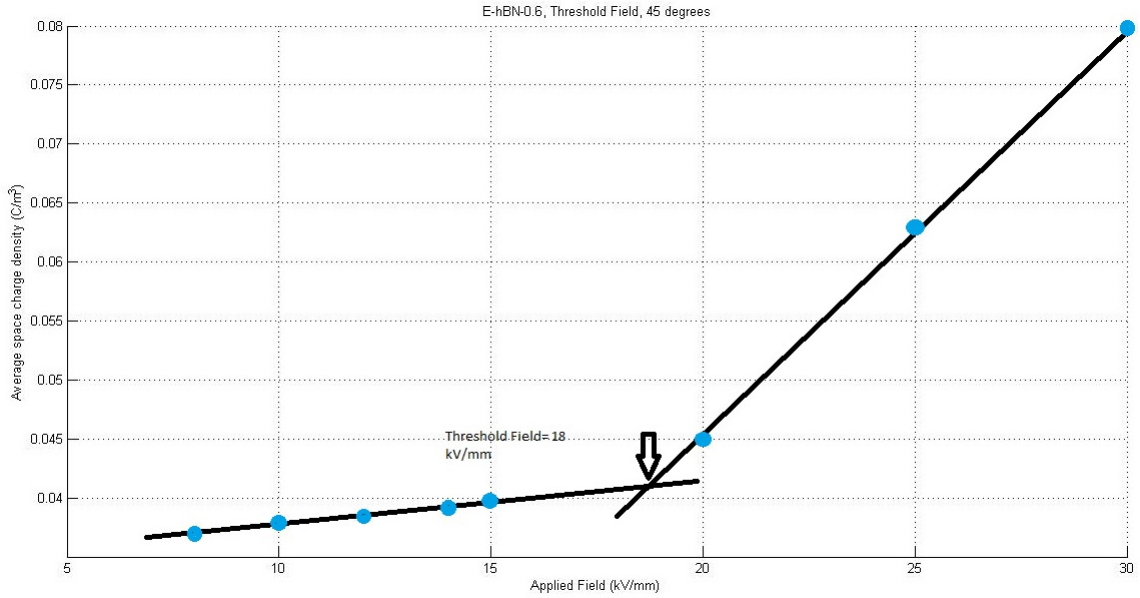

Figure 4.4.4: E-hBN-0.6 threshold field plot, 45 degrees

Figure-4.4.4 depicts the similar threshold field value (18 kV/mm) for sample E-hBN-0.6 in comparison with the threshold field value for sample E-hBN-0.5 (Figure-4.4.3), even though a slight increase in fill grade is present.
Proceeding as per increasing fill-grade, the next best performer is E-hBN-1-C. This was previously determined to be the relatively superior performer to the samples present in the 1 volume% group.

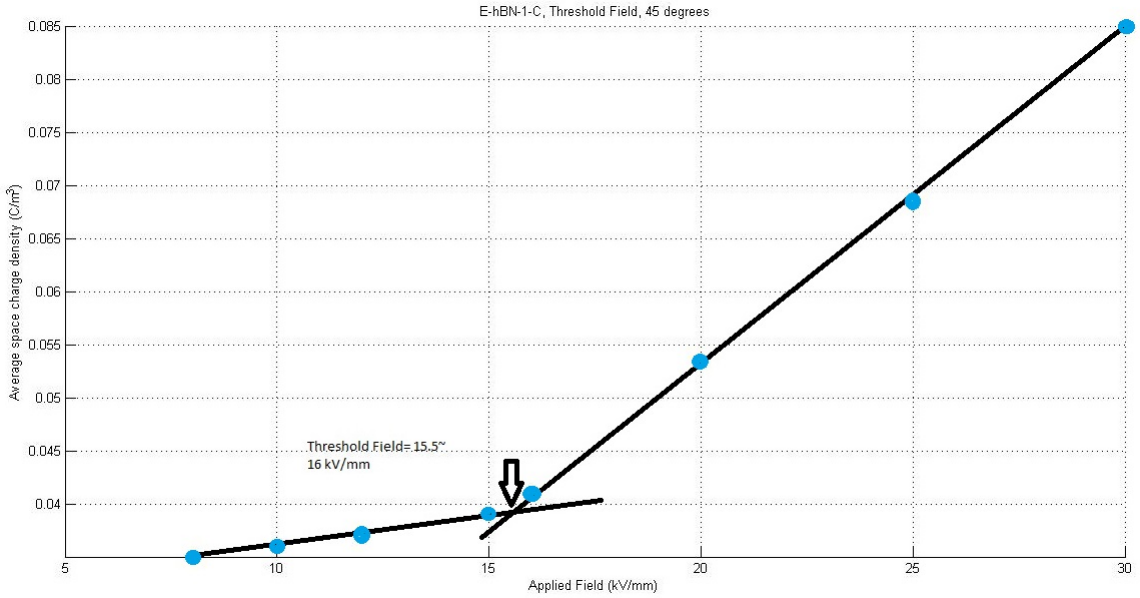

Figure 4.4.5: E-hBN-1-C threshold field plot, 45 degrees

Here, an interesting phenomenon occurs. It is seen from Figure-4.4.5 that the threshold field value shifts down to a lower value than the previous trend of an increase. As has been mentioned in previous sections, 0.6% fill grade possibly represents a point of shift in space charge behaviour for the epoxy nanocomposite samples.
Proceeding as per increasing fill-grade, the final best performer is E-hBN-5-B.

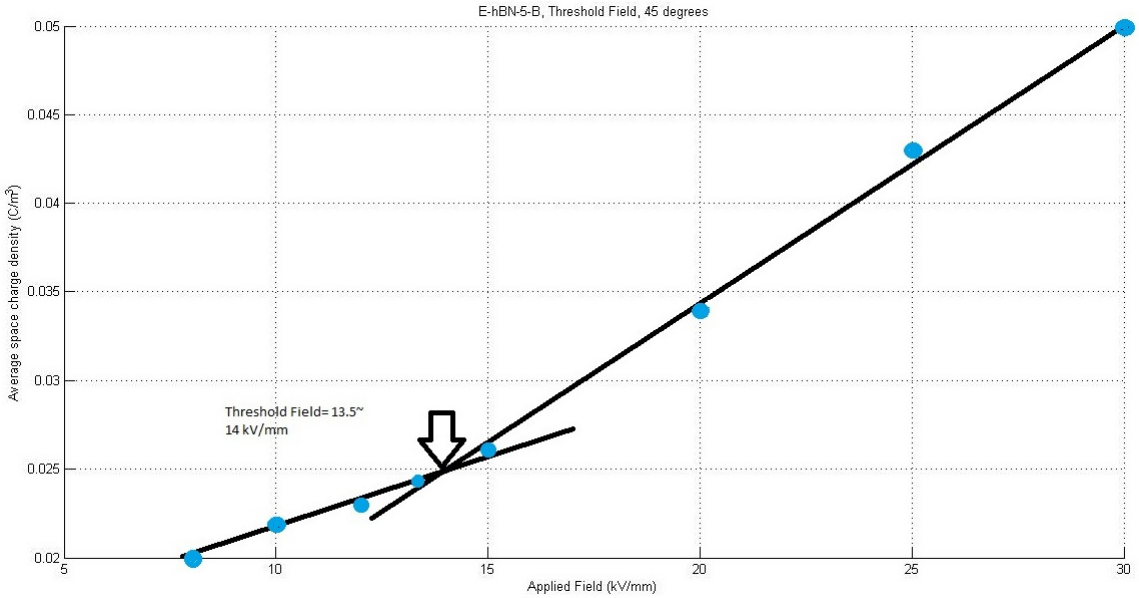

Figure 4.4.6: E-hBN-5-B threshold field plot, 45 degrees

Figure-4.4.6 depicts the threshold field value for E-hBN-5-B- an interesting observation can be made here. Even though the threshold field is lowered than neat epoxy, the rate of charge accumulation in the sample as a function of increasing applied electric field is much slower than neat epoxy. (Figures-4.4.1 & 4.4.6 depict this fact) This might possibly present the situation: *Charges may be injected quicker into sample E-hBN-5-B initially, but then accumulation of charges as homocharges near the interfacial region of the injecting electrode quickly slows down the rate.*
Thus, from all the results presented, we can observe that the threshold increases maximally till 18 kV/mm, for an increase in filler grade concentration from 0.2 % volume till 0.6 % volume, with a decrease starting from 1 volume % till 5 volume%. So, 0.5-0.6 volume% filler concentration might be called a *pivot point* in terms of threshold field for space charge accumulation. The fitting line slopes are thus calculated and presented beneath:

- **Neat Epoxy**: The slope is equal to 0.017
- **E-hBN-0.2-C**: The slope is equal to 0.0011
- **E-hBN-0.5**: The slope is equal to 0.0018
- **E-hBN-0.6**: The slope is equal to 0.003
- **E-hBN-1-C**: The slope is equal to 0.003
- **E-hBN-5-B**: The slope is equal to 0.001

As is highly interesting to note, the steepest slope values pertains to neat epoxy, than the epoxy-based nanocomposites. As this research work clearly demonstrates earlier on, that suppression of charge injection due to interfacial charge accumulation of homocharges, and possible band structure alteration by nanoparticles is also a vital factor in determining the threshold field, at which space charge onset is observed. The relevant contour plots are placed under Appendix III, for the interested reader.

Thus, this section is concluded with the aforementioned results.

4.5 The Ultrasonic measurement of sound velocity in Epoxy-hBN nanocomposites

The space resolution of space charge distribution is mainly determined by the duration ΔT_p of the pulse electric field for the PEA method, and the speed of sound in the specimen under test. The higher the absolute resolution, the better the measurement- and better accuracy & reproduciblity of data of the measuring system. As per the *CIGRE TF D1-12 -01* guidelines, relative spatial resolution (% space resolution) should be optimally between 2-5%, at the minimum. Since the spatial resolution depends upon the thickness of the transducer, and also upon pulse duration through the nanocomposite specimens (which depends on acoustic velocity via them), hence, it ws considered an excellent idea to perform basic ultrasonic measurements upon neat epoxy & the related polymer nanocomposites. All the measurements were conducted at the Aerospace NDT laboratory of TU Delft, under the august supervision of postdoctoral researcher, Dr. A.G. Anisimov.

4.5.1 Basic mathematics behind calculations & an important observation

Assume the thickness of the sample is d and the duration of the pulse voltage is ΔT_p. The relative spatial resolution η is given by the equation provided below:

$$\eta = \frac{\Delta T_p}{\frac{d}{Velocity_{sound}}} * 100 \tag{4.1}$$

The term $\frac{d}{Velocity_{sound}}$ in the denominator is the transit time at which the acoustic pulse propagates through the sample. **Thus, from the above equation it is immediately clear that the quicker the sound travels through the sample, the better resolution is achieved.** Physically, this can be attributed to much less reflections and attenuations of the acoustic pulse, which leads to higher resolution for subsequent measurements.

4.5.2 Equipment, measurement & results

The OmniScan MX2 Phased Array Flaw detector was used, in conjunction with a 10 MHz ultrasound frequency probe to detect the approximate speed of sound in the samples[80]. All fill grades were detected, except 0.6 volume% filler content, since that particular fill grade did not presently have a thicker sample (other than the thin plaque) associated with it. In cases of samples from the same fill grade, the thickest sample was chosen, so that the associated time for the sound wave to reflect off the bottom surface is possible to detect with a level of accuracy, as per the instrument and geometry of the provided samples (which are not of uniform thickness everywhere, as perceived by measurement with a micrometer). 5 successive measurements are taken, by setting appropriate gain parameters onto the measuring device, and the average of those 5 measurements are calculated as an approximation of the actual sound speed inside the sample. The probe with the wedge was always placed on the mid-portion of the samples in question, both for consistency and accuracy purposes.
Some relevant diagrams have been mentioned here, and the interested reader may refer to Appendix II for more interesting setup photographs.

Figure 4.5.1: The Phased Array Ultrasonic Flaw detector Omniscan MX2, ©Olympus NDT Canada, Inc.

Figure 4.5.2: The sample, wedge connected to setup for measurement.

The calculated average acoustic velocities for neat epoxy and the composites tested are presented below:

- **Neat Epoxy**: The velocity of sound was measured as 2671.44 m/s.
- **The 0.2% fill grade**: The velocity of sound was measured as 2711.56 m/s.
- **The 0.5% fill grade**: The velocity of sound was measured as 2745.74 m/s.
- **The 1% fill grade**: The velocity of sound was measured as 2750.22 m/s.

- **The 5% fill grade**: The velocity of sound was measured as 2753.4 m/s.

Thus, it can be seen, that velocity of sound increases steadily from 0% fill grade till 1% fill grade, where it flattens out into a plateau. This fact can be clearly seen in the graph presented herein.

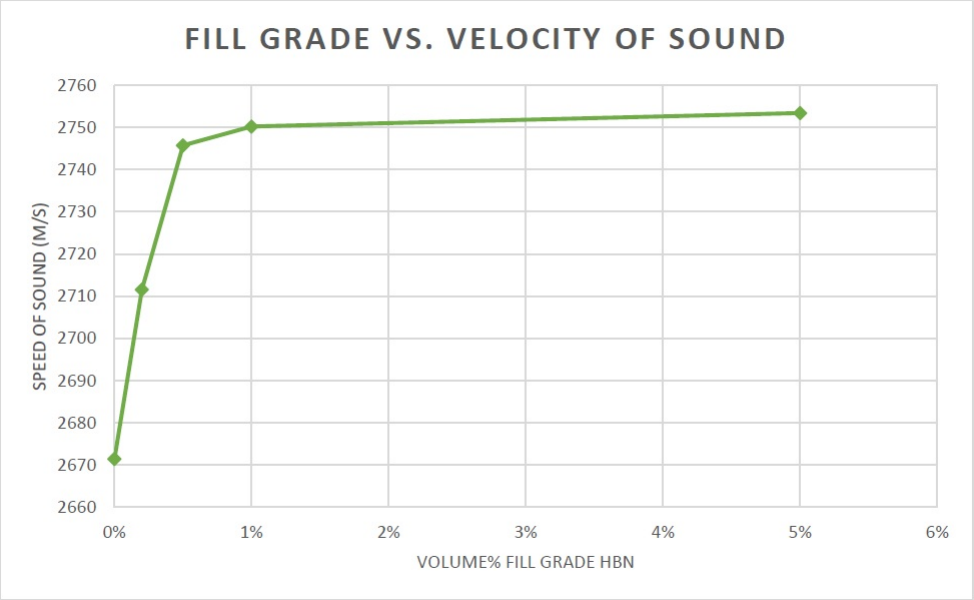

Figure 4.5.3: Fill grade vs. Acoustic velocity

As is clear from Figure-4.5.4 presented, there is extensive overlap between 0.5 volume fill-grade, & the 1 and 5 fill-grades. This is also a conclusion that is evident from the *plateau nature* of the curve presented previously. It has been reported in research literature[74] that the values of fiber content & ultrasonic wave velocity in investigated materials bear a close relationship. As quoted in the paper, *"The results show that in general the ultrasonic velocity increases with an increase in glass content."* Also, P.N. Bindumadhavan & H. K. Wah published results that agree with this relationship[75].The plateau nature of the curve can probably be attributed to the fact that the longitudinal wave velocity of the epoxy matrix reaches close to the maximum at 1% fill-grade, and from then on, the content of fill-grade does not relate to a steady rise in sound velocity through the samples under consideration.

Ultrasonic response of filled polymers depends strongly on the concentration, particle size and dispersion of fillers.

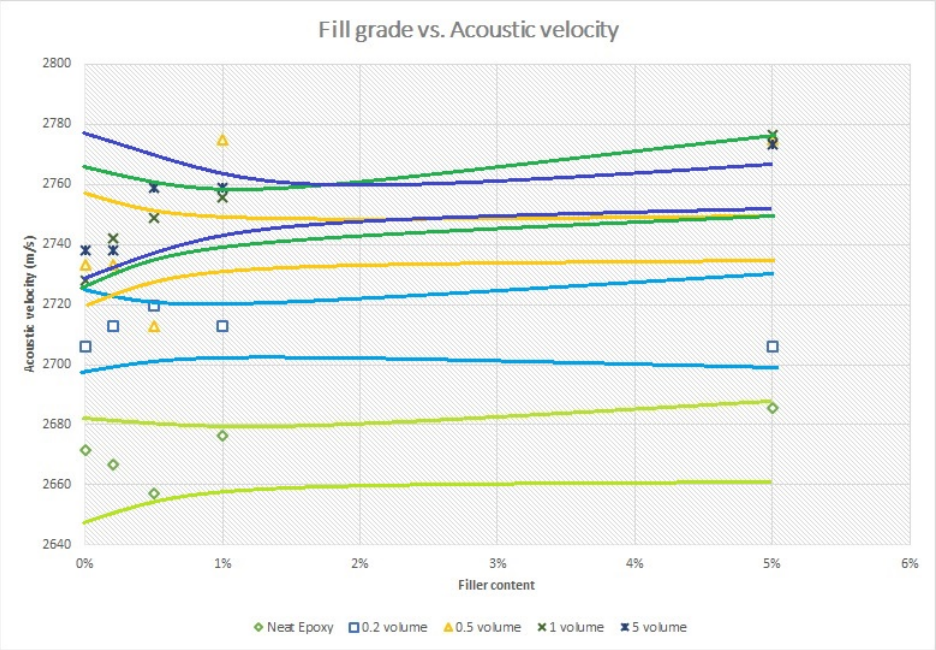

Figure 4.5.4: Fill grade vs. Acoustic velocity(95% C.I.)

But, this much can be stated: **With increasing fill-grade, the velocity of sound increases in the epoxy-nanofiller matrix, as compared to neat epoxy.** This leads to an important conclusion for the measurements presented in this research work: ***As the fill-grade increases, the relative spatial resolution of the measurements increase. This leads to greater clarity of space charge detection for the higher fill-grades. The fact that the highest fill grade performs as good as the lowest fill grade for a particular technique, according to the space charge measurements- can be strongly corroborated with the fact that increased resolution still does not detect any remarkable development of charges, and hence it can be concluded that there is indeed lesser charge development as compared to unfilled epoxy.***

This section is hereby concluded, as well as the chapter devoted to experimental results & subsequent relevant discussion.

In the end, it doesn't even matter.

Linkin Park, Hybrid Theory

5

Conclusion & Recommendations for future work

In this chapter, a holistic *bird's eye* view is taken over the entire spectrum of results presented in this research work. Two main questions were posed at the onset:

- **What is the effect of the nanoparticles upon space charge behaviour of the epoxy composite in general, and how does filler content loading affect relevant electrical behaviour?**
- **What is the effect of the dispersion techniques used in this work upon space charge behaviour, and can there be a possible correlation between filler content loading effects & synthesis technique corresponding to the same?**

The next section deals with the conclusions inferred from the experimental results.

5.1 Conclusions

All relevant conclusions and possible explanations have been advanced on the following pages.

- The primary observation on incorporation of hBN nanoparticles, of average size 70 nm, into the epoxy host material has been a reduction in the amount of space charge accumulated over the poling period, and the secondary observation has been the stabilization of the growth rate during poling period for some fill-grade specimens. This has been attributed to a multiplicity of possible factors(Section 4.2): Strong interfacial dynamics at play in lower fill-grades, the possible development of trap sites close to the interfacial region (in good agreement with depoling trends & results), to the fact that the filler added to base resin acts as an *"induced dipole"* under DC electric field and it works as a trap site, the development of homocharges due to low injection depth into the PNC (Polymer nano-composite) around the electrode-semicon-insulator region which prevents further charge injection into the sample, and finally the possible alteration of band structure, surface energy state by the interaction of the nanoparticles with the polymer matrix. Increasing number of nano-interfaces possibly leads to development of more trapping sites. Greater number of trapping sites can lead to more trapping of charges quickly as soon as they are injected from the metal across the metal-semicon-insulator interface, at the region close to the metal-insulator interface zone. This accumulation

of 'homocharges', in turn raises the barrier potential at the metal-semicon-insulator interface, lowers the local electric field distribution- due to the rise in barrier potential, it is more difficult now for charges to be injected into the sample, since higher energy possessed charges are required. This probably results in a net reduction of charges in the specimen, which of course is the amount of charge detected by the PEA system in use. However, it must be kept in mind that beside gradual charge injection suppression mechanism, other competing processes may also contribute towards the lesser amount of charge in the nanocomposite specimens towards the end of the poling period.

- The secondary observation of the stabilization of growth rate of space charge in some specimens can be dealt with by considering the fact that two main forces are at play for the injection of charges in an insulator bulk, across the metal-semicon-insulator interface: The ease of injection, which depends on the work function of the metal constituting the electrode & the ease of transport of the charges across the specimen length after possible injection. Since, as observed in this work, the charges dominant upon injection are positive polarity charges (same polarity as the HV electrode)- it points to the development of homocharges after some initial injection of charges across the potential barrier. These homocharges distort the Laplacian field distribution in the specimens, lower the local electric field distribution close to the interface and increase the barrier height for injection- hence the growth rate of charges slows down in the sample. The slowing down of the growth rate in these specimens could thus be attributed to 2 factors: Either the charge injection mechanism is suppressed, or else trap site introduction prevents continued charge injection & results in net lower charge detected by the PEA system.

- The final clue inferred from the space charge measurements conducted in this thesis, relates to the strikingly similar performance of the relatively superior performers across increasing filler grades. As has been pointed out in (Section 4.3), an increase in filler loading from 0.2 volume% till a 5-fold increase up to 1 volume%, followed by a further increase in fill grade loading, again by a factor of 5, till the highest concentration of 5 volume% should introduce an enormous increase in effective surface area of the nanoparticles, which should have had a remarkable effect upon the specimen behaviour. But, the observations presented herein in this research work do not reveal such a fact (at least across the spectrum of the Nanomizer synthesis technique). Various proposed models in research literature state that the interaction between the nanoparticles & polymer matrix reduces the mobility of epoxy chain in the bulk material, which results in a reduction of the effective permittivity of epoxy nanocomposites. Lower filler loading implies larger interparticle distances, while relatively higher filler loading leads to smaller interparticle distances. At lower filler content, the amount of the immobilized polymer around the particles is small, allowing for sufficiently strong interactions between the loosely bound polymer and the particles. As the amount of immobile polymer increases at higher nanoparticle contents, such interactions will become weaker. In the former case, it may be that there are more number of interactions between the polymer-filler particles, since lesser amount of polymer chain is immobilized; in the latter case, even though the number of nano-particles & resulting interfaces are greater in number, not all of them interact with the greater immobilized polymer chain. As a result, if electrical interactions between the nano-particles and the polymer chains do not increase as per higher filler content loading- it may explain why behaviour across a range of increasing filler content, for a synthesis technique, remains similar.

- The importance of dispersion techniques adopted is highly stressed herein. As has been stressed earlier, interfacial effects are very important for nano-filler & polymer matrix interaction- and interfacial phenomena depend on filler dispersion in the nanocomposite. 3 techniques were studied in this research work, namely- The Nanomizer technique, The Solvent technique & The Speedmixer technique. A relative ranking of superiority between them was conducted, with Nanomizer coming out on top, the speedmixer technique second, followed finally by the solvent technique. Interestingly, it was observed that for relatively lower filler loadings(0.2% till 0.6%), synthesis techniques were dominant & differences in space charge accumulation behaviour were observed. For relatively higher loadings(1% till 5%), the effect of fill grade is probably more dominant. For 0.5% and 0.6% filler grade concentration, an interesting observation can be made- the space charge accumulation is improved with respect to neat epoxy in both cases. This might point towards the fact that a small increase in an already determined beneficial fill grade con-

centration does not necessarily drastically change space charge behaviour, or charge dynamics, for better or worse. (These two specimens, E-hBN-0.5 & E-hBN-0.6 behave similarly, as has been determined earlier in Chapter 4.) The technique and the filler concentration are like the two arms of a scissor- the right balance must be struck to prevent agglomerations, and achieve improved space charge accumulation behaviour.

- Finally, the issue of incorporation of nano-fillers into the host insulation material, and its effect upon threshold fields for space charge accumulation is discussed. It has been observed in this research work (in Section 4.5) that for filler loading till 0.6 volume%, the threshold field for space charge accumulation keeps on increasing in comparison to neat epoxy, with much less steeper fitting line slope characteristics. From 1% till 5%, the threshold field gradually starts decreasing- and finally ends up lesser as compared to neat epoxy. This probably signals towards a correlation between filler grade concentration and threshold field detection. A possible hypothesis for the decrease of threshold field at higher filler loadings might be attributed to the fact that possibly recombination processes might be dominant in comparison to charge injection processes, due to introduction of more sites- a fact which would lead to net lesser space charge accumulation, and detection by the PEA system. So, the onset of space charge accumulation might start earlier- but overall, lesser charge is accumulated in the nanocomposite system as compared to neat epoxy.

The final section deals with a presentation of possible scope for future research work.

5.2 Future scope of research work

- **Conduction current measurements**: Conduction current measurements may be possibly performed upon the best performing specimens, as determined from this work. This can help in further insight into the conduction mechanism prevalent in the nanocomposite systems- as well as the activation energy, sample dynamic resistance, and other factors of interest.

- **Acquisition of an improved PEA system**: One of the prime problems encountered whilst signal processing in this work, was due to the imperfect nature of the applied pulse signal. Due to the high operation voltage and the high switching frequency, the noise immunity is crucial for a reliable pulse generator using a solid-state switch (also recommended). Components with low inductance should be chosen, wire-wound resistors should never be used. The line connection should be kept as short as possible, the line inductance should be considered and kept low. The human error is vital in a high voltage involved experiment such as space charge distribution measurement, especially when the experimental period is considerably tiringly long- possible automation of the setup using LabView software may be taken into account. A higher resolution PEA system would be a prime consideration as well.

- **Further research into deconvolution techniques**: It is possible that even with ill-conditioned matrices obtained due to imperfect equipment, the obtained space charge profile can reveal factually consistent data upon careful processing. Towards this end, advanced mathematical techniques can be adopted to carefully deconvolute the recorded signal, and obtain required data.

- **Incorporation of higher fill grades, and production of newer samples**: Aging of any dielectric, due to repeated exposure to temperature, electric stress and other ambient conditions is a well-established fact. Newer samples production could possibly mitigate these effects over time. Higher fill-grades could reveal more into the behavioral nature of these nanocomposites, and sample conductivity as a function of electric field & temperature could be tested to ascertain whether incorporation of inorganic nano-fillers into insulation materials, beyond a certain filler loading, can lead to generation of better inter-particle networks, and consequently, conductivity increases. The mobility of the charges could then be observed to deduce further theories into the same.

- **Further research into synthesis techniques**: This work well supports the importance of particle distribution into host material matrix, and at this juncture, it is also necessary to take the entire production process into account while analyzing for key electrical behaviour. More insight into the multiple processes prevalent during production of these

nanocomposites, could yield a deeper understanding of the possible changes in the polymer morphology later introduced when the nanoparticles have been dispersed into the host matrix material.

This section is hereby concluded.

References

[1] T. J. Lewis, "Nanometric Dielectrics", IEEE Transactions on Dielectrics and Electrical Insulation, Vol:1, pp 812-25, 1994.

[2] P.O. Henk, T.W. Kortsen and T. Kvarts, "Increasing the electrical discharge endurance of acid anhydride cured DGEBA epoxy resin by dispersion of nanoparticle silica", High Performance Polymers, Vol:11, pp 281-296, 1999.

[3] J.K. Nelson, J.C. Fothergill, "Internal charge behaviour in nanocomposites", Nanotechnology, Vol:15, pp 586-9, 2004.

[4] S. Singha, M.J. Thomas, "Dielectric Properties of Epoxy Nanocomposites", IEEE transactions on Dielectrics and Electrical Insulation, Vol:15(1): p. 12-23, February 2008.

[5] A. Hajiyiannis, G.Chen, C. Zhang, G. Stevens, "Space Charge Formation in Epoxy Resin Including Various Nanofillers", in Annual Report Conference on Electrical Insulation Dielectric Phenomenon, Canada, 2008.

[6] M. Roy, J.K. Nelson, R.K. MacCrone, L.S. Schadler, C.W. Reed, R. Keefe, W. Zeneger, "Polymer Nanocomposite Dielectrics – The Role of the Interface.", IEEE Transactions on Dielectrics and Electrical Insulation,Vol:12(4): p. 629-643, August 2004.

[7] T.J. Lewis, "Interfaces are the Dominant Feature of Dielectrics at the Nanometric Level.", IEEE Transactions on Dielectrics and Electrical Insulation, Vol:11(5): p. 739-753, October 2004.

[8] T. Imai, T. Nakano, T. Ozaki, T. Shimizu, M. Kozako, T. Tanaka,, "Effects of nano- and Micro-filler Mixture on Electrical Insulation Properties of Epoxy based Composites.", IEEE Transactions on Dielectrics and Electrical Insulation, 13(1): p. 319-326, February 2006.

[9] M. Roy, J.K. Nelson, L.S. Schadler, C. Zou, J.C. Fothergill., "The influence of physical and chemical linkage on the properties of nanocomposites", in Annual Conference Report on Electrical Insulation and Dielectric Phenomena, CEIDP, UK, October 2005.

[10] P.M. Ajayan, L.S Schadler, P.V. Braun, "Nanocomposite science and technology.", Wiley-VCH, July 2003.

[11] G. Tesoro, "Epoxy resins-chemistry and technology", Journal of Polymer Science Part C: Polymer Letters, 26(12): p. 539, 1988.

[12] T. Andritsch, P.H.F. Morshuis., "Nanotechnology for HVDC Applications- Literature Survey Tailored Insulation Material, in Truimvirate IV", Report 1, TU Delft, January 2007.

[13] R.M. Laine, J. Choi, I. Lee, "Organic-Inorganic Nanocomposites with Completely Defined Interfacial Interactions.", Advanced Materials, Vol:13(11): p. 800-803, 2001.

[14] Y. Murata , M. Nemoto, Y. Sekiguchil, Y. Inoue, M. Kanaokal, N. Hozumi, M. Nagao, "Effects of Nano-sized MgO-filler on Electrical Phenomena under DC Voltage Application in LDPE",in Annual Conference Report on Electrical Insulation and Dielectric Phenomena, CEIDP, Japan, October 2005.

[15] T. Tanaka, G.C. Montanari, and R. Mulhaupt, "Polymer Nanocomposites as Dielectrics and Electrical Insulation-perspectives for Processing Technologies, Material Characterization and Future Applications.", IEEE transactions on Dielectrics and Electrical Insulation, Vol:11(5): p. 763-784, October 2004.

[16] J.C. Fothergill, J.K Nelson, M. Fu, "Dielectric properties of epoxy nanocomposites containing TiO_2, Al_2O_3, and ZnO fillers", in Annual Conference Report on Electrical Insulation and Dielectric Phenomena, CEIDP, UK, 2004.

[17] T. Takada, J. Holboell, A. Toureille, J. Densley, N. Hampton, J. Castellon, R. Hegerberg, M. Henriksen, G.C. Montanari, M. Nagao, P. Morshuis, "Space charge measurement in dielectrics and insulating materials.", Cigre Task Force D1.12.01, February 2006.

[18] N. Adachi, X.Q., Y. Tanaka, T. Takada, "Comparison between the PEA Method and The PWP Method for Measuring Space Charge Distributions.", IEEE transactions on Dielectrics and Electrical Insulation, Vol:5(6): p. 944-951, December 1998.

[19] Juan Martinez-Vega, "Dielectric materials for electrical engineering", Wiley Publishing, 2010.

[20] D.R. Paul & L.M. Robeson, "Polymer nanotechnology: Nanocomposites", 2008.

[21] J.M. George, Z. Lodi, "Design and selection criteria for HVDC overhead transmission lines insulators", CIGRE Canada, Toronto, October 4-6, 2009.

[22] M. F. Frechette, M.L. Trudeau, H.D. Alamdar, S. Boily, "Introductory Remarks on Nanodielectrics", Dielectrics and Electrical Insulation, IEEE Transactions on (Volume:11 , Issue:5) pp. 808-818, 2004.

[23] J.K. Nelson, Breakdown strength of solids, Engineering Dielectrics, Vol 2A, Chapter 5, ASTM, 1983.

[24] D. L. Chapman, "A contribution to the theory of electrocapillarity", Philos Mag 25: 475–481, 1993.

[25] J. K. Nelson, Y. Hu, "Nanocomposite dielectrics – Properties and implications", Journal of Physics D: Applied Physics, Issue:2, DOI:10.1088/0022-3727/38/2/005, 2005.

[26] J. K. Nelson, J. C. Fothergill, L. A. Dissado and W. Peasgood, "Towards an understanding of nanometric dielectrics", Annual Report Conference Electrical Insulation and Dielectric Phenomena, pp. 295–298, 2002.

[27] G. Chen, Y.L. Chong, M. Fu, "Calibration of the pulsed Electroacoustic technique in the presence of trapped charge.", Measurement Science and Technology, 17(7): p. 1974-1980, 2006.

[28] M.J.P. Jeroense, "Charges and discharges in HVDC cables, in particular in mass impregnated HVDC cables", TU Delft: Delft, 1997.

[29] J. Castellon, A. Toureille, "Space Charge Measurement Applied to the Ageing of Industrial Insulating Composite Materials" CSC'3, Toisième conféenc internationale sur la Charge Electrique des Isolants Solides, Tours, France, pp. 679-683, 1998.

[30] M. Wadamori, M. Fukuma, T. Maeno, K. Fukunaga and M. Nagao, "Proposal of Numerical Analysis Model of Acoustic Wave Propagation and Generation on PEA Method", Proceedings ICPADM(2003), pp.863-866, 2003.

[31] Y. Li, K. Murata, Y. Tanaka, T. Takada, M. Aihara, "Space Charge Distribution Measurement in Lossy Dielectric Materials by Pulsed Electroacoustic Method.", in Proceedings of the 4th International Conference on Properties and Application of Dielectric Materials, Australia, July 1994.

[32] R. Bodega, "Space Charge Accumulation in Polymeric High Voltage DC Cable Systems", Delft University of Technology: Delft, 2006.

[33] D. Fabiani, G.C. Montanari, C. Laurent, G. Teyssedre, P. H. F. Morshuis, R. Bodega, L. A. Dissado, A. Campus, U. H. Nilsson, "HVDC Cable Design and Space Charge Accumulation. Part 1: Insulation/ Semicon Interface.", IEEE Electrical Insulation Magazine, 23(6): p. 11-19, November/December 2007.

[34] L. A. Dissado , J.C. Fothergill, "Electrical Degradation and Breakdown in Polymers", ed. G.C. Stevens, Peter Peregrinus Ltd. on behalf of IEEE, 1992.

[35] C.P. Wong, R.S. Bollampally, "Thermal conductivity, elastic modulus, and coefficient of thermal expansion of polymer composites filled with ceramic particles for electronic packaging.", Journal of Applied Polymer Science, Vol 74:pp:(3396–

3403), 1999.

[36] K.P. Donnelly, B.R. Varlow, "Non-linear dc and ac conductivity in electrically insulating composites.", IEEE Transactions on Dielectrics and electrical insulation, Vol:10,pp:(610–614), 2003.

[37] M. Harada, M. Morimoto, M. Ochi, "Influence of network chain orientation on the mechanical property of epoxy resin filled with silica particles.", Journal of Applied Polymer Science, Vol:87,pp:(787–794), 2003.

[38] S. Holé, A. Sylvestre, S. Rowe, "The influence of filler particles on space charge measurements.", Journal of Physics D: Applied Physics, Vol:37,pp:(1869–1876), 2004.

[39] O. Gallot-Lavallee, G. Teyssedre, C. Laurent, S. Rowe, "Space charge behaviour in an epoxy resin: the influence of fillers, temperature and electrode material.", Journal of Physics D: Applied Physics, Vol:38, pp:2017–2025, 2005.

[40] K.R. Bambery, R.J. Fleming, "The temperature dependence of space charge accumulation in crosslinked polyethylene.", Journal of Thermal Analysis and Calorimetry, Vol:50,pp:(19–31), 1997.

[41] D. Mary, C. Laurent, G. Teyssedre et al., "Threshold of Space Charge Injection and Electroluminescence in Polymeric Insulation", Annual Report Conference on Electrical Insulation and Dielectric Phenomena, 2004.

[42] T. Lebey, C. Laurent, "Charge injection and electroluminescence as a prelude to dielectric breakdown", Journal of Applied Physics, Vol:68, pp.275-282, 1990.

[43] G. Teyssedre, C. Laurent, G.C. Montanari, F. Palmieri, A. See, L.A. Dissado, J.C. Fothergill, "Charge distribution and electroluminescence in XLPE under dc fields", Journal of Physics D,Vol:34, pp. 2830-2844, 2001.

[44] L.A. Dissado, C. Laurent et al., "Demonstrating a Threshold for Trapped Space Charge Accumulation in Solid Dielectrics under dc Field", IEEE Transactions on Dielectrics and Electrical Insulation Vol. 12, No. 3; June 2005.

[45] J. M. Alison, J.V. Champion, S.J. Dodd, G. C. Stevens, "Dynamic Bipolar Charge Recombination Model for Electroluminescence in Polymer Based Insulation During Electrical Tree Initiation", Journal of Physics D: Applied Physics, Vol:28, pp:1693-1701, 1995.

[46] A. Many, G. Rakavi, "Theory of Transient Space Charge Limited Current in Solids in the Presence of Trapping", Physical Review, Vol: 126, pp. 1980-1988, 1962.

[47] A. Rose, "Space-charge-limited Currents in Solid", Physical Review, Vol:97, pp. 1538-1544, 1955.

[48] N. F. Mott, R. W. Gurney, "Electronic Processes in Ionic Crystals", Oxford University Publishers, New York, 1940.

[49] D. A. Seanor, Electrical Properties of Polymers, Academic Press, 1982.

[50] G. C. Montanari, D. Fabiani, "Evaluation of dc Insulation Performance Based on Space-charge Measurements and Accelerated Life Tests",IEEE Transactions on Dielectrics & Electrical Insulation, Vol:7, pp. 322-328, 2000.

[51] D. Fabiani, G.C. Montanari, R. Bodega et al., "The Effect of Temperature Gradient on Space Charge and Electric Field Distribution of HVDC Cable Models", IEEE, 2006.

[52] G.C. Montanari, P. Morshuis, "Space charge phenomenology in polymeric insulating materials", IEEE Trans. on Dielectrics and Electrical Insulation, Vol:12, No:4, pp. 754-767, June 2005.

[53] Peng Liu (State Key Lab. of Electr. Insulation & Power Equip)., Xi'an Jiaotong Univ., Xi'an, China , Zhen Xiang ; Xin Ning ; Hua Feng ; Zongren Peng, "Effect of electrode material on space charge behavior in epoxy resin", Electrical Insulation and Dielectric Phenomena (CEIDP), IEEE Conference, 2013.

[54] H. Okubo, "Enhancement of electrical insulation performance in power equipment based on dielectric material techniques", IEEE Conference on Electrical Insulation and Dielectric Phenomena (CEIDP), 2011.

[55] T. Andritsch, "Epoxy Based Nanocomposites for High Voltage dc Applications – Synthesis, Dielectric Properties and Space Charge Dynamics.", PhD thesis, Delft University of Technology, ISBN 978-90-5335-331-8, 2010.

[56] I.A. Tsekmes, "Electrical Characterization of Polymeric DC Mini-Cables by means of Space Charge & Conduction Current Measurements", Delft University of Technology, August 2012.

[57] K. Fukunaga, H. Tanaka et al, "In Situ Space Charge Measurement of PCB Insulations During the Ageing Test", 2005.

[58] Y. Zhang, J. Lewiner et al, "Evidence of strong correlation between space-charge buildup and breakdown in cable insulation", IEEE Transactions on Electrical Insulation, Vol:3(6):pp:778, Dielectrics and Electrical Insulation, IEEE Transactions on (Volume:3 ,Issue:6), 1996.

[59] X. Chun et al.,"Electric Field Analysis of Space Charge Injection from a Conductive Nano-Filler Electrode", Chinese Physics Letters Vol:27, No.7 (2010) 077303, 2010.

[60] G. Blaise, W. J. Sarjeant, "Space charge in dielectrics energy storage and transfer dynamics from atomistic to macroscopic scale", IEEE Transactions on Electrical Insulation, Vol:5(5):pp:779, 1998.

[61] P. Gonon, A. Boudefel, "Electrical properties of epoxy/silver nanocomposites", Journal of Applied Physics, Vol:99, pp: 024308(1)-024308(8), 2006.

[62] G. Tsagaropoulos, A. Eisenberg, "Dynamic Mechanical Study of the Factors Affecting the Two Glass Transition Behavior of Filled Polymers. Similarities and Differences with Random Ionomers", Macromolecules, Vol:28, pp: 6067-6077, 1995.

[63] Devin R. Merrill, Daniel B. Moore, "Misfit Layer Compounds and Ferecrystals: Model Systems for Thermoelectric Nanocomposites", Materials: Volume 4, 2015.

[64] L. Zhang et al., "Effect of Nanoparticle Surface Modification on Breakdown and Space Charge Behavior", 2014.

[65] T. Takada et al,"Space charge trapping in electrical potential well caused by permanent and induced dipoles for LDPE/MgO nanocomposite", Dielectrics and Electrical Insulation, IEEE Transactions on (Volume: 15, Issue: 1), 2008.

[66] H. Chakraborty, A. Sinha et al., "Effect of Space Charge Density and High Voltage Breakdown of Surface Modified Alumina Reinforced Epoxy Composites", Transactions on Electrical and Electronic Materials, Vol:14, Issue:3, pp:121-124, 2013.

[67] J. Rebouel, "Metal-Organic Frameworks: Coordination Polymer Nanoparticles and Macrostructures", Wiley Publishing, 2014.

[68] S.K. Bhattacharya, "Metal filled Polymers", Marcel Dekker Publishers, USA, 1986.

[69] C. Raman et al, "Thermally conductive but electrically insulating plastics for thermal management applications", Momentive Performance Materials Inc, 2015.

[70] Internet site: www.nanomizer.co.jp, visted on 21-06-2015.

[71] D. J. McClements, "Nanoparticle- and Microparticle-based Delivery Systems", CRC press, ISBN 9781482233155 - CAT K22935, 2014.

[72] Y.W. Mai, Z. Yu, "Polymer Nanocomposites", Woodhead Publishing, 28 February 2006.

[73] D. Pitsa, M.G. Danikas, "Interfaces features in polymer nanocomposites: a review of proposed models", NANO: Brief Reports and Reviews Vol:6, No.6 (2011), pp:497–508, World Scientific Publishing Company, 2011.

[74] G. Wróbel, S. Pawlak, "The effect of fiber content on the ultrasonic wave velocity in glass/polyester composites", Journal of Achievements in Materials and Manufacturing Engineering, Volume-20, Pages 295-298, 2007.

[75] P.N. Bindumadhavan, H. K. Wah, "Assessment of particle-matrix debonding in particulate metal matrix composites using ultrasonic velocity measurements", Materials Science and Engineering, 323 (2002) 42-51, 2002.

[76] P. H. F. Morshuis, "Lecture notes: High voltage dc", Delft University of Technology, 2010.

[77] F. H. Kreuger, Industrial high DC voltage. Delft University Press, 1995.

[78] G. Mazzanti, G. C. Montanari, and J. M. Alison, "A space-charge based method for the estimation of apparent mobility and trap depth as markers for insulation degradation: theoretical basis and experimental validation," IEEE Transactions on Dielectrics and Electrical Insulation, Vol:10, No:2, pp:187-197, 2003.

[79] A. K. Jonscher, "Dielectric relaxation in solids", Journal of Physics D: Applied Physics, Vol:32, No:14, pp:57-70, 1999.

[80] Phased Array Ultrasonic Flaw Detector manual, Omniscan MX2, Olympus NDT Canada Inc.

[81] N.H. Ahmed, N.N. Srinivas, 1997, IEEE Transactions on Dielectrics and Electrical Insulation, Vol:4, pp:644.

[82] F. Rogti et al., "Space Charge Behavior at Physical Interfaces in Cross-linked Polyethylene under DC Field", IEEE Transactions on Dielectrics and Electrical Insulation Vol: 15, No. 5; October 2008.

[83] V. Griseri, L.A. Dissado, J.C. Fothergill, G. Teyssedre, C. Laurent, "Electroluminescence Excitation Mechanisms in an Epoxy Resin Under Divergent and Uniform Field", IEEE Transactions on Dielectrics and Electrical Insulation, Vol. 9, No. 1, February 2002.

[84] T. Iizuka, K. Yoshimoto, H. Takai, K. Fukunaga and T. Maeno, "Measurement of space charge distribution in epoxy resin", Electrical Engineering in Japan, Volume:129, Issue:3, pp:9–16, 30 November 1999.

[85] G. Chen, T.Y.G Tay et al, "Electrodes and Charge Injection in low density polyethylene: using the Pulsed Electroacoustic technique", IEEE Transactions on Dielectrics and Electrical Insulation, Vol:8, No:6, December 2001.

[86] K. Fukunaga, T. Maeno, "Space charge formation at the interface between a charge transport layer and a polyester film", Dielectrics and Electrical Insulation, IEEE Transactions on (Volume:5 , Issue:2), 1998.

[87] D. Fabiani, G.Chen, G.C. Montanari et al, "Space Charge Dynamics in Nanostructured Epoxy Resin", 2008.

[88] I.A. Tsekmes, R. Kochetov, P.H.F Morshuis, J.J. Smit, "The role of particle distribution in the dielectric response of epoxy-boron nitride nanocomposites", Journal of Materials Science, Vol:50, Issue(3), pp:(1175-1186), October 2014.

[89] R. Kochetov, T. Andritsch, P.H.F Morshuis, J.J. Smit, "Anomalous behaviour of the dielectric spectroscopy response of nanocomposites.", IEEE Transactions on Dielectrics and Electrical Insulation, Vol:19, pp:107–117, 2012.

[90] I.A. Tsekmes, R. Kochetov, P.H.F. Morshuis, J.J. Smit, "Evaluating the Effect of Particle Distribution and Dispersion on the Dielectric Response of Boron Nitride - Epoxy Nanocomposites", Electrical Insulation Conference, Philadelphia, Pennsylvania, USA,2014.

[91] M. F. Fréchette, A Vijh, L Utracki, M. L. Trudeau, A Sami, C Laurent, P Morshuis, T Andritsch, R Kochetov, A Vaughan, E David, J Castellon, D Fabiani, S Gubanski, J Kindersberger, C Reed, A Krivda, J Fothergill, S Dodd, F Guastavino, H Alamdari, "Nanodielectrics: A Panacea for Solving All Electrical Insulation Problems?", International Conference on Solid Dielectrics, Potsdam, Germany, July 4-9, 2010.

[92] Y. Li, M. Yasuda, T. Takada, "Pulsed Electroacoustic Method Measurement of Charge for Accumulation in Solid Dielectrics", IEEE transactions on Dielectrics and Electrical Insulation, Vol:1(2): pp:(188-195), 2004.

[93] J.M Alison, "Pulsed electro-acoustic system for space charge and current density measurements at high fields over a temperature range 25°C- 80°C", Proceedings of CSC'3, pp:(711-714), 1998.

[94] T. Maeno, T. Futami, H. Kushibe, T. Takada and C. M. Cooke, "Measurement of Spatial Charge Distribution in Thick Dielectrics using the Pulsed Electroacoustic Method", IEEE Transactions on Dielectrics and Electrical Insulation, Vol:23, pp:(433-140),1988.

[95] P. Bloss, H. Schafer, "Investigations of polarization profiles in multilayer systems by using the laser intensity modulation method", Review of Scientific Instruments, Vol:65, pp: 1541-1550, 1991.

[96] S.B. Lang, D.K. Dasgupta, "Laser-intensity-modulation method: a technique for determination of spatial distributions of polarization and space charge in polymer electrets", Journal of Applied Physics, Vol: 59, pp:(2151-60), 1986.

[97] G.M. Sessler, "LIPP investigation of piezoelectricity distributions in PVDF poled with various methods", Ferroelectrics, Vol:76, pp:(489-96), 1987.

[98] K. Fukunaga, "Industrial applications of space charge measurement in Japan", IEEE Electrical Insulation Magazine, Vol:15, No:5, pp:(6-18), Sept/Oct 1999.

[99] T. Mizutani, "Space charge measurement techniques and space charge in polyethylene", IEEE Transactions on Dielectrics and Electrical Insulation, Vol:1, pp:(923-33), 1994.

[100] I.M. Zimmerling, "Space charge development in XLPE model cables", Master of Science thesis, Delft University of Technology, April 2015.

[101] M.A. Lampert, "Simplified Theory of Space-Charge-Limited Currents in an Insulator with Traps", Physical Review Volume: 103, Number:6, September 15, 1956.

[102] P. Morshuis, "Interfaces: to be avoided or to be treasured?", IEEE International Conference on Solid Dielectrics, Bologna, Italy, June 30 – July 4, 2013.

Appendix I
General signal processing

Deconvolution of signal

The electrical signal is not a correct representation of the space charge profile as the amplifier acts as a high pass filter which distorts the original pressure signal. According to convolution theorem, once the signal response of a linear system is known, the relation between the input and output of that circuit can be calculated. So, the system response H can give the relationship between the detected signal at the oscilloscope $U_{det}(t)$ and the original signal $U_{orig}(t)$. If the system response is known, it is possible to compute the original signal by using the inverse system response H^{-1}. Therefore, in the frequency domain, the equation provided below holds.

$$U_{det}(f) = H(f)U_{orig}(f) \tag{5.1}$$

In the time domain the original signal $U_{orig}(t)$ is given by equation 5.2.

$$U_{orig}(t) = F^{-1}\frac{U_{det}(f)}{H(f)} \tag{5.2}$$

It is worth noting that the deconvoluted signal $U_{decon}(t)$ is never identical to the original signal $U_{orig}(t)$. Thus, the deconvoluted signal is designated. The deconvolution process is explained with the aid of the diagram presented below.

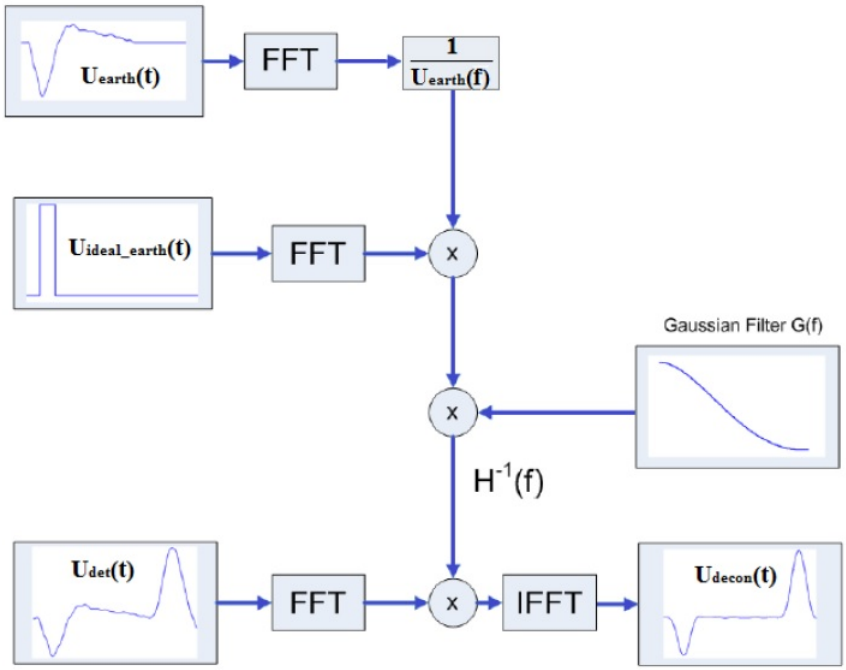

Figure 5.2.1: Schematic representation: Deconvolution technique

As the system response is not known, equation 5.2 cannot be applied directly. The system response is determined by using the signal $U_{earth}(t)$ which represents the earth electrode and the bulk of the material which is part of the detected signal $U_{det}(t)$. Usually, the earth electrode is chosen because the acoustic signal of this charge does not experience any attenuation and dispersion by the sample material.

Also, the ideal signal $U_{ideal-earth}(t)$ from the electrode charge is used. So, it is a signal without the response of the sensor and the amplifier. This ideal signal is represented by a pulse which has approximately the same width as the earth electrode in the detected signal $U_{det}(t)$ and has a height of 1. This height is usually much larger than the height of the electrode signal in the detected signal.

The ideal signal $U_{ideal-earth}(t)$ and the measured signal $U_{earth}(t)$are converted into the frequency domain. Then the former is divided by the latter and the inverse response function $H^{-1}(f)$ can be calculated. However, the presence of high frequency components can affect the final deconvoluted signal $U_{decon}(t)$. In order to eliminate or attenuate these high frequency components a low pass Gaussian filter with transfer function G(f) is used.

However, the deconvoluted signal is still an approximation as the height of the ideal signal is one and the resulting deconvoluted signal does not have the correct value. Therefore, a correction factor $K_{cor}$is required. This factor can be obtained by

dividing the maximum value of the deconvoluted signal by the maximum value of the detected signal according to equation 5.3.

$$K_{cor} = |\frac{max(U_{decon}(t))}{max(U_{det}(t)}| \tag{5.3}$$

So, the final deconvoluted signal $U_{f-decon}(t)$ is obtained by using equation 5.4.

$$U_{f-decon}(t) = \frac{U_{decon}(t)}{K_{cor}} \tag{5.4}$$

The deconvolution process is performed correctly only when the signal is free of space charge. Otherwise, the signal $U_{earth}(t)$ cannot be flat outside the charge region.

5.2.1 Attenuation & Dispersion

A general expression for a planar acoustic wave p(x,t) travelling through an ideal medium can be described in the frequency domain by equation 5.5.

$$p(x, \omega) = P_o(\omega)exp(-i\beta\omega) \tag{5.5}$$

Where $P_o(\omega)$ represents the magnitude of the pressure wave with angular frequency ω at zero location $(P_o(o, \omega))$. This wave propagates without attenuation and its velocity v is related to the phase coefficient β according to equation 5.6.

$$\beta = \frac{v}{\omega} \tag{5.6}$$

An acoustic wave p(x,t) travelling through a lossy and dispersive medium can be described in the frequency domain by equation 5.7.

$$p(x, \omega) = P_o(\omega)exp(-a(\omega)x)exp(-i\beta(\omega)x) \tag{5.7}$$

Where $a(\omega)$ is the frequency-dependent attenuation factor and $\beta(\omega)$ is the frequency-dependent phase factor. The former takes into account that the wave magnitude decreases as the wave travels through the medium and the latter takes into account the frequency dependence of the speed of sound in the medium.

$$G(x, \omega) = \frac{p(x, \omega)}{p(o, \omega)} = exp(-a(\omega)x)exp(-i\beta(\omega)x) \tag{5.8}$$

The coefficients $a(\omega)$ and $\beta(\omega)$ are calculated with the use of two acoustic waves at two different locations in the sample. The acoustic wave generated at the HV electrode $p(d, \omega)$ and the corresponding acoustic wave detected at the sensor $p(o, \omega)$ are used. Thus, equation 5.9 is valid.

$$G(d, \omega) = \frac{p(d, \omega)}{p(o, \omega)} = exp(-a(\omega)d)exp(-i\beta(\omega)d) \tag{5.9}$$

When the function $G(d, \omega)$ is defined, the coefficients $a(\omega)$ and $\beta(\omega)$ can be calculated. In this way the function $G(x, \omega)$ can be determined and the pressure distribution p(x,t) inside the sample can be derived according to equation 5.10. The initial acoustic wave at any location is determined by the acoustic wave detected at the sensor.

$$p(x, t) = F^{-1}[p(o, \omega)G(x, \omega)] \tag{5.10}$$

The pressure distribution p(x,o) corresponds to the acoustic wave at its initial location where it is generated and the pressure distribution p(o,t) corresponds to the acoustic wave at the sensor location after travelling through the sample.

In order to implement the procedure described above, the original signal at the HV electrode which corresponds to the acoustic wave $p(d, \omega)$ is required. If the sample is space charge free, the recovered signal at the HV electrode represents the electrode charge only. This charge can be calculated when a known voltage is applied across the sample. It is worth noting that the recovered signal does not exactly correspond to the original signal as some of the higher frequencies of the original signal may be totally attenuated.

The calculation of the coefficients $a(\omega)$ and $\beta(\omega)$ with the use of the function $G(d, \omega)$ includes some difficulties. Firstly, the function $G(d, \omega)$ is defined as the ratio of two other functions. So, if the denominator contains zeros, the division cannot be performed. Secondly, during the mathematical procedure high frequencies of the signal are amplified more than the low frequencies. Thus, if noise is present in the detected signal, it is amplified as well. These two problems can be tackled with

defining two approximating equations for the calculation of the coefficients $a(\omega)$ and $\beta(\omega)$.

$$a(\omega) = A + a(\omega^2) \tag{5.11}$$

$$\beta(\omega) = b\omega \tag{5.12}$$

Equations 5.11 and 5.12 are valid under the assumption that the original waveform y1(t) and the detected waveform y2(t) are Gaussian functions according to equations 5.13 and 5.14.

$$y_1(t) = A_1 exp(-a_1(t-\tau_1)^2) \tag{5.13}$$

$$y_2(t) = A_2 exp(-a_2(t-\tau_2)^2) \tag{5.14}$$

In the frequency domain equations 5.13 and 5.14 can be written according to equations 5.15 and 5.16.

$$Y_1(\omega) = A_1\sqrt[1]{\frac{\pi}{a_1}} exp(-i\tau_1\omega - \frac{\omega^2}{4a_1}) \tag{5.15}$$

$$Y_2(\omega) = A_2\sqrt[1]{\frac{\pi}{a_2}} exp(-i\tau_2\omega - \frac{\omega^2}{4a_2}) \tag{5.16}$$

As a result, the function $G(d,\omega)$ can be written according to equation 5.17.

$$G(d,\omega) = \frac{Y_1}{Y_2} = \frac{A_1}{A_2}\sqrt[1]{\frac{a_2}{a_1}} exp(-i\omega(\tau_1 - \tau 2) - \frac{\omega^2}{4}(\frac{1}{a_1} - \frac{1}{a_2})) = exp(-d(A + a\omega^2))exp(-ib\omega d) \tag{5.17}$$

Where the terms A,a and b are determined from equations 5.18, 5.19 and 5.20 respectively.

$$A = -\frac{1}{d}\ln(\frac{A_1}{A_2}\sqrt[1]{\frac{a_2}{a_1}}) \tag{5.18}$$

$$a = \frac{1}{4d}(\frac{1}{a_1} - \frac{1}{a_2}) \tag{5.19}$$

$$b = \frac{1}{d}(\tau_1 - \tau_2) \tag{5.20}$$

The values of the above parameters depend on the type of the medium and approximate values are used. Therefore, the coefficients $a(\omega)$ and $\beta(\omega)$ can be determined according to equations 5.11 and 5.12 respectively.

Appendix II
Setup photographs

Technical specifications & photographs of the PEA setup

This part mainly deals with photographs of the test setup used at the High Voltage Laboratory of TU Delft, by the author, to conduct the experiments- the results of which have been discussed in this work.

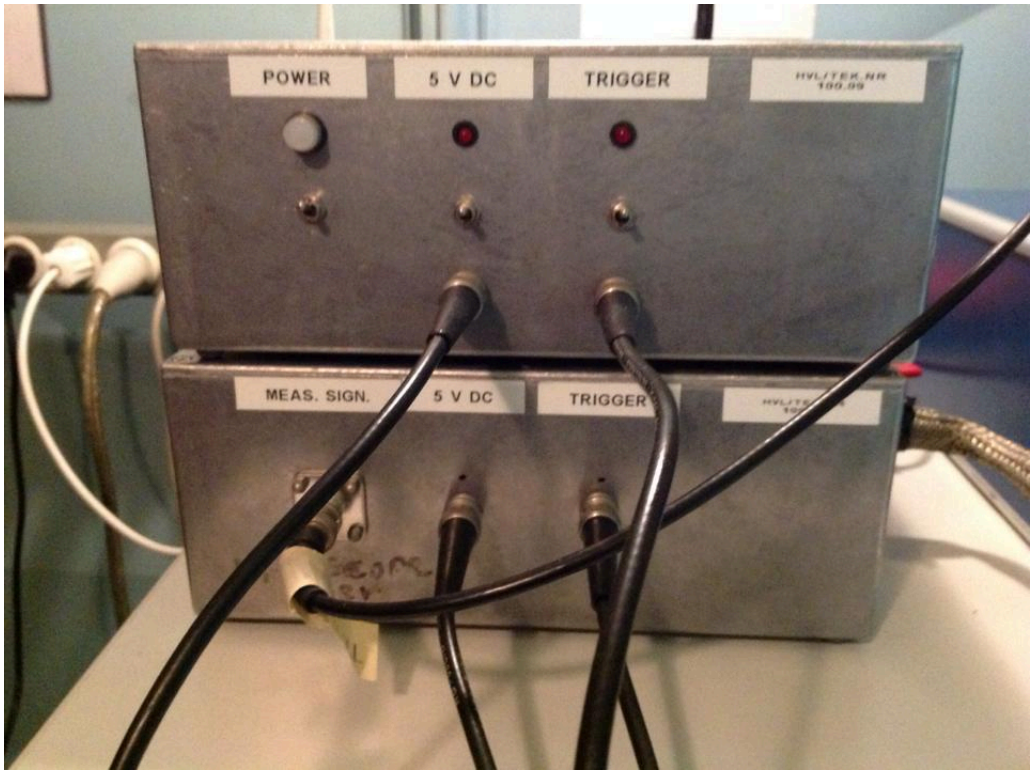

Figure 5.2.2: Switch box for PEA setup

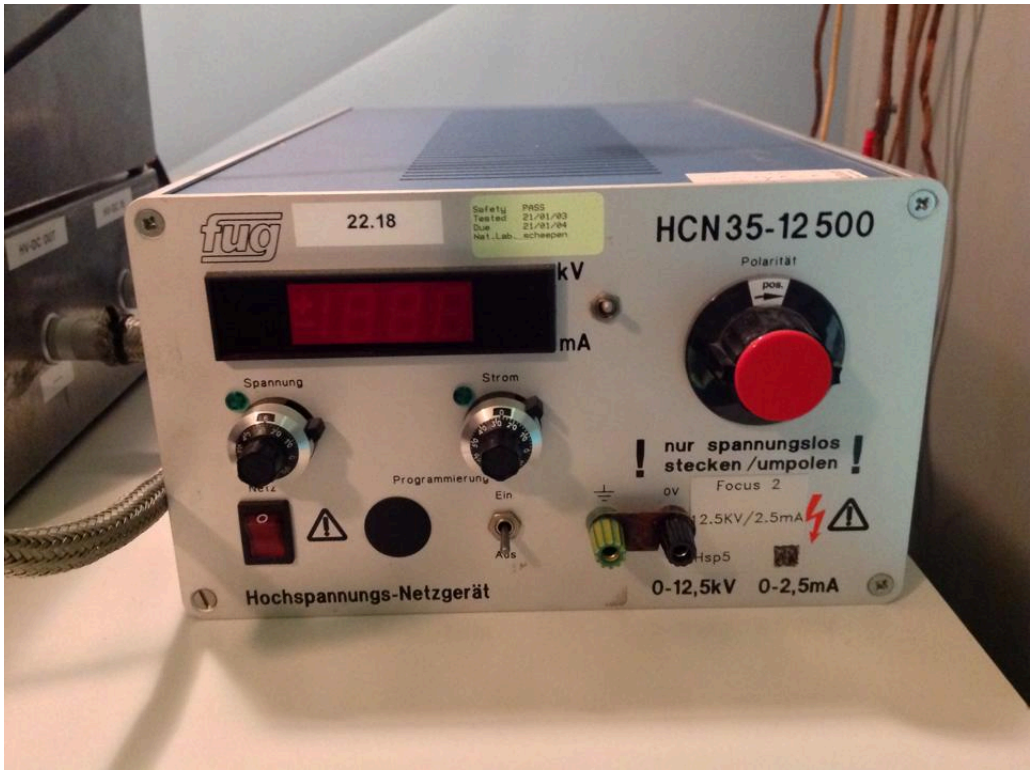

Figure 5.2.3: HVDC pulse generator for PEA setup

Equipment	Make type	Input	Output
HVDC generator(Fig-5.2.3)	FUG HCN35-12500	230 V	12.5 kV, 2.5 mA
Switch box(Fig-5.2.2)	TU Delft	-	-

Figure 5.2.4: HVDC supply for PEA setup

Equipment	Make type	Input	Output
HVDC supply(Fig-5.2.4)	FUG HCN35-65000	230 V	65 kV, 0.5 mA

Figure 5.2.5: Oscilloscope used for data acquisition from PEA setup

Equipment	Sample Rate, RIS	Bandwidth	Averaging
LeCroy WaveRunner 6050(Fig-5.2.5)	5 GS/sec, 200 GS/sec	500 MHz	Upto 1 million sweeps

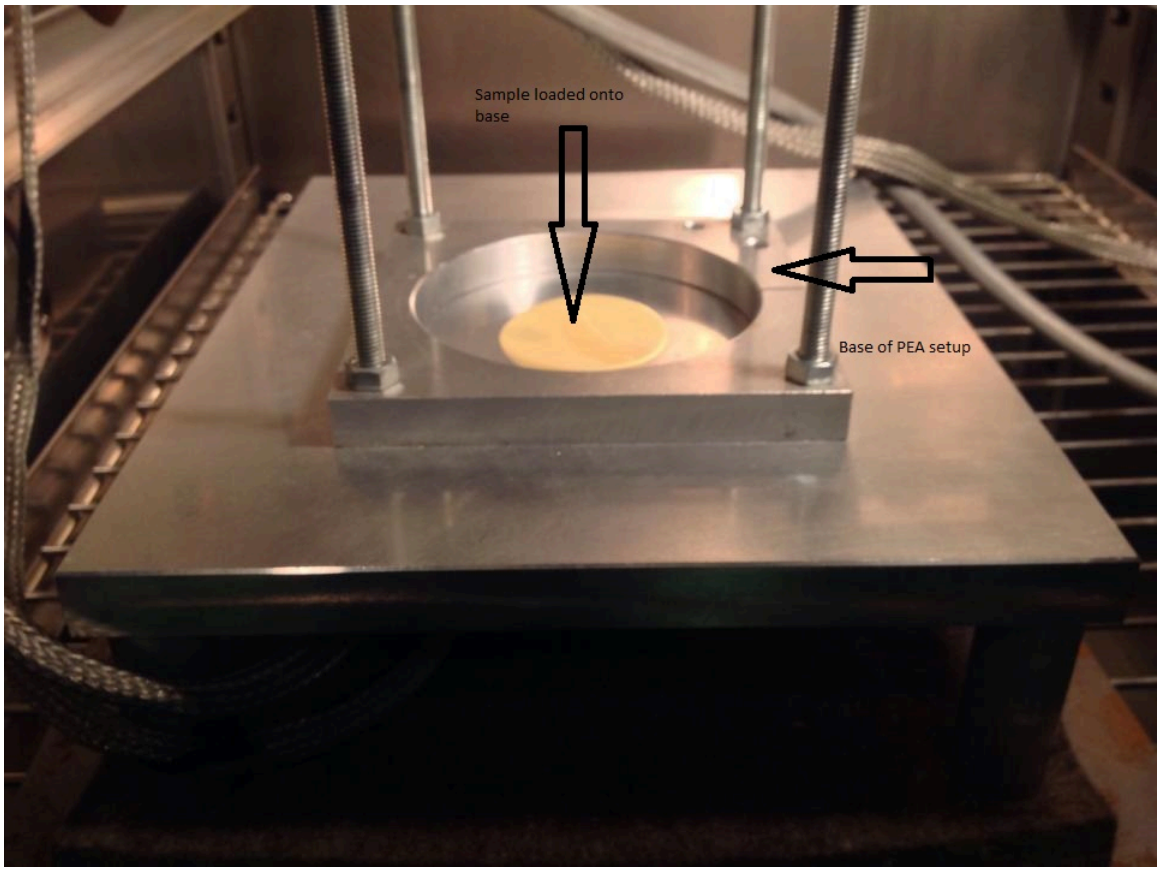

Figure 5.2.6: PEA setup, sample loaded onto base

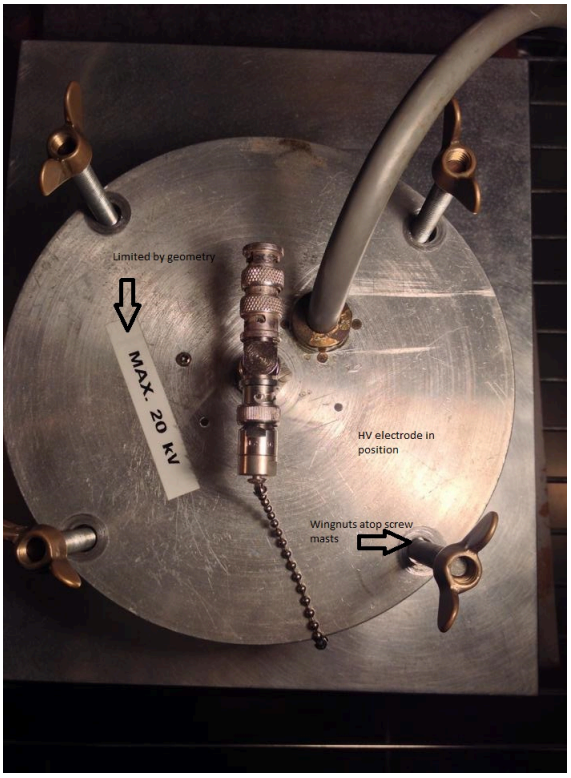

Figure 5.2.7: PEA setup, HV electrode in position

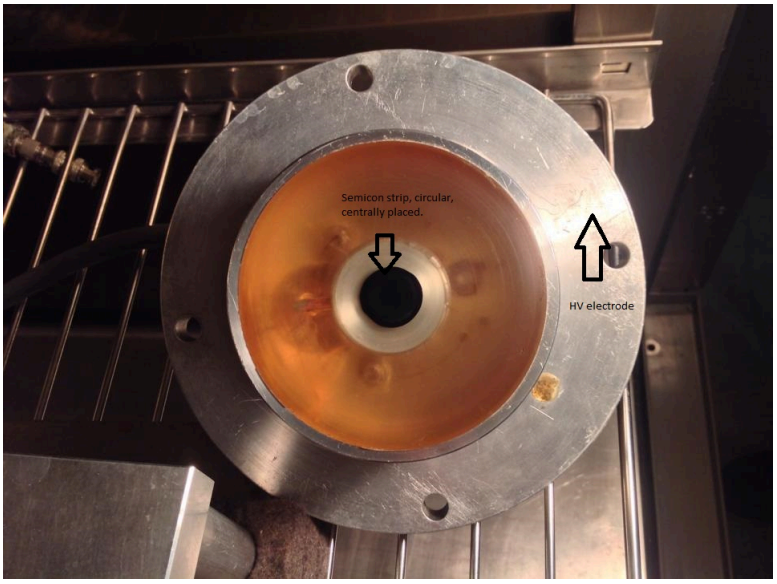

Figure 5.2.8: PEA setup, HV electrode with semicon strip

Photographs of the setup, for acoustic measurements

This part mainly deals with photographs of the test setup used at the Aerospace NDT Laboratory of TU Delft, by the author in collaboration with Dr. A.G. Anisimov, to conduct the experiments- the results of which have been discussed in this work.

Figure 5.2.9: The Omniscan MX2 Flaw detector

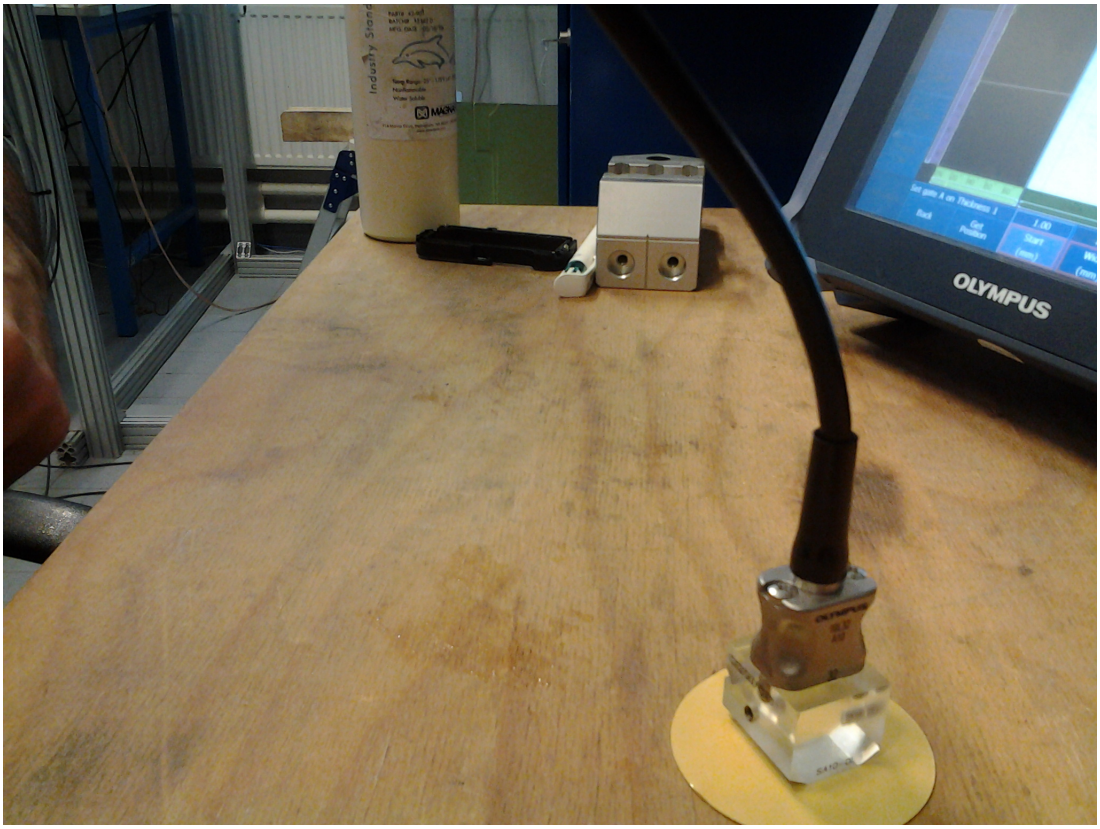

Figure 5.2.10: The Omniscan MX2 Flaw detector, sample underneath optical wedge, gel for application on surface

Appendix III
Contour plots & other diagrams of relevance

E-hBN-0.5, 30 kV/mm, 45 degrees- a selection of traces

Primarily, the space charge profile for the specimen under consideration is presented in Figure-5.2.11. The relevant portion is magnified in Figure-5.2.12 to make the exposition made on Page-71 clear to the reader.

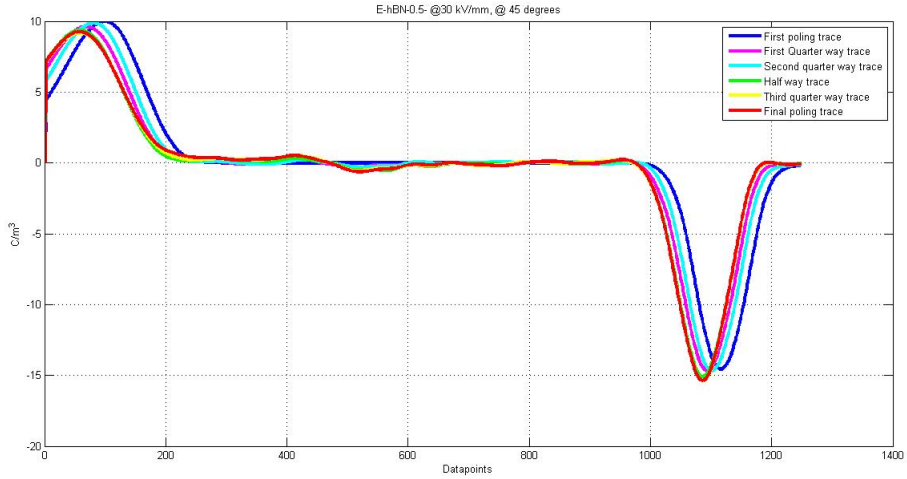

Figure 5.2.11: The selection of traces, for E-hBN-0.5, 30 kV/mm, 45 degrees

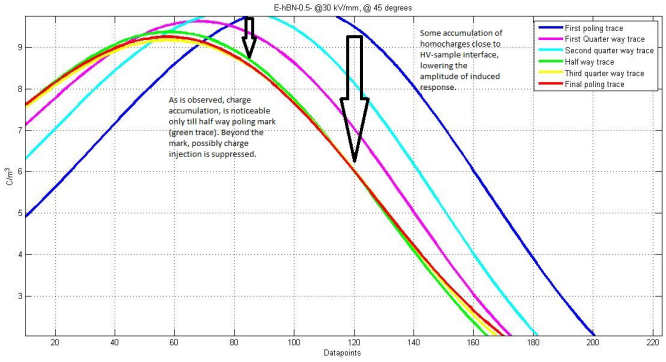

Figure 5.2.12: The selection of traces, for E-hBN-0.5, 30 kV/mm, 45 degrees[magnified]

The next section deals with the contour plots, used for the threshold measurements, for the best performing samples as determined earlier in Chapter-4.

A collection of contour plots

Primarily, the collection of the contour plots for neat epoxy is presented in Figure-5.2.13 & Figure-5.2.14.

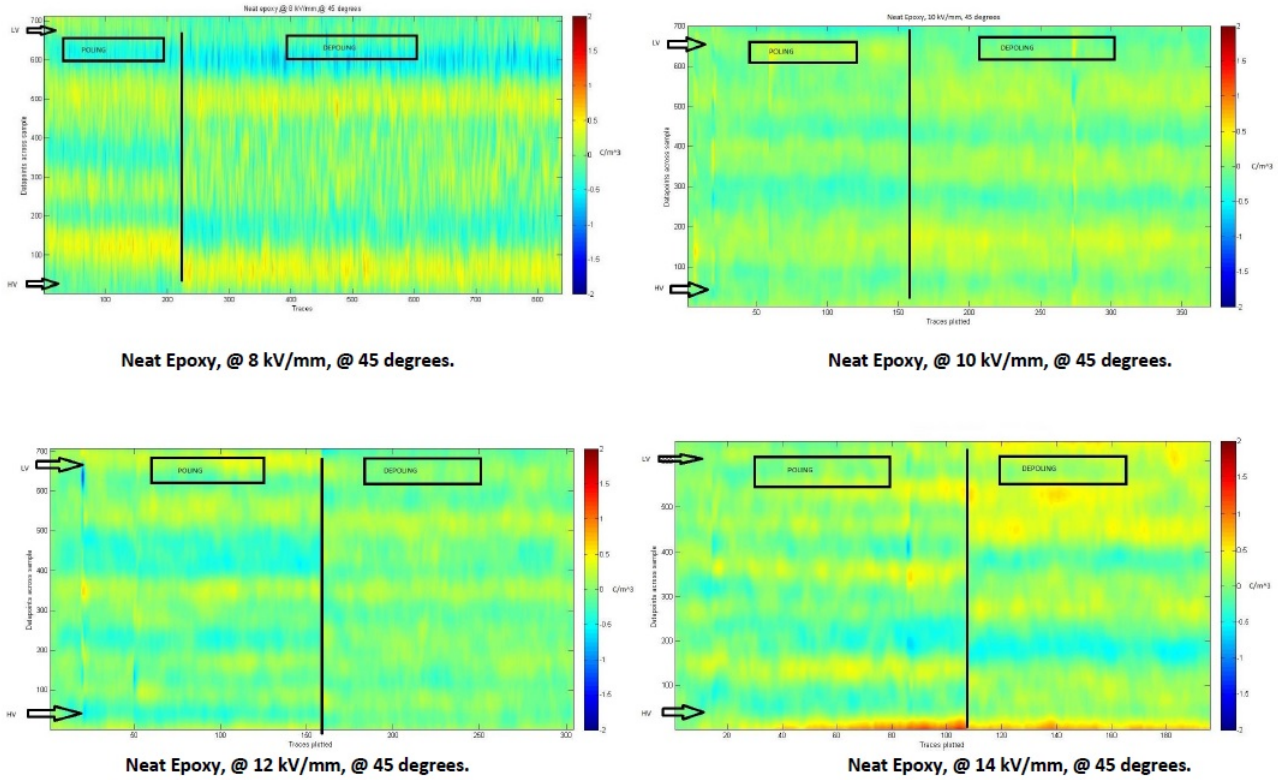

Figure 5.2.13: Neat epoxy contour plots-1

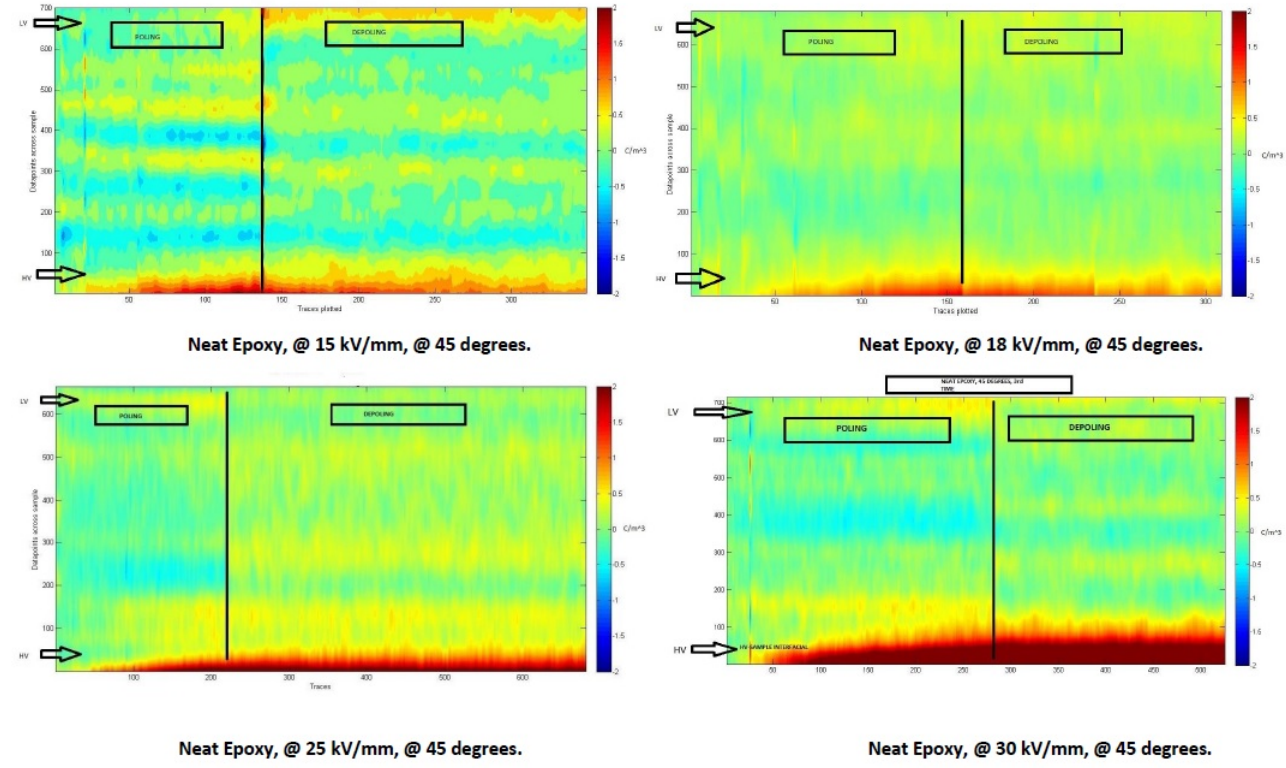

Figure 5.2.14: Neat epoxy contour plots-2

Next, the collection of the contour plots for E-hBN-0.2-C is presented in Figure-5.2.15 & Figure-5.2.16.

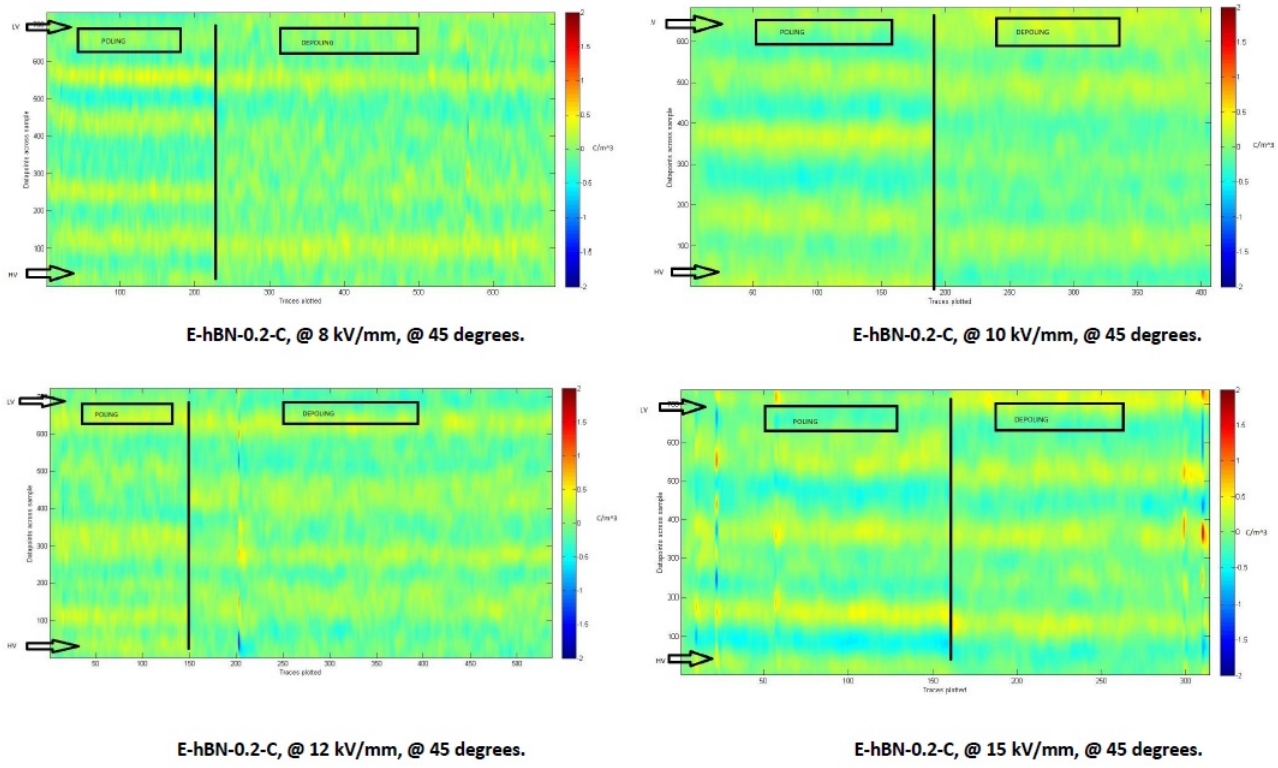

Figure 5.2.15: E-hBN-0.2-C contour plots-1

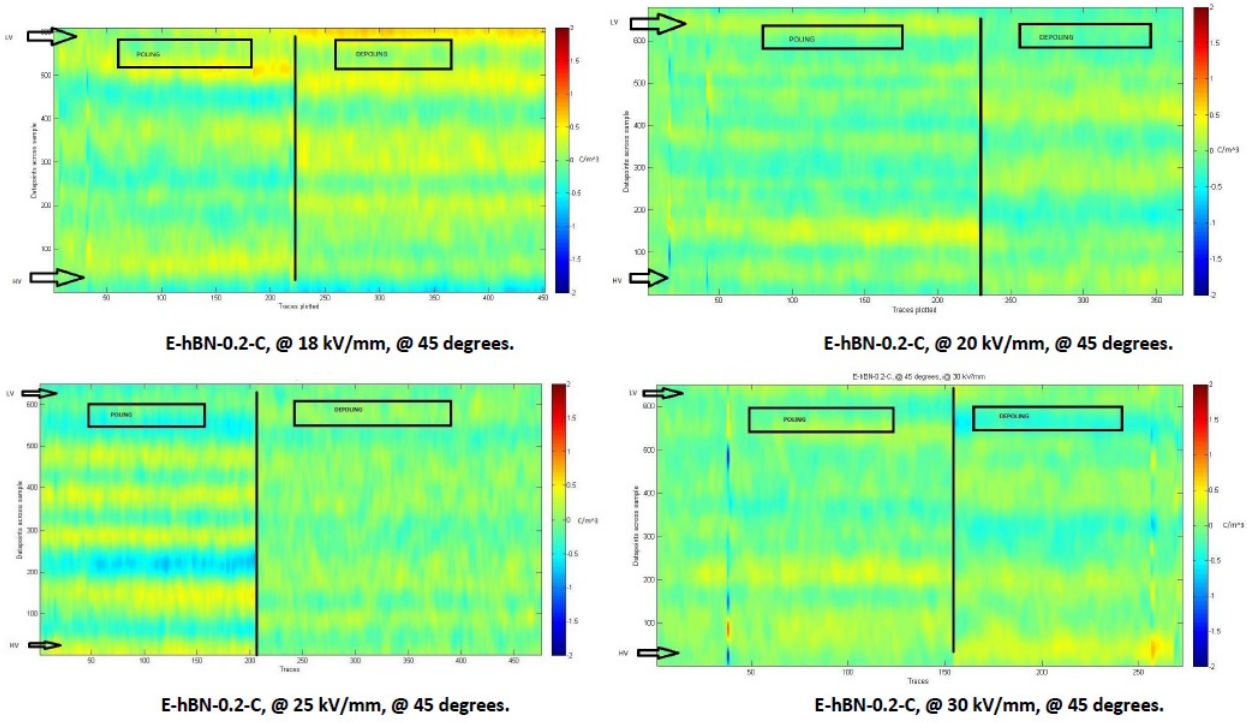

Figure 5.2.16: E-hBN-0.2-C contour plots-2

Next, the collection of the contour plots for E-hBN-0.5 is presented in Figure-5.2.17 & Figure-5.2.18.

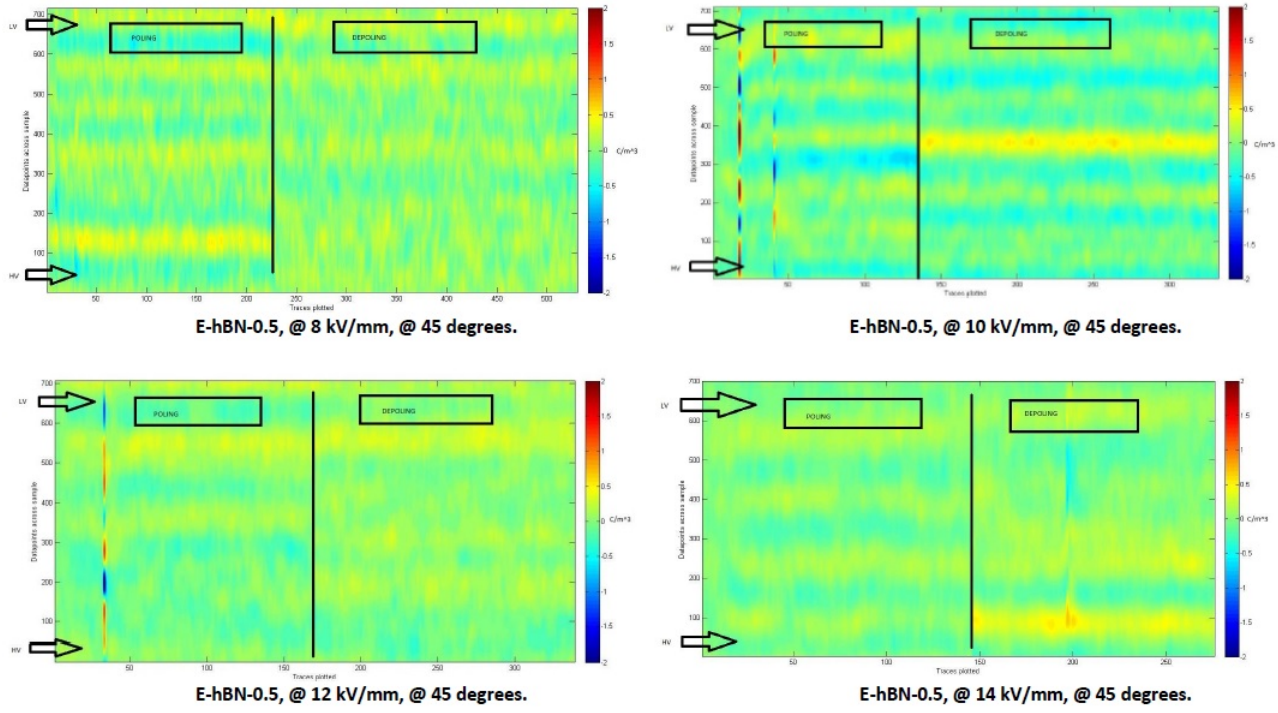

Figure 5.2.17: E-hBN-0.5 contour plots-1

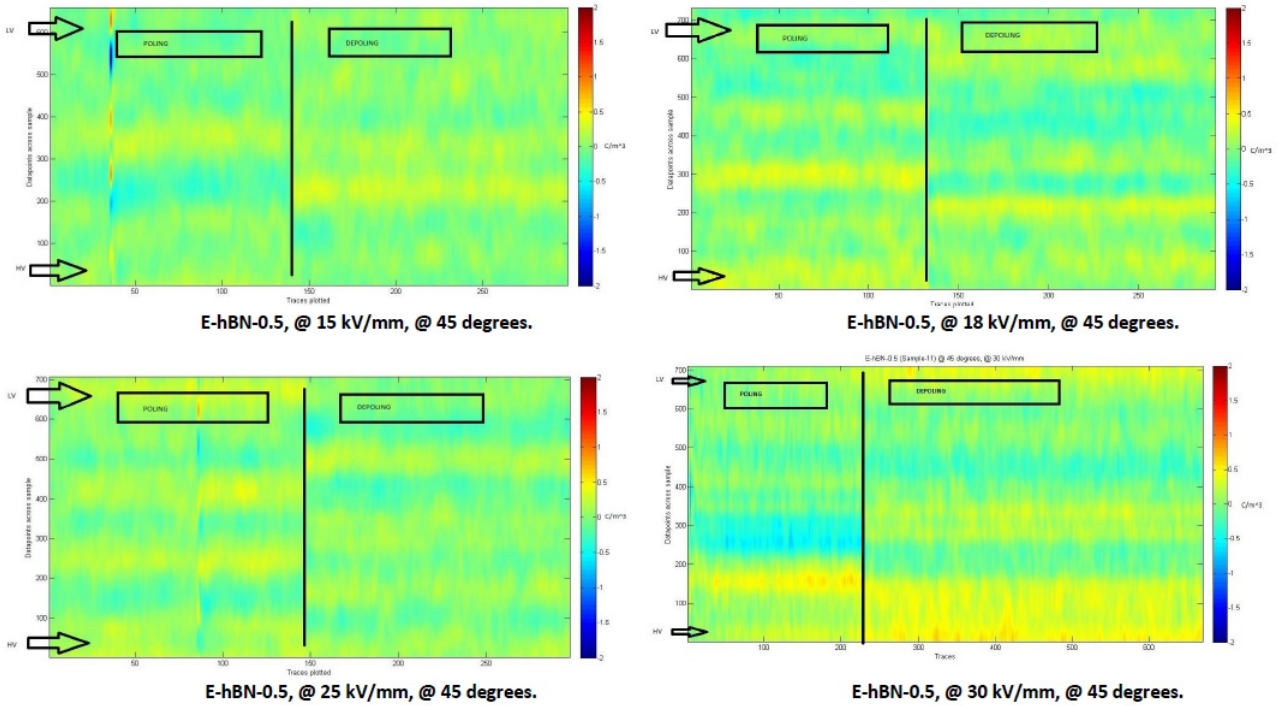

Figure 5.2.18: E-hBN-0.5 contour plots-2

Next, the collection of the contour plots for E-hBN-0.6 is presented in Figure-5.2.19 & Figure-5.2.20.

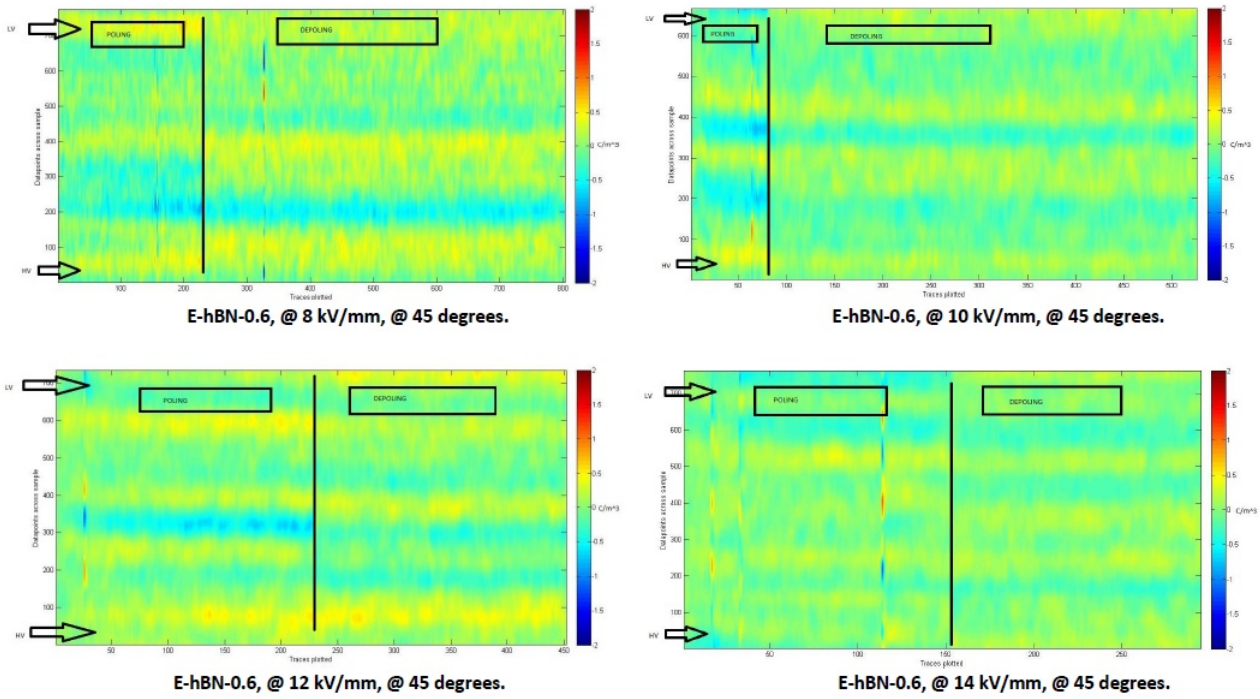

Figure 5.2.19: E-hBN-0.6 contour plots-1

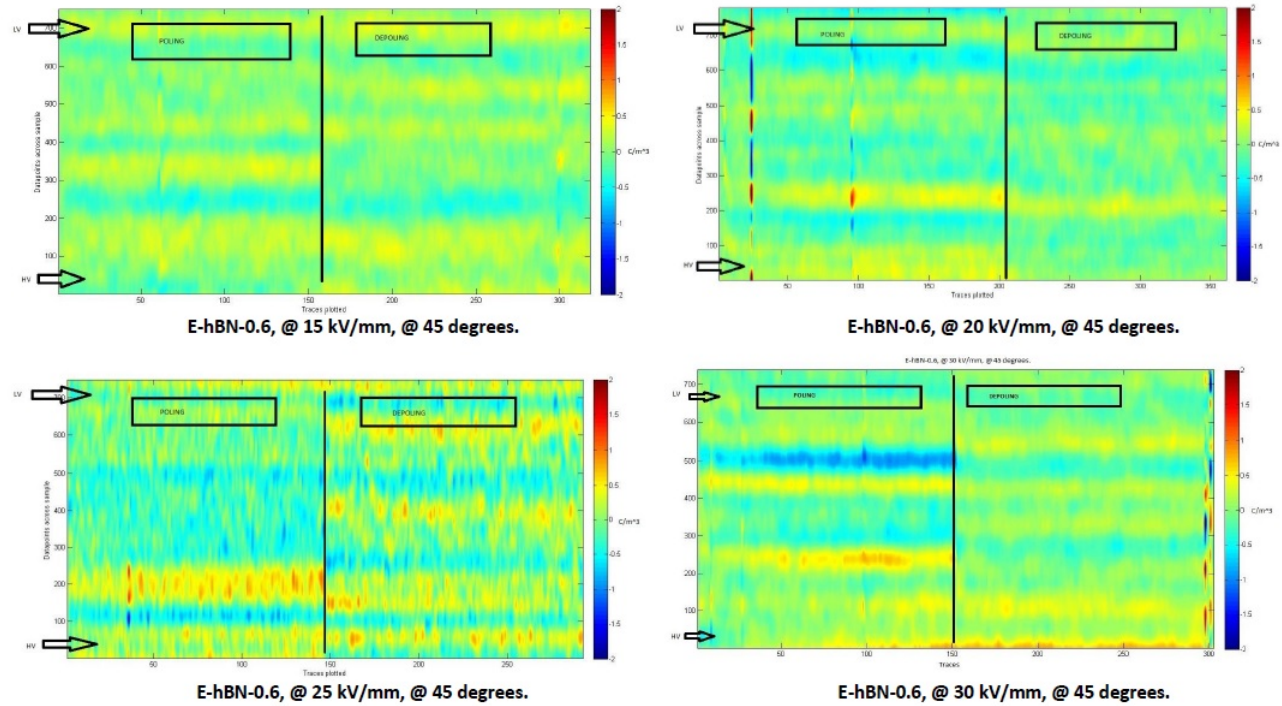

Figure 5.2.20: E-hBN-0.6 contour plots-2

Next, the collection of the contour plots for E-hBN-1-C is presented in Figure-5.2.21 & Figure-5.2.22.

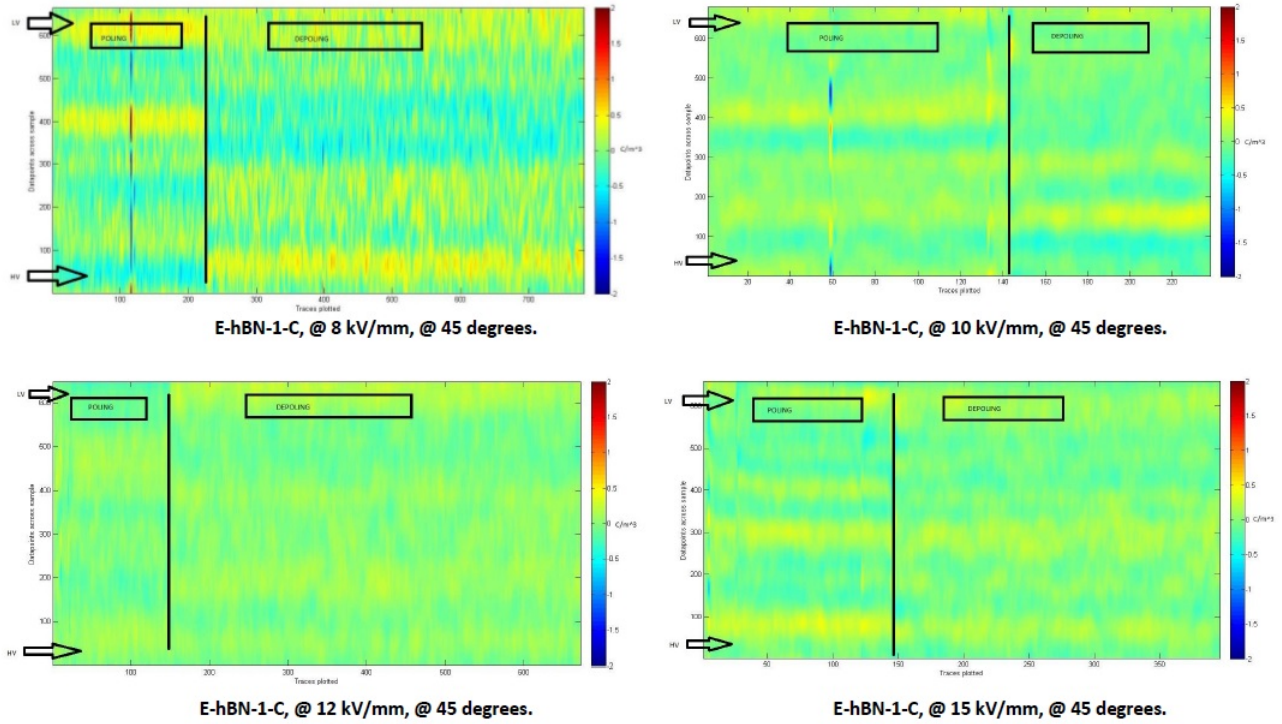

Figure 5.2.21: E-hBN-1-C contour plots-1

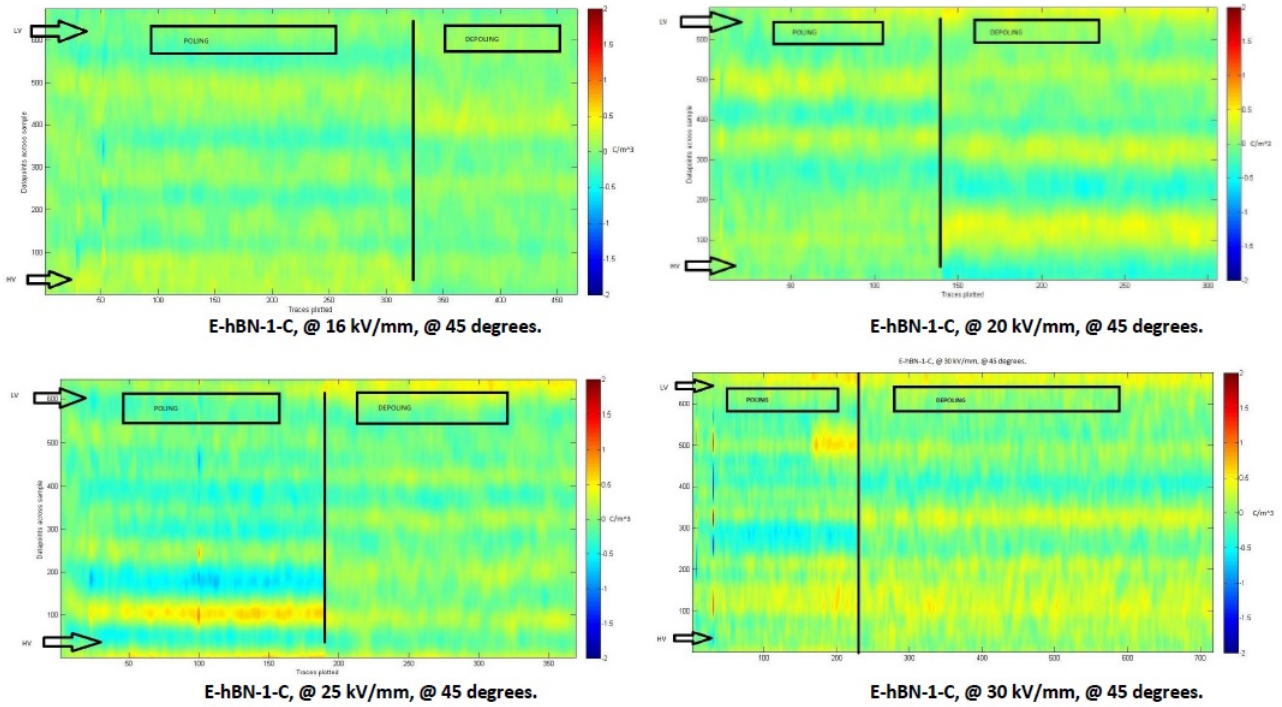

Figure 5.2.22: E-hBN-1-C contour plots-2

Finally, the collection of the contour plots for E-hBN-5-B is presented in Figure-5.2.23 & Figure-5.2.24.

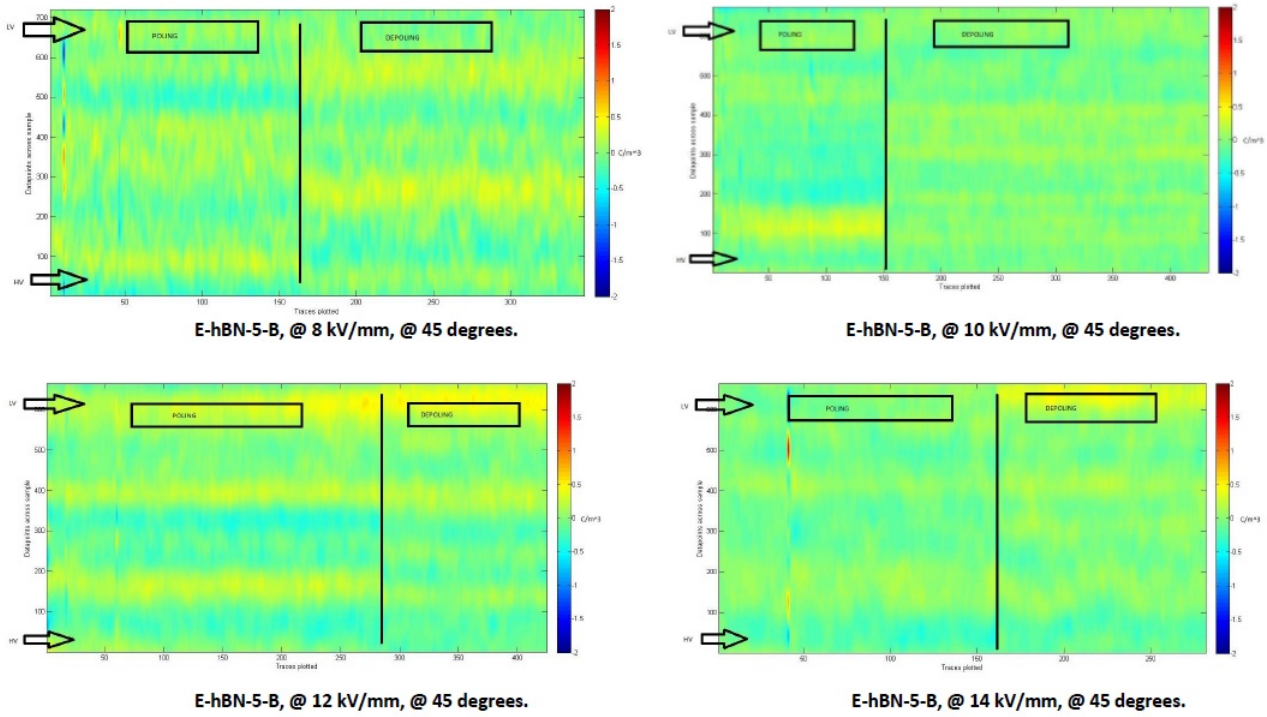

Figure 5.2.23: E-hBN-5-B contour plots-1

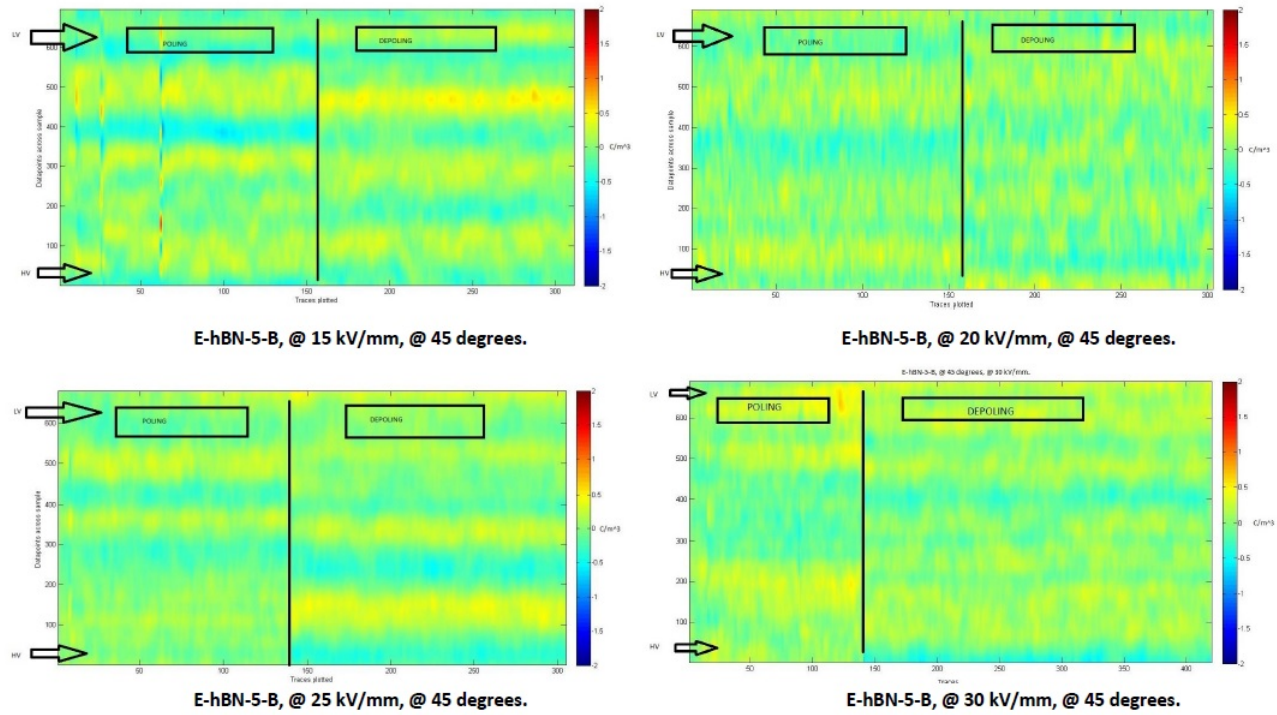

Figure 5.2.24: E-hBN-5-B contour plots-2

This part is hereby concluded.

Space Charge!: An epilogue

I got them in my cross-hairs,
I tracked the little devils down-
They had made new friends in their quantum world,
and they greeted my nudges with a wily frown!
Their world is draped in a camouflage of matter,
their actions show up as white noise and chatter-
They defy many notions of conventional physics,
and our hypotheses' fall off with a clatter!
Waves strike the shore of the ocean, and frothy foam obscures the glint of blue-
Many were the days I strode about life, without a pointer or a clue!
My brain had his fun, he wandered off without a map or a plan, and all he could do in life was scoff-
But when I needed him most, and all felt lost- he returned right back, and picked up where he left off!
I have paced down long corridors, trying to make sense of it all, when it came to me-
Their actions made perfect sense to the grand order of life, a beautiful theory would be the key!
Two decades and five I made plans for my future self, while life passed me by-
It took a journey with the smallest of things, to bring the biggest of truths to my eye!

— Debarshi Saha (July 01, 2015)